論文 / 著書情報
Article / Book Information

題目(和文)	ニッケル及び銅単結晶上に調製した酸化薄膜の研究
Title(English)	Study of Oxide thin films formed on Nickel and copper single crystals
著者(和文)	松本健俊
Author(English)	
出典(和文)	学位:博士(理学), 学位授与機関:東京工業大学, 報告番号:甲第4750号, 授与年月日:2001年3月26日, 学位の種別:課程博士, 審査員:堂免 一成
Citation(English)	Degree:Doctor (Science), Conferring organization: Tokyo Institute of Technology, Report number:甲第4750号, Conferred date:2001/3/26, Degree Type:Course doctor, Examiner:
学位種別(和文)	博士論文
Type(English)	Doctoral Thesis

Study of Oxide Thin Films Formed on Nickel and Copper Single Crystals

Thesis submitted to

Tokyo Institute of Technology

for Doctor Thesis

March 2001

by

Taketoshi Matsumoto

Contents

1 General introduction

Surface science emerged in the 1960s with the development of ultrahigh vacuum apparatus [1]. Metal single crystals were examined by low-energy electron diffraction (LEED) to reveal the surface structures, and the composition of the surface was determined by electron and infrared spectroscopies. The products through the surface reactions were measured by quadrupole mass spectrometer. Scanning tunneling microscopy (STM) and atomic force microscopy (AFM) [1-3] enabled to observe the local surface structure at atomic resolution, while short-lived intermediates were detected by laser spectroscopy in the last two decades. Some of these techniques were applied to the observation of the single crystal surfaces at the pressure range from 10^{-9} Torr to the ambient pressure giving solution to the pressure gap problems [4]. Especially, infrared reflection absorption spectroscopy (IRAS) has advantages in sensitivity and resolution under in-situ conditions [5-8]. These techniques provided information about the relationships between surface conditions and catalytic reaction rates. In this way, surface science has contributed in expanding our understanding of catalytic reactions [9].

Various metal oxides have been used as essential industrial catalysts in water gas shift reactions, partial oxidation of organic compounds, and so on [10]. For the study of the model oxide catalysts, oxide thin films have been utilized because of their sufficient electron conductivity, heat conductivity, and reflectivity for traditional surface science techniques [11]. The oxide thin films are often grown epitaxially on metal single crystal surfaces by exposure to oxygen [12]. Recent years have seen commercialization of oxide photocatalysts [10], and research and development of oxide

electronic materials with downsizing electronic devices [13, 14]. Basic research of oxide films at atomic level is growing in importance in various fields.

In this thesis, the observations of oxygen adsorption on Ni(111) and Cu(111) surfaces using STM, and reactions on the oxidized surfaces using IRAS are reported. Adsorption and decomposition of formic acid and carbon dioxide are observed on NiO(111)/Ni(111) and oxidized Cu(111) surfaces. The work described in this thesis is summarized as below.

Chapter 2 Basic principles and concepts of IRAS and STM are discussed. Apparatuses constructed and used in the experiments are also shown.

Chapter 3 Adsorption of oxygen on Ni(111) at elevated temperatures was observed by STM and LEED. The oxidation process and the temperature dependence of the surface structure are discussed.

Chapter 4 Decomposition of formic acid on NiO(111)/Ni(111) was observed using IRAS. The sites of dehydrogenation and dehydration reactions were revealed by using adsorbed CO as a probe.

Chapter 5 Adsorption of carbon dioxide on NiO(111) /Ni(111) and OD/NiO(111) /Ni(111) were observed by IRAS. The structure of the carbonate and the reactivity with hydroxyl species are discussed.

Chapter 6 Oxygen adsorption on Cu(111) was observed by STM and LEED. The oxidation process and the temperature dependence of the surface structure are discussed. Models of the oxidized surface structures are suggested.

Chapter 7 Adsorption and decomposition of formic acid were observed on the oxidized Cu(111) surface using TPD and IRAS. The decomposition temperatures are compared with those on other copper surfaces reported previously.

Chapter 8 Summary of this study is described.

References

[1] G. A. Somorjai, Introduction to Surface Chemistry and Catalysis (John Wiley & Sons Ltd, N. Y., 1994).

[2] C. Bai, Scanning Tunneling Microscopy and Its Application (Springer, Berlin, 1999).

[3] R. Wiesendanger, Scanning Probe Microscopy and Spectroscopy (Cambridge university press, Cambridge, 1994).

[4] R. J. Madix, Adv. Catal. 29 (1980) 1.

[5] J. W. Walles and R. Smith, Surface Science Techniques (Elsevier Science Ltd, Oxford, 1994).

[6] R. I. Masel, Principles of Adsorption and Reaction on Solid Surfaces (John Wiley & Sons Ltd, N. Y., 1996).

[7] R. J. H Clark and R. E. Hester, Spectroscopy of Surfaces (John Wiley & Sons Ltd, New York, 1988).

[8] F. M. Hoffmann, Surf. Sci. Rep. 3 (1983) 107.

[9] G. Ertl, Adv. Catal. 45 (2000) 1.

[10] V. E. Henrich and P. A. Cox, The Surface Science of Metal Oxides, 1st ed. (Cambridge U.P., New York, 1994).

[11] C. Xu and D. W. J. Goodman, Chem. Soc. Faraday Trans. 91 (1995) 3709.

[12] H.-J. Fruend, Angew. Chem. 109 (1997) 444.

[13] G. Timp, Nanotechnology (Springer, New York, 1999).

[14] M. C. Roco, R. S. Williams and P. Alivisatos, Nanotechnology Research Directions (Kulwer Academic Publishers, Boston, 2000).

2 Infrared reflection absorption spectroscopy (IRAS) and scanning tunneling microscopy (STM)

2.1 IRAS

The surface electric fields arising from *s*- and *p*-polarization components of both the incident and reflected rays are shown in Fig. 2.1 [1-3]. At all angles of incidence, the phase of the *s*-polarized component is almost exactly reversed on reflection, so that the field from the reflected beam opposes that from incident one. Since the reflection coefficients of metals are close to unity in the infrared, almost complete cancellation of two fields occurs in the vicinity of the surface. Accordingly, the surface field from the *s*-component is very small, and there can be little interaction with the dipoles of adsorbed molecules. The phase of the *p*-component is also changed on reflection, but the change depends on the angle of incidence. While the resultant field has a component parallel to the surface which is always small, the perpendicular component is large at angles of incidence close to grazing.

Since the infrared absorption intensity of a molecule dipole is proportional to the square of the oscillating electric field component along the dipolar axis, the principle selection rules are established for IRAS at metal surfaces.

(i) Only *p*-polarized radiation is adsorbed to significant extent by the adlayer.

(ii) Only vibrations which have a component of the induced dipole perpendicular to the surface are infrared active.

The first rule is used in the method of polarization of modulation: by processing the beams from the two polarization components separately and comparing the absorption of each, an effective double beam spectroscopy is achieved which is insensitive to fluctuations in source intensity, detector responsiveness, absorption by gas

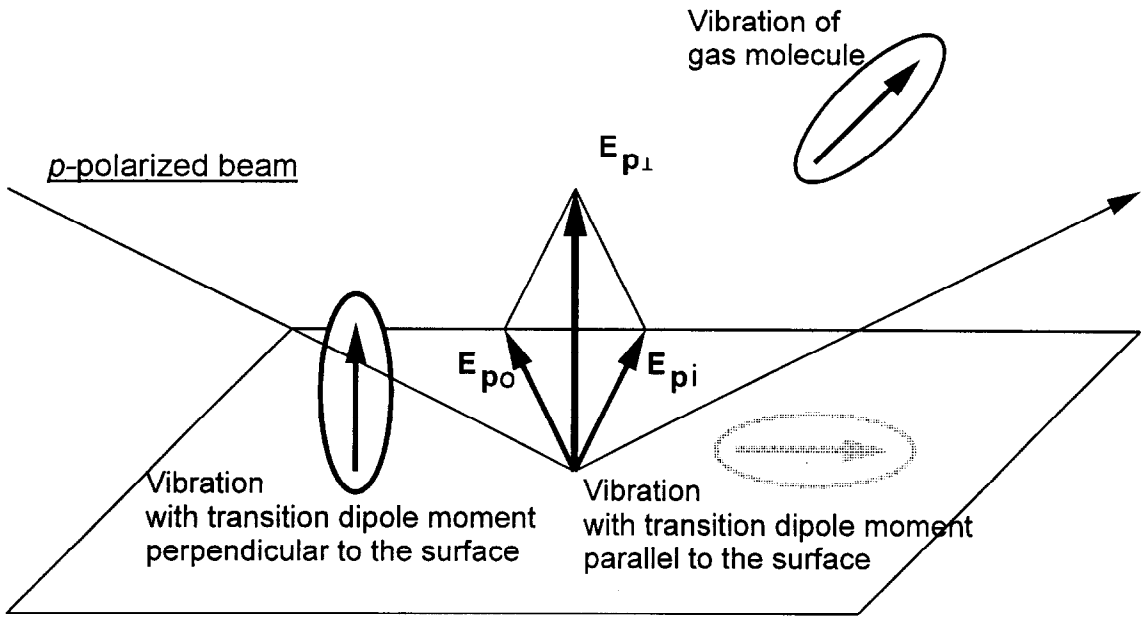

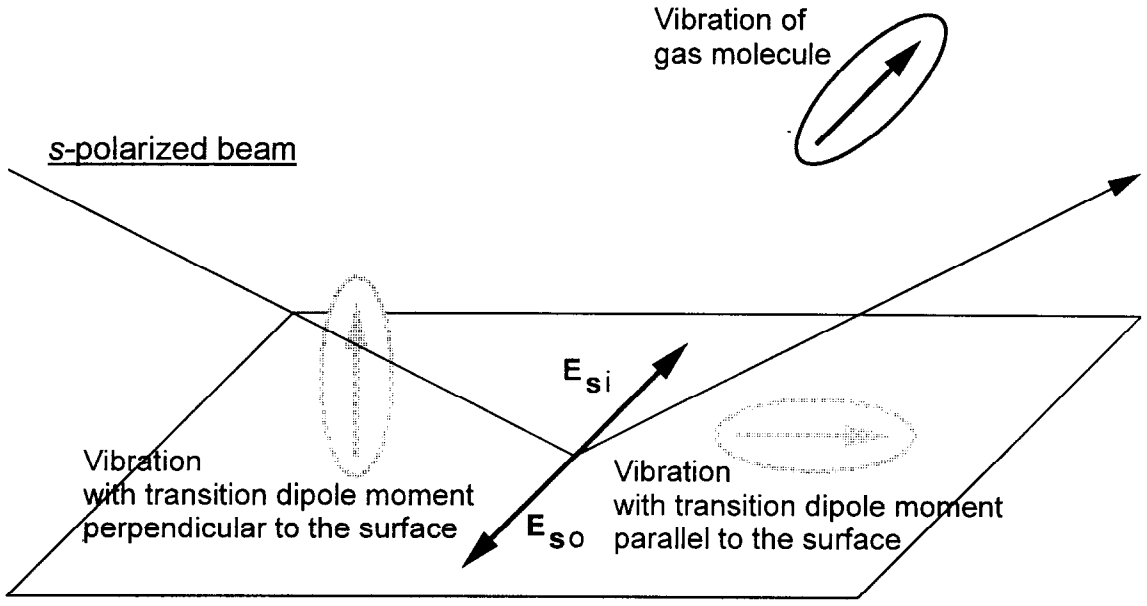

Fig. 2.1. Electric vectors of the *s*- and *p*-polarized components and radiation on a metal surface. Vibrations of adsorbed molecules with transition dipole moment perpendicular to the surface and gas molecules can be observed by *p*-polarized beam. Only vibrations of adsorbed molecules with transition dipole moment perpendicular to the surface can be observed by *s*-polarized beam.

molecules and other factors which influence both components equally.

2.2 STM

Conventional STM is based on the control of the tunneling current I through the potential barrier between the surface to be investigated and the probing metal tip [4-5]. If a small bias voltage is applied between the sample surface and the tip (in the best case, an atomically sharp tip), a tunneling current will flow between the tip and sample when the gap between them is reduced to a few atomic diameters. It takes advantages of the strong dependence of the tunneling probability of electrons on the electrode separation. There it is well known that the tunneling current I (at a low voltage V and low temperature) behaves as

$$I \approx 18 \frac{V}{10^4 \Omega} \frac{k}{s} A_{eff} \exp(-2ks) \tag{1}$$

where $2k$ [Å^{-1}] = $1.025\Phi_B^{1/2}$ [eV], Φ_B is the effective barrier height between the two electrodes. $A_{eff} = \pi \times (1/2L_{eff})^2$ is the effective area determining the lateral resolution $L_{eff} \approx 2 \times [(R_t+s)/k]^{1/2}$ which applies when the separation s becomes smaller than the Radius R_t of the tip. For typical metals ($\Phi_B \approx 5$ eV) the predicted change in I by one order of magnitude for the change $\Delta s \approx 1$ Å has been verified. If the current is kept constant to within, e.g. 2 %, then the gap s remains constant to within 0.01 Å. This fact represents the basis for interpreting the image as simply a contour of constant height above the surface [1].

It is considered that the tip has highly localized dangling bond d or p type states traces out the contours of fictitious surface with the dangling bond type states on each sample atoms [1, 5]. These contours show atomic corrugations an order magnitude greater than those of charge-density distribution. Experiments show that atoms can be identified on metal surfaces where the atomic separation is less than 0.2 nm.

There are five main parameters that can be varied in an STM. These are x and y (area), z (height), V (bias voltage), and I (tunneling current). Three main modes of operation are as follows.

(i) Current imaging mode, where z and V are kept constant, x and y are varied by rastering the tip and I is measured.

(ii) Constant current mode, where I and V are kept constant, x and y varied by rastering the tip and z is measured.

(iii) Spectroscopy mode, where parameters are varied in a variety of ways.

The constant current mode, which is most popular, was applied in this study.

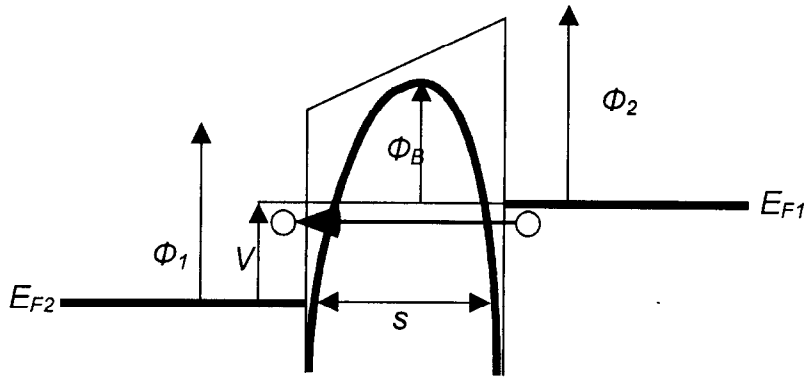

Fig. 2.2. Energy diagram of the tunneling gap E_{F1} and E_{F2} Fermi levels of tip and surface, Φ_1 and Φ_2 work functions of tip and surface, Φ_B effective barrier height, effective tunneling gap s and V tip bias.

2. 3 Instrumental

All experiments were carried out in UHV chambers with ~10^{-8} Pa base pressure.

The IRAS system used for the experiments on the NiO(111) and copper oxide surfaces are shown in Fig. 2.3. The FT-IR JEOL-100 and InSb/MCT two color infrared detector were used for the measurement of IRA spectra. It took ten minutes for getting an effective spectrum after 500 times integration. The pass of infrared beam was purged with dry air. The UHV chambers for IRAS experiments on nickel and copper oxide surfaces are illustrated in Figs. 2.4 and 2.5, respectively. The TPD (temperature-programmed desorption), LEED/AES (low energy electron diffraction / Auger electron spectroscopy), and IRAS methods are available. The chambers have windows for the irradiation of the UV-light. A high-pressure reactor designed for use at 1 atm gas pressure is attached inside the chamber as depicted in Fig. 2.5.

The STM systems used for the observation of the NiO(111) and copper oxide surfaces are shown in Fig. 2.6 (JEOL JSPM-4500S, operative above 30 K) and Fig. 2.7 (W. A. Technology VT STM, operative at above room temperature), respectively. Tips were prepared by electrochemical etching of tungsten wires.

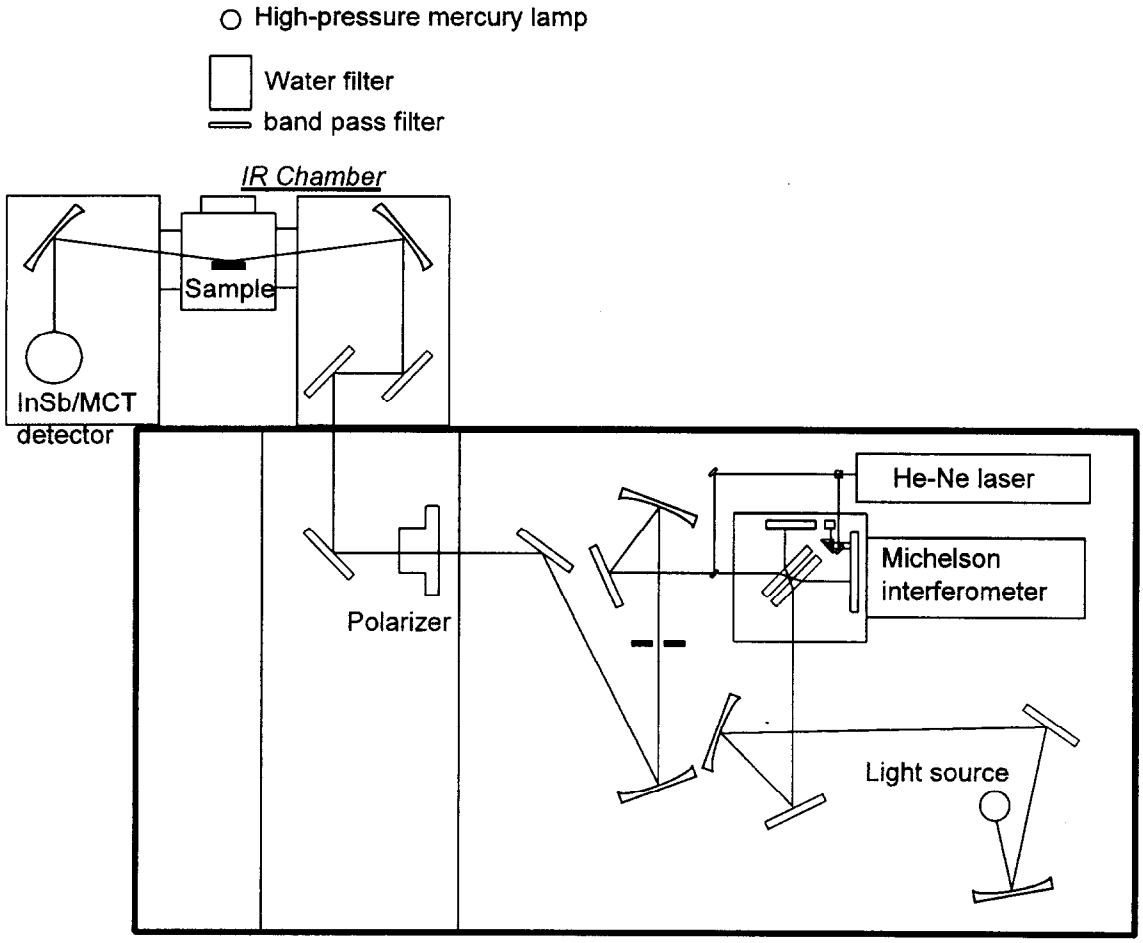

Fig. 2.3. Schematic view of IRAS system.

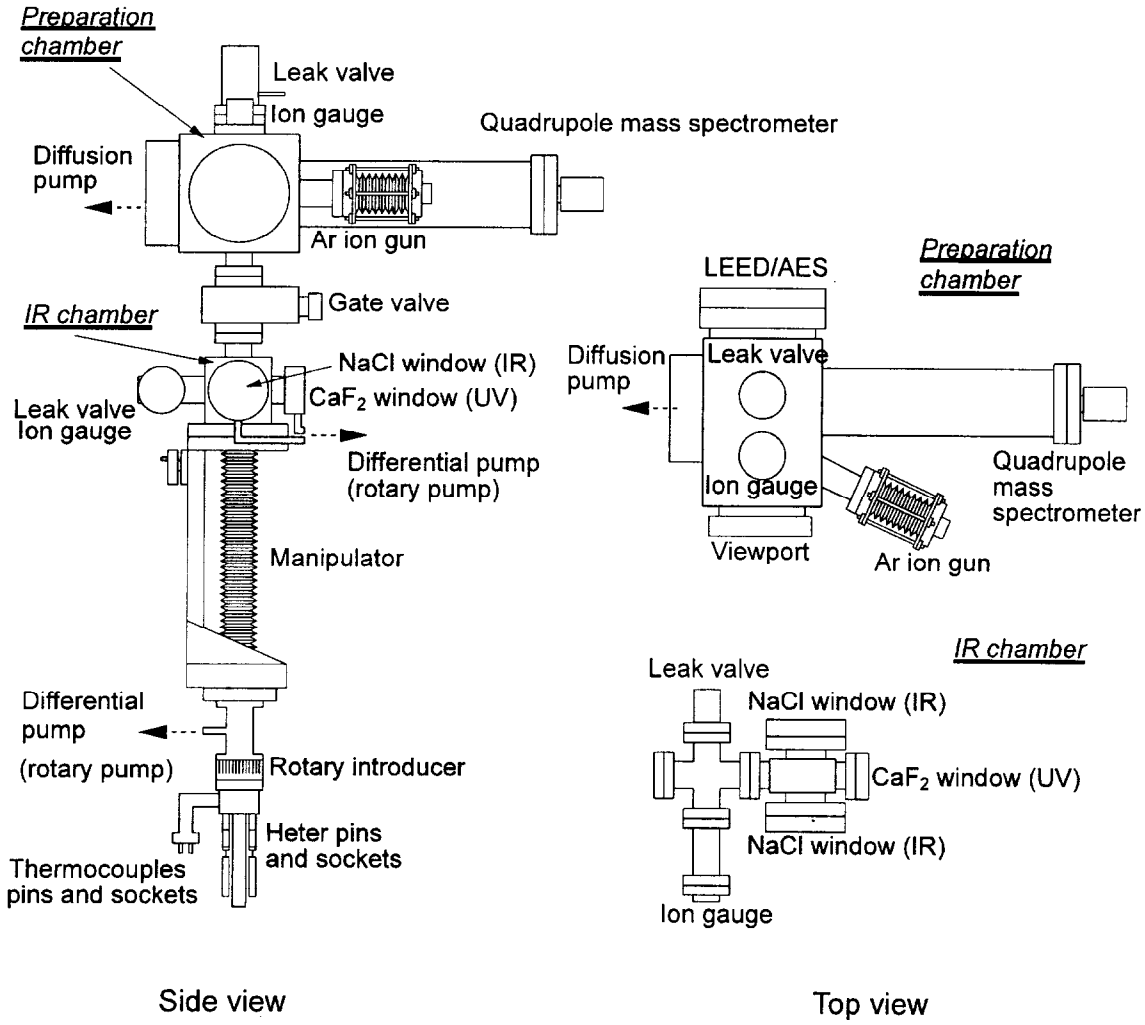

Fig. 2.4. Schematic view of UHV chambers used for IRAS observation of NiO(111).

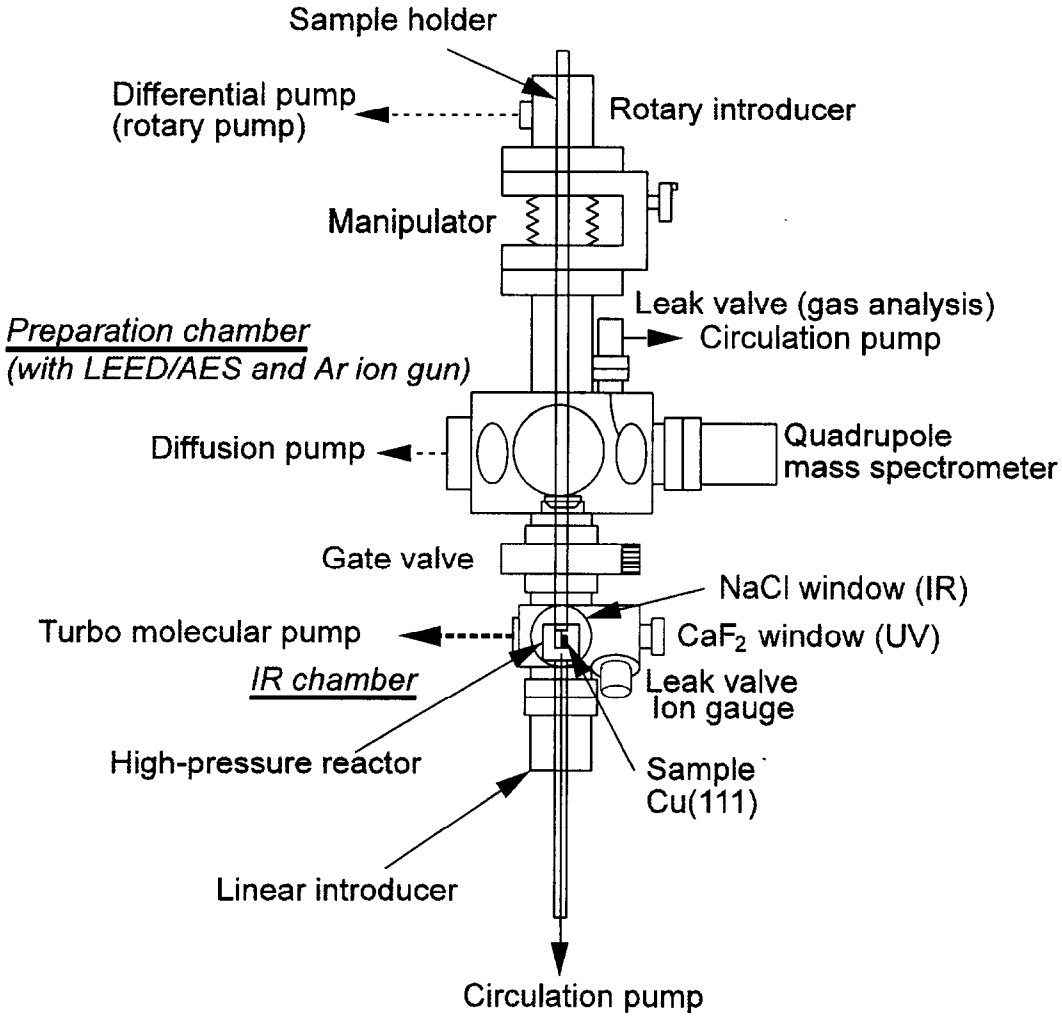

Fig. 2.5. Schematic view of UHV chambers used for IRAS observation of copper oxide surface.

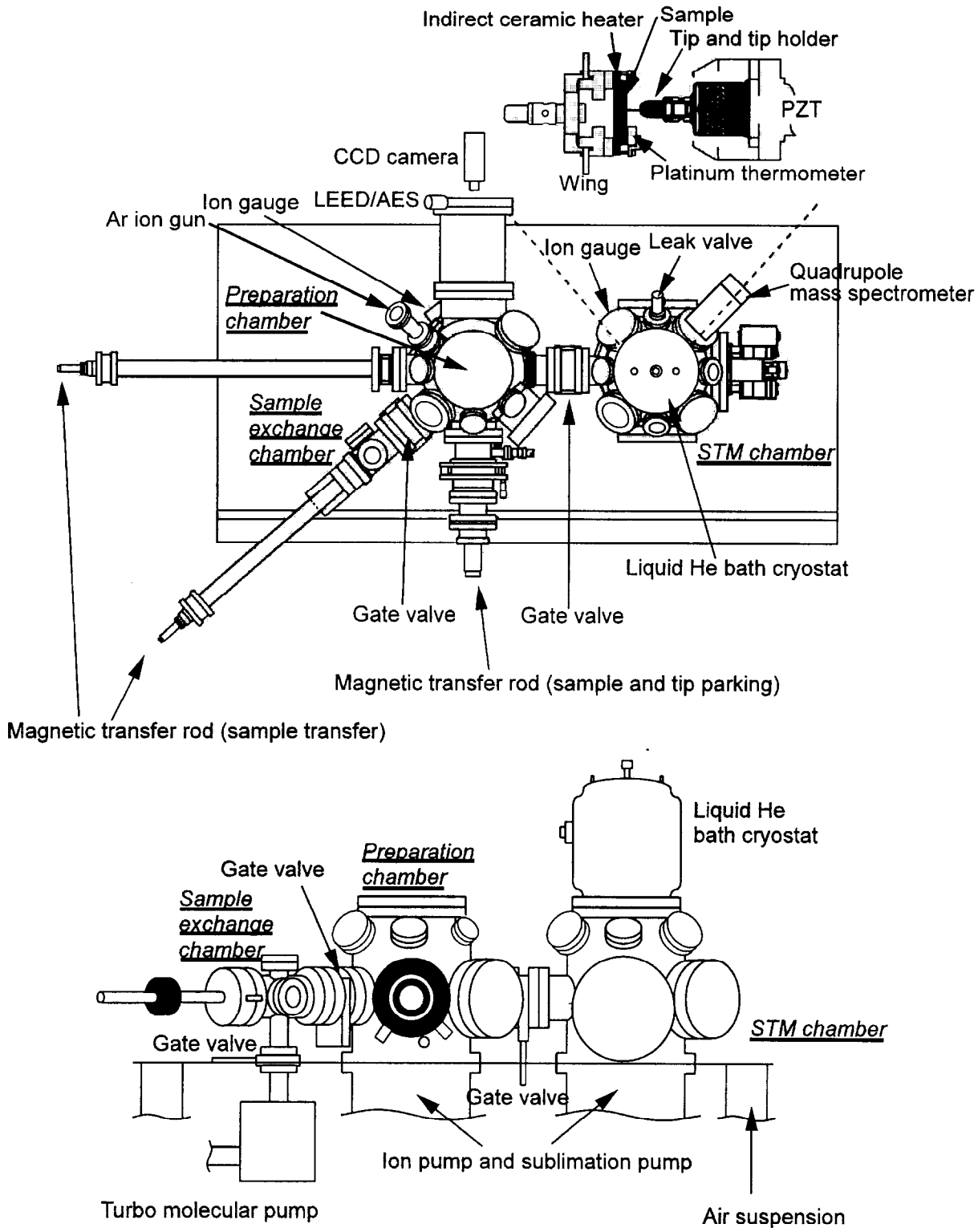

Fig. 2.6. Schematic view of UHV chambers used for STM observation of NiO(111).

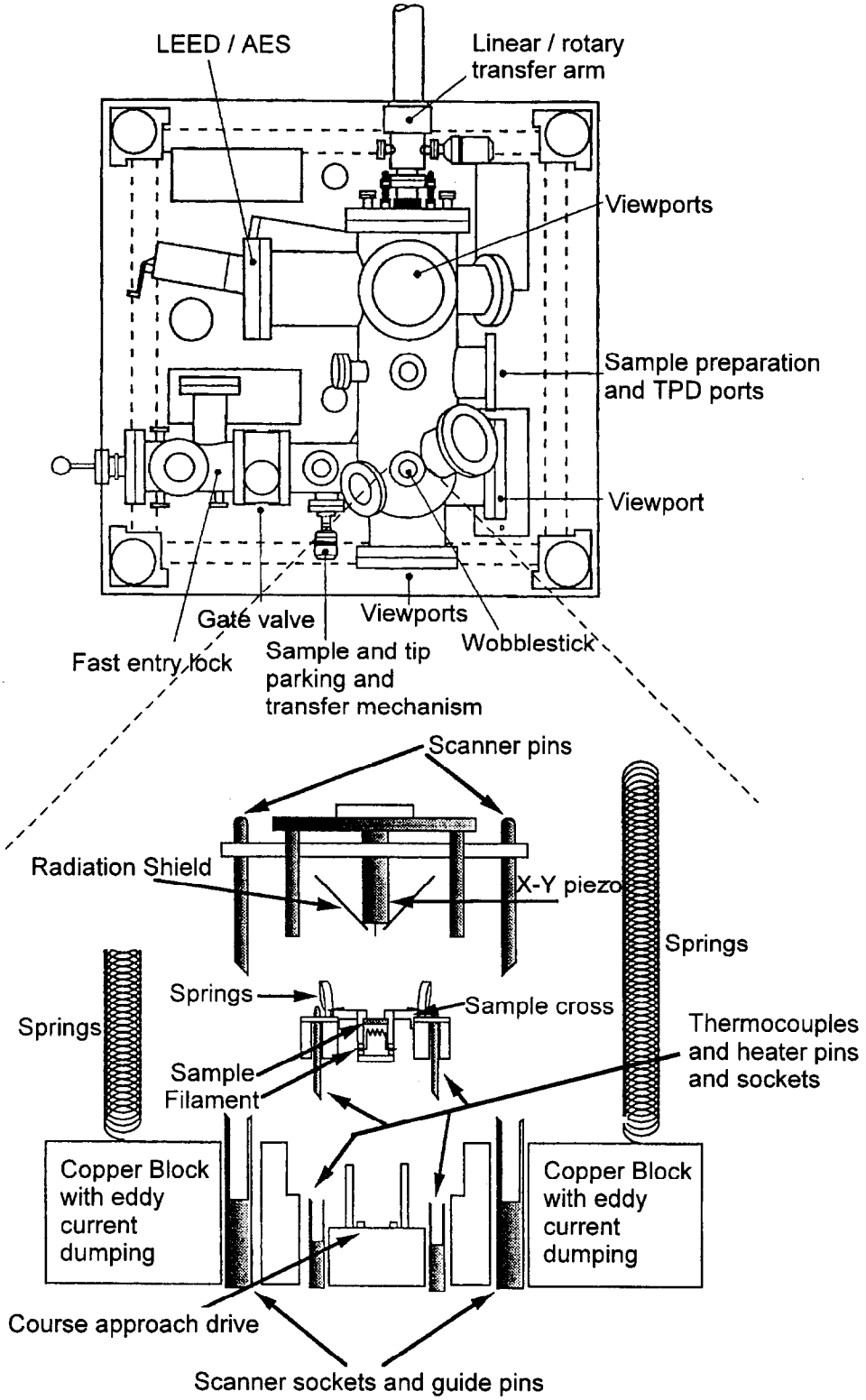

Fig. 2.7. Schematic view of UHV chambers used for IRAS observation of copper oxide surface.

References

[1] J. W. Walles and R. Smith, Surface Science Techniques (Elsevier Science Ltd, Oxford, 1994).

[2] R. J. H Clark and R. E. Hester, Spectroscopy of Surfaces (John Wiley & Sons Ltd, New York, 1988).

[3] F. M. Hoffmann, Surf. Sci. Rep. 3 (1983) 107.

[4] C. Bai, Scanning Tunneling Microscopy and Its Application (Springer, Berlin, 1999).

[5] R. Wiesendanger, Scanning Probe Microscopy and Spectroscopy (Cambridge university press, Cambridge, 1994).

3 STM studies of oxygen adsorption on Ni(111)

Abstract

The oxidation process of the Ni(111) surface including the structural change on exposure to O_2 was studied using scanning tunneling microscopy (STM) and low-energy electron diffraction (LEED). STM revealed that two oxidation processes proceeded in parallel at 573 K. Flat oxide formed at early stage of oxidation, followed by the formation of oxide islands on top of the flat oxide followed. The (2×2) structure domains derived after flashing the surface up to 623 K. The domain sizes were very small and estimated to be a few nanometers.

3.1 Introduction

The NiO(111) thin film formed on the Ni(111) surface has been investigated because of the interests in the reconstruction of the surface structure and the chemical reactions on its surface [1-3]. It has been reported that the (2×2)-NiO(111) surface, observed by low energy electron diffraction (LEED) after oxidizing and annealing the Ni(111) surface at around 600 K, reconstructed to the (1×1) structure with formation hydroxyl species on exposure to water vapor [1]. The LEED spots corresponding to the (2×2) structure were reported to be diffuse [1], and it has been considered that the local surface structure should be specified by scanning tunneling microscopy (STM). The (1×1)-NiO(111), the (2×2)O-Ni(111) and the NiO(100) structures produced on the Ni(111) surface were observed by STM [3]. The oxidation process and the local (2×2)-NiO(111) structure is unknown on the Ni(111) surface. In this study, the oxidation process of the Ni(111) surface was observed at elevated temperatures and the (2×2)-NiO(111) structure were observed by LEED and STM.

3.2 Experimental

The fresh Ni(111) crystal surface was cleaned by many cycles of Ar ion bombardment and annealing. The clean surface was prepared before experiments by 6 cycles of ion bombardment at room temperature for 15 minutes and vacuum annealing at 973 K for 4 minutes. Contamination on the surface was negligible as verified by Auger electron spectroscopy. All STM images were acquired in the constant-current mode.

3.3 Results and discussion

Fig. 3.1 (a) shows the LEED pattern of the Ni(111) surface. Sharp spots and low background intensity indicate that the surface is well-ordered. A STM topograph of the surface is shown in Fig. 3.1 (b). Bright dots arraying hexagonally correspond to each Ni surface atoms.

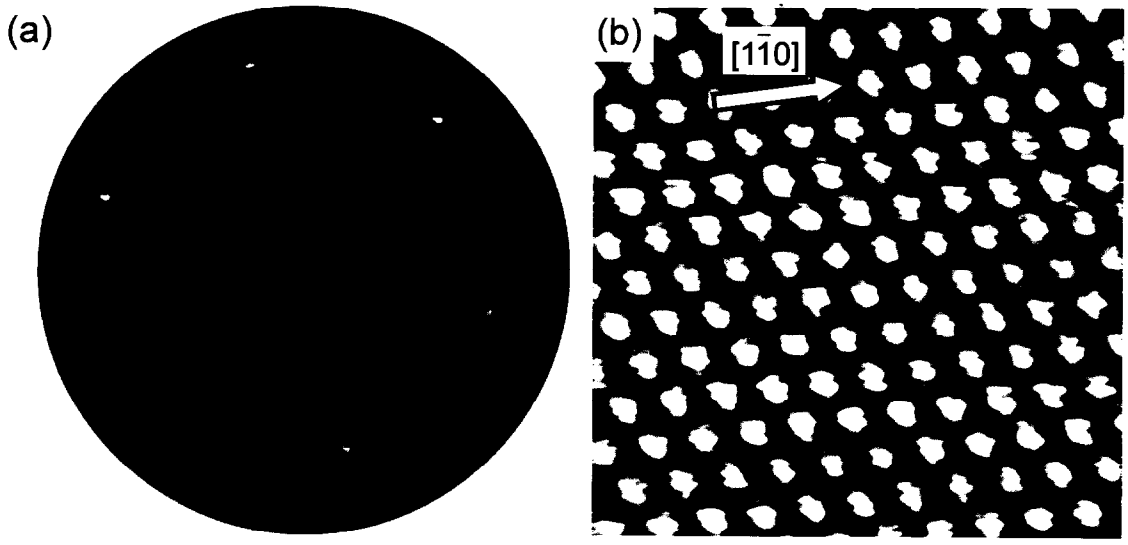

Fig. 3.1. LEED pattern and STM topographs of Ni(111) at 300 K. (a) LEED pattern (163 eV). (b) STM topograph at atomic resolution (26×26 Å^2, Vs=0.08 V, It=5 nA). The arrow indicates the crystallographic direction.

When the Ni(111) surface was exposed at 573 K to O_2 of 2-5 $\times 10^{-5}$ Pa pressure, the STM topographs changed to those shown in Fig. 3.2 by exposure time. The clean Ni(111) surface before the exposure to O_2 at 573 K is shown in Fig. 3.2 (a). Ni(111) terraces having several hundreds angstroms width and straight step edges were observed. The bright areas which are considered to be composed of oxides (indicated by an arrow) were found along step edges changing their shapes from the straight lines to the curved lines as seen in Fig 3.2 (b) (exposure to 0.4 L O_2). Flat oxide areas grew over Ni(111) terraces, and bright small islands (indicated by an arrow) appeared on the flat oxide areas in Fig. 3.2 (c) (1.2 L). A flat oxide layer was formed over the terrace surfaces and the number of small islands increased when the exposure reached 2 L (Fig 3.2 (d)). After the exposure of 4 L, the STM image changed as shown in Fig. 3.2 (e), and one sees that the expansion and increase of the small islands area distinctly slower than the growth of the flat terraces. Thus, two processes in the oxidation of the Ni(111) surface were observed; one is the formation of flat oxide layer on terraces as seen in Figs. 3.2 (b)-(d), and the other is the formation of small islands on the flat oxide as seen in Figs. 3.2 (c)-(e). Fig. 3.2 (f) is the magnified image of the oxidized Ni(111) surface observed at 300 K after the evacuation of O_2 gas from the system that gave the image shown in Fig. 3.2 (e). The surface consisted of oxide particles having the sizes of a few hundreds angstroms width and the large corrugation of ~40 Å. The surface structure was not evident at atomic resolution.

A LEED pattern was examined at 300 K after flashing to 623 K the surface that gave the images in Fig. 3.2 (f). The LEED patterns assignable to Ni(111) and (1×1)-NiO(111) phases were observed as shown in Fig. 3.3 (a). As reported previously [1], very diffuse spots were observed between the center and the (1×1)-NiO(111) spots. The surface is thus considered to be only partialy ordered since the LEED spots assigned to NiO(111) are diffuse. Fig. 3.3 (b) and (c) are the STM topographs of the same surface at different magnifications: the presence of the

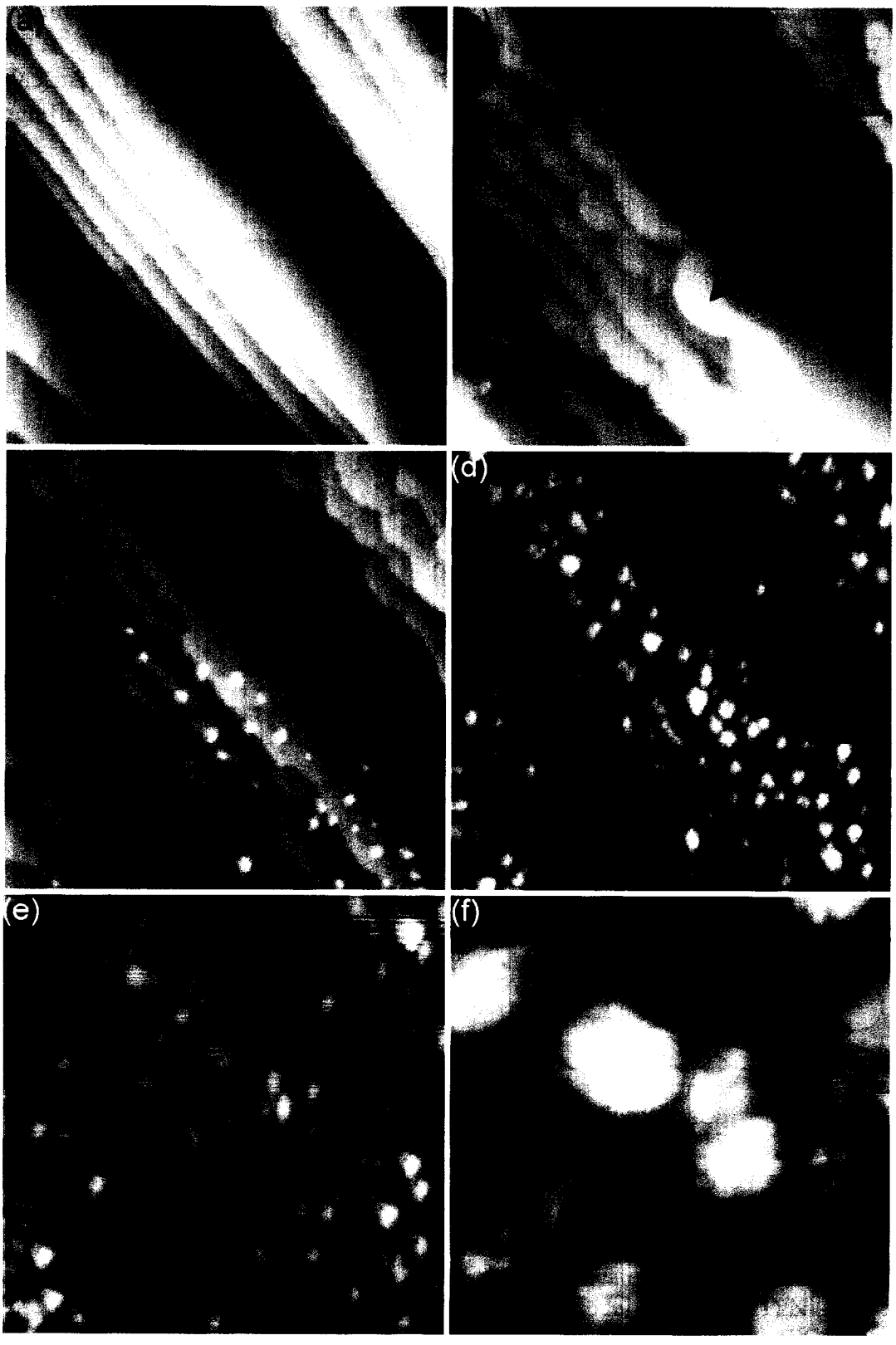
(d)
(e)
(f)

Fig. 3.2. STM topographs of Ni(111) surface exposed to O_2 at 573 K. (a) Clean Ni(111) before exposure (1800×1800 Å^2, Vs=0.7 V, It=0.5 nA). (b) After 0.4 L exposure (1400×1400 Å^2, Vs=0.7 V, It=0.5 nA). (c) After 1.2 L exposure(1800×1800 Å^2, Vs=0.7 V, It=0.5 nA). (d) After 2 L exposure (1800×1800 Å^2, Vs=0.7 V, It=0.5 nA). (e) After 4 L exposure (1800×1800 Å^2, Vs=0.7 V, It=0.5 nA). (f) Magnified view in UHV (900×900 Å^2, Vs=0.7 V, It=0.5 nA).

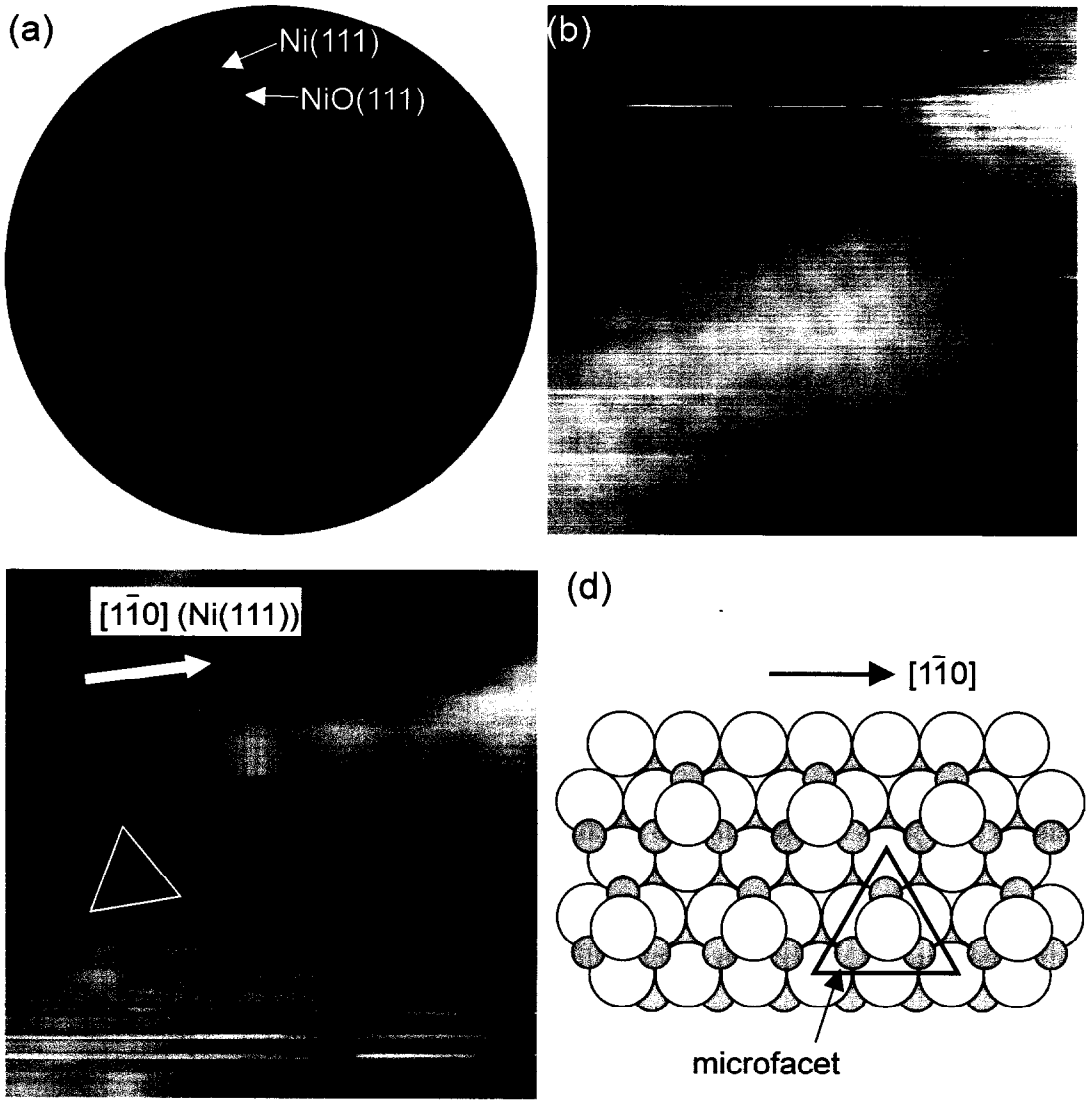

Fig. 3.3. LEED pattern and STM topographs of NiO(111)/Ni(111) at 300 K. (a) LEED pattern (89 eV). (b) STM topograph (60×60 Å^2,Vs=0.4 V, It=0.5 nA). (c) Magnified view of the surface observed in figure (b) STM topograph (30×30 Å^2,Vs=0.7 V, It=0.5 nA). The arrow indicates the crystallographic direction of the substrate Ni(111) surface. (d) Model of NiO(111)/Ni(111). The arrow indicates the crystallographic direction of the substrate NiO(111) surface.

partially ordered structure can be seen in Fig. 3.3 (b), and the twice magnified image shown in Fig. 3.3 (c) displays the bright areas (highlighted) arrayed hexagonally with the nearest-neighbor distances of ~6 Å. These bright areas are assignable to the trigonal pyramids of the microfacets of NiO(111) (Fig. 3.3 (d)). The ordered areas were only a few tens angstroms wide, but the images with atomic resolution could not be obtained. The arrow in Fig.3.3 (c) indicates the crystallographic direction of the substrate Ni(111) surface. As seen in Fig. 3.3 (c), the NiO[$1\bar{1}0$] direction (Fig. 3.3 (d)) is parallel to the Ni[$1\bar{1}0$] directions as suggested by the LEED pattern in Fig. 3.3 (a). This result is in correspondence with that reported for small (1×1)-NiO(111) island produced on the Ni(111) surface and observed by STM at 300 K [2].

3.4 Conclusion

The Ni(111) surface under oxidation process was observed by means of STM and LEED. Three major findings emerged as,

1. two oxidation processes were observed on Ni(111) at 573 K by STM; flat oxide formation and oxide islands formation on the flat oxide.
2. the (2×2) NiO(111) structure with the sizes of a few nanometers width was observed.
3. the NiO(111) thin films grew epitaxially with the direction of the NiO[$1\bar{1}0$] parallel to the Ni[$1\bar{1}0$].

These findings indicate that NiO(111) thin films grew epitaxially as particles rather than flat terraces with the (2×2) structure on the Ni(111) surface.

References

[1] F. Rohr, K. Wirth, J. Libuda, D. Cappus, M. B. Öumer and H.-J. Freund, Surf. Sci. 315 (1994) L977.

[2] M. A. Langell and M. H. Nassir, J Phys. Chem. 99 (1995) 4162.

[3] N. Kitakatsu, V. Maurice and P. Marcus. Surf. Sci. 411 (1998) 215.

4 Adsorption and reaction of formic acid on (2×2)-NiO(111)/Ni(111) surface

Abstract

The decomposition of formic acid on (2×2)-NiO(111)/Ni(111) was studied by IRAS. Formic acid molecules adsorbed dissociatively on the surface to form formate which decomposed to H_2, CO_2, H_2O, and CO at 340-415 and 520 K. The vacant sites after decomposition of formate were probed by the adsorption of CO at 100 K. On clean NiO(111) at 100 K, IRAS peaks of two types of adsorbed CO were observed at 2146 and 2079 cm^{-1}, which were assigned to the CO on fully-oxidized Ni cation sites and less-oxidized Ni cation sites, respectively. The CO peaks were not observed on the formate precovered surface. The IRAS peak of adsorbed CO at 100 K on the fully-oxidized Ni cation sites appeared when the surface was heated to decompose formate around 340-415 K. After decomposition at 520 K, the intensities of both peak of CO were recovered to the initial intensities. It was thus concluded that the sites of decompositions at 340-415 and 520 K are the fully-oxidized Ni cation sites and less-oxidized Ni cation sites, respectively. The behavior of hydroxyl species produced by dissociative adsorption of formic acid was next investigated using deuterated formic acid (DCOOD). Hydroxyl species (-OD) formed by the dissociative adsorption of formic acid (DCOOD) was observed at 2536 cm^{-1} below 343 K, while the isolated OD groups appeared at 2713 cm^{-1} and around 500 K. The mechanism of decomposition of formate at each temperature is discussed.

4.1 Introduction

Considerable attention has been paid to the study about adsorptions and reactions of molecules on single-crystal oxide surfaces to understand the catalytic

properties of oxides. The study of oxide surfaces lags behind that of metal and semiconductor surfaces since electron spectroscopies and infrared reflection absorption spectroscopy (IRAS) have been difficult to apply on such surfaces especially in early times because of the low electron conductivity and high transparency [1]. Recently developed technique to prepare epitaxially grown films of oxides on metal substrates enables us to apply these spectroscopies, and there has been large interest of these surfaces in the past several years [2-13].

NiO single crystal films on substrates of single crystal metals are typical examples of epitaxial films applied to the study of adsorptions of molecules by several methods [4, 5, 7-13]. The NiO(111) surface is known to be more active for chemical reactions than NiO(100) because Ni cations at the surface are in lower coordination number [8]. NiO(111) is reconstructed to the (2×2) structure terminated by oxygen atoms in vacuum, thus trigonal pyramids of the microfacets are disposed in order [5, 9].

A significant intermediate in water-gas shift, methanol synthesis, and selective oxidation reactions has been considered to be thr carboxylate species on the surface. One of the simplest way to produce carboxylate is dissociative adsorption of carboxyl acid on the surface as reported on TiO_2(100) [14], NiO(100) [4], NiO(111) [7, 8], MgO(100) [15], ZnO(0001) [16], and ZrO_2(100) [17]. Our group has investigated the adsorption and decomposition of formic acid on NiO(111) prepared by oxidation of Ni(111) under vacuum and steady-state conditions [10, 11]. It was found that formic acid adsorbs on NiO(111) to form formate even at 163 K which decomposes to desorb as H_2, CO_2, H_2O and CO at 340-415 and 520 K in vacuum. Formates were found to be in tilted bidentate configuration in vacuum and in both bidentate and monodentate configuration under flow of formic acid. Formic acid on a thick layer of NiO(111) prepared on a Mo(110) substrate was reported to decompose at 555 K by Xu and Goodman [7, 8]. The question is why the formate decomposes at two different temperatures, 340-415 and 520 K, on our surface. The further examination of the

behavior of formate and that of the hydroxyl species, which may play an important role in the decomposition of formate, is required.

In this work, we investigated the characteristics of the reaction sites for decomposition of formic acid on NiO(111) using CO molecules as a probe. The behavior of hydroxyl species during decomposition of formic acid was also examined by using deuterated formic acid.

4.2 Experimental

The experiments were carried out in an ultra-high vacuum chamber evacuated to 10^{-8} Pa as described in detail in the previous papers [11]. The clean Ni(111) surface was prepared by Ar ion bombardment and annealing at 1023 K and characterized by Auger electron spectroscopy (AES) and low energy electron diffraction (LEED). The NiO film was grown on the clean Ni substrate by the cycles of exposure to oxygen gas at 1000 L (1 L = 10^{-6} Torr s, 1 Torr = 133 Pa) and 570 K and annealing at 650 K. The thickness of the NiO film was estimated to be 5-10 monolayers from the AES peak intensities. The hexagonal LEED pattern which indicates (2×2)-NiO(111) was observed on the NiO film. It should be noted that the amount of oxygen on the NiO(111) estimated by AES did not change after several repetitions of thermal desorption of formic acid or CO.

IRA spectra were acquired using JEOL JIR-100 Fourier transform infrared spectrometer (FTIR) with an InSb/MCT composite detector. The resolution of the spectra was 4 cm^{-1} and the spectra were averaged over 512 scans.

The commercially purchased gases were purified by passing them through a cold trap or by vacuum distillation before use. The amounts of exposure are derived from the apparent pressures displayed by an ionization gauge without any correction and calibration.

4.3 Results and discussion

4.3.1 Characterization of reaction sites using CO

Temperature-programmed desorption (TPD) spectra of formic acid on NiO(111) at 10 L are shown in Fig. 4.1. The desorption of H_2, CO_2, and CO were observed as products of decomposition. The desorption of H_2O, which is the decomposition partner of CO, was not observed because of a high background signal. H_2 and CO_2 as the products of dehydrogenative decomposition desorbed in two temperature regions, 340-390 and 520 K. The presence of two regions indicates that there are two kinds of sites or two kinds of decomposition mechanisms. CO desorbed at 415 and 520 K. These desorptions can be classified into two groups which are observed at around 340-415 K and 520 K. Xu and Goodman reported the decomposition temperature of formic acid on a thick layer of NiO(111) is around 555 K where they used NiO(111) prepared on a Mo(110) substrate by evaporation of Ni in oxygen environment [7, 8]. The desorption at 520 K in the present study may correspond to that at 555 K in their study. The aim of this study is to consider the reason why formic acid is decomposed at two temperature regions.

CO molecule is often used to probe the adsorption sites as the vibrational frequency reflects the state of adsorption sites such as electronegativity. The IRA spectra of adsorbed CO on NiO(111) at 100 K and various exposures are shown in Fig. 4.2. Two peaks were observed at 2146 and 2079 cm^{-1}. It is known that the high and low frequency peaks are corresponding to the adsorbed CO on the fully- and less-oxidized Ni cation sites (denoted as HF and LF sites), respectively [18]. We consider that the HF sites are located at the (2×2)-NiO(111) terrace since the frequency is close to that on other typical oxides [19]. The frequency of the band for the CO on the LF sites is close to that of Ni metal surfaces and the sites are regarded as defect sites such as oxygen vacancies, steps, or boundaries of crystal domains. The CO desorbed

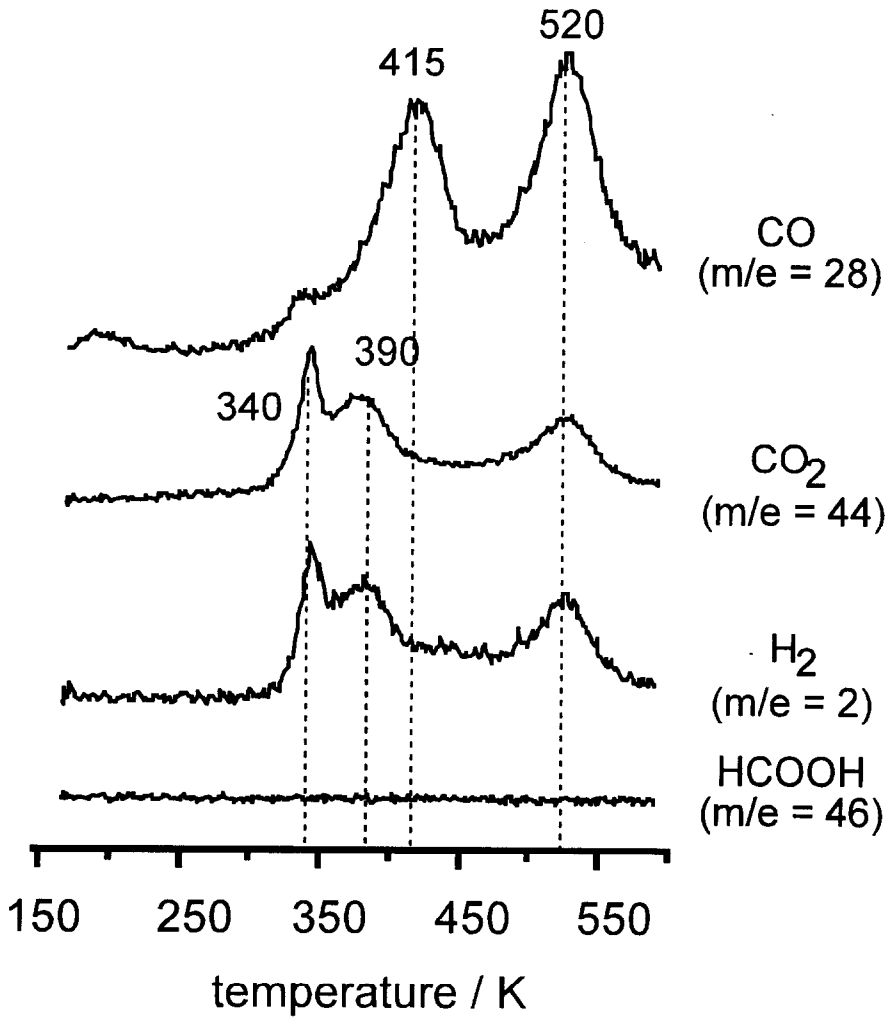

Fig. 4.1. TPD spectra of HCOOH-dosed NiO(111) surface. The surface was exposed to 10 L of HCOOH at 163 K.

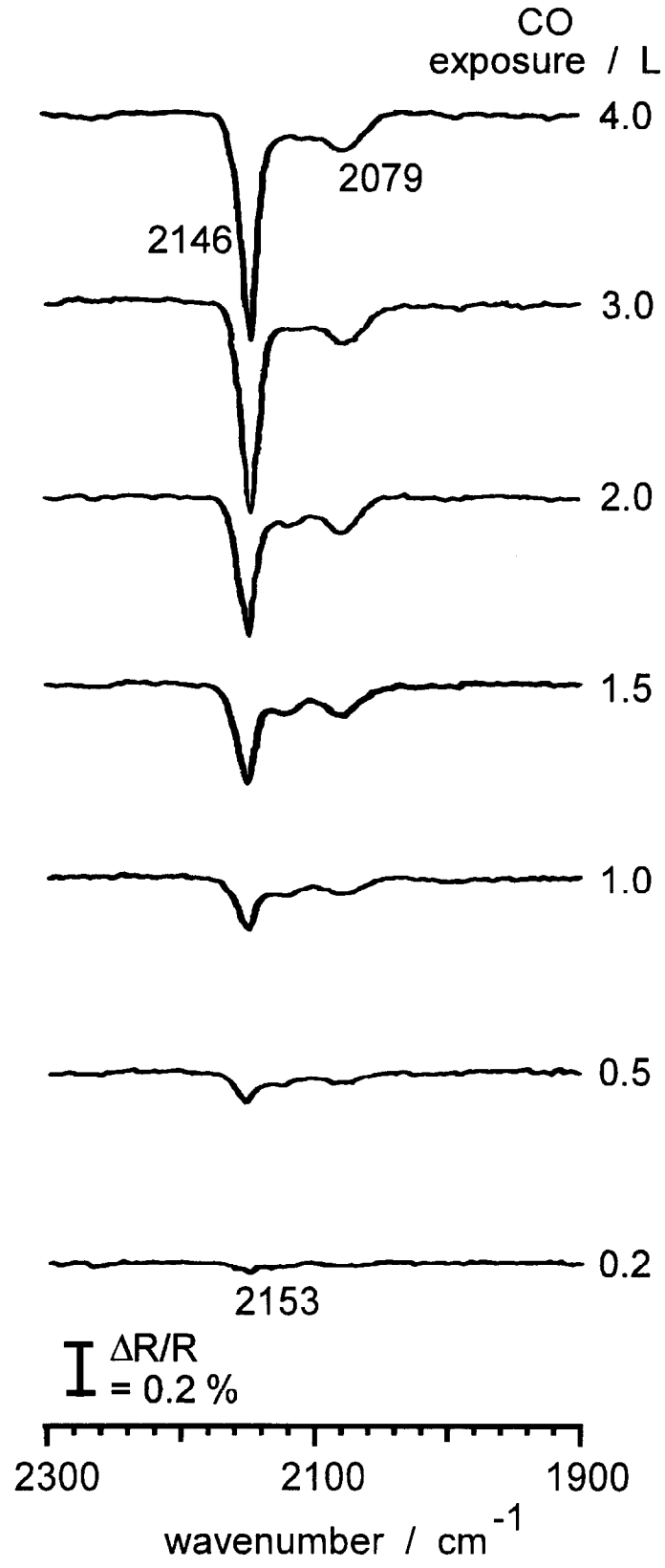

Fig. 4.2. IRA spectra of CO adsorbed on NiO(111) surface at 100 K with various exposures.

at 125 K and no CO_2 was produced during thermal desorption indicating that CO adsorbs only weakly without any reaction on NiO(111).

Temperature-dependence of the IRA spectra of the NiO(111) surface dosed by formic acid are shown in Fig. 4.3. The surface was exposed to the saturation coverage of formic acid at 163 K and the sample was subsequently heated to the stated temperatures. Peaks were observed at 2860, 1570, 1360, and 778 cm^{-1} and are assigned to the C-H stretching, asymmetric O-C-O stretching, symmetric O-C-O stretching and in-plane deformation modes, respectively, of bidentate formate [10]. The appearance of the band of the O-C-O asymmetric stretching mode indicates that the formate molecules inclined on the surface. The peak at 2947 cm^{-1} was possibly due to the C-H stretching mode of the physisorbed formic acid molecule which disappeared at around 273-323 K. The intensities of the formate peaks decreased at higher temperature as formate decomposed. The band of the symmetric O-C-O stretching mode at 1360 cm^{-1} disappeared at 373 K, but its shoulder peak at 1317 cm^{-1} remained until 473 K indicating that the formate species giving the peaks at 1360 and 1317 cm^{-1} decomposed at 340-390 and 520 K in the TPD measurement, respectively. It is hard to discuss the difference in structures and adsorption sites of the two kinds of formate from frequencies of the symmetric O-C-O stretching mode alone and we proceeded to use CO as the probe of the adsorption sites of formate.

Shown in Fig. 4.4. are the IRA spectra observed after the CO-adsorption of the formate-covered NiO(111); the surface was heated to the stated temperatures for a few minutes in vacuum, cooled to 100 K, and dosed by CO to the saturation coverage. The behavior of the formate peaks at 2860, 1570, 1360, and 778 cm^{-1} in Fig. 4.4 is similar to that in Fig. 4.3 suggesting that the adsorbed CO does not affect the structure and decomposition of the remaining formate. The changes in the area intensities of the formate and CO bands by the heated temperatures are displayed in Fig. 4.5. The surface heated at 228 K was solely covered by formate to the saturation coverage and

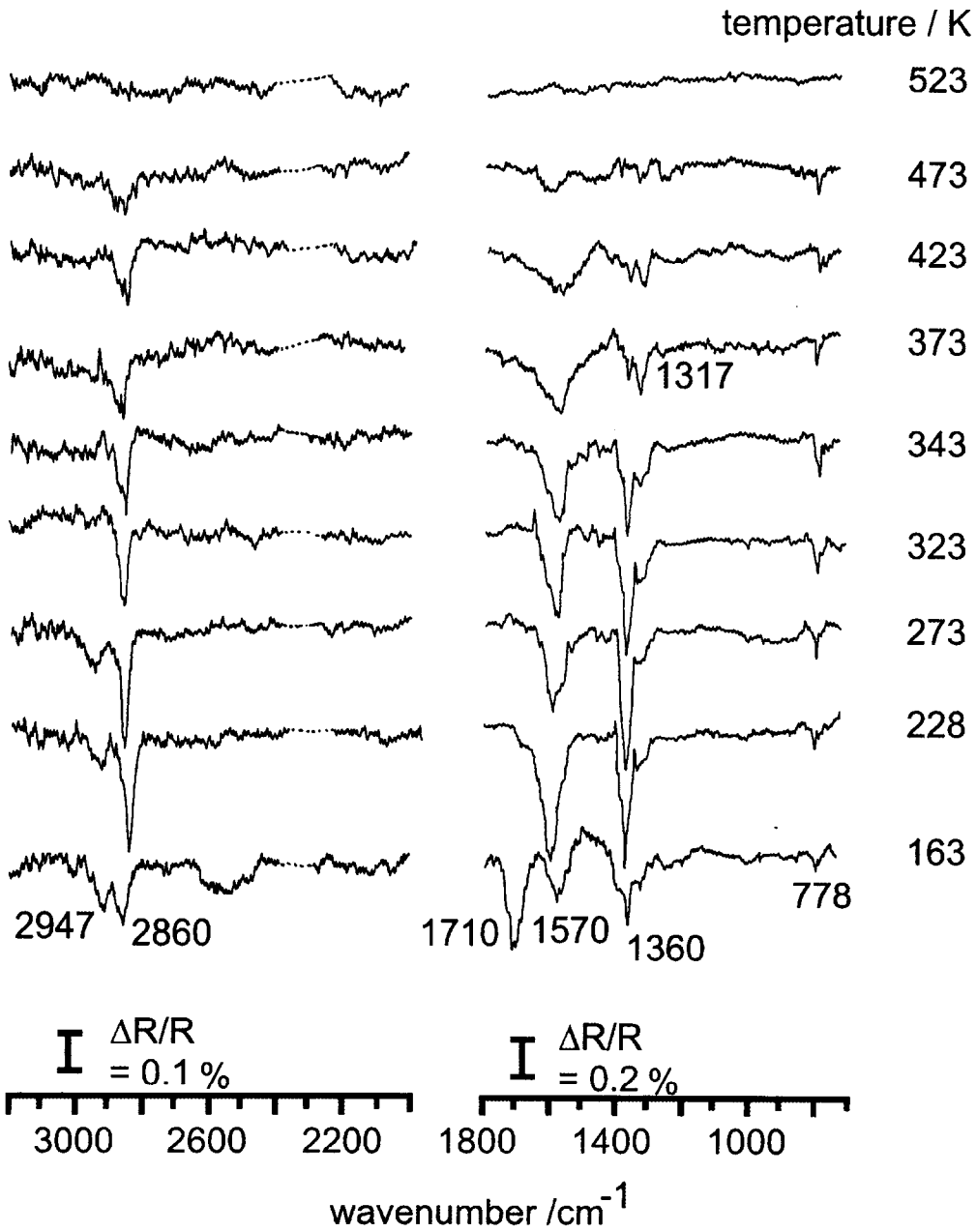

Fig. 4.3. Temperature dependent IRA spectra of formate adsorbed on NiO(111). The surface was first exposed to HCOOH (10 L) at 163 K and then heated to the stated temperatures.

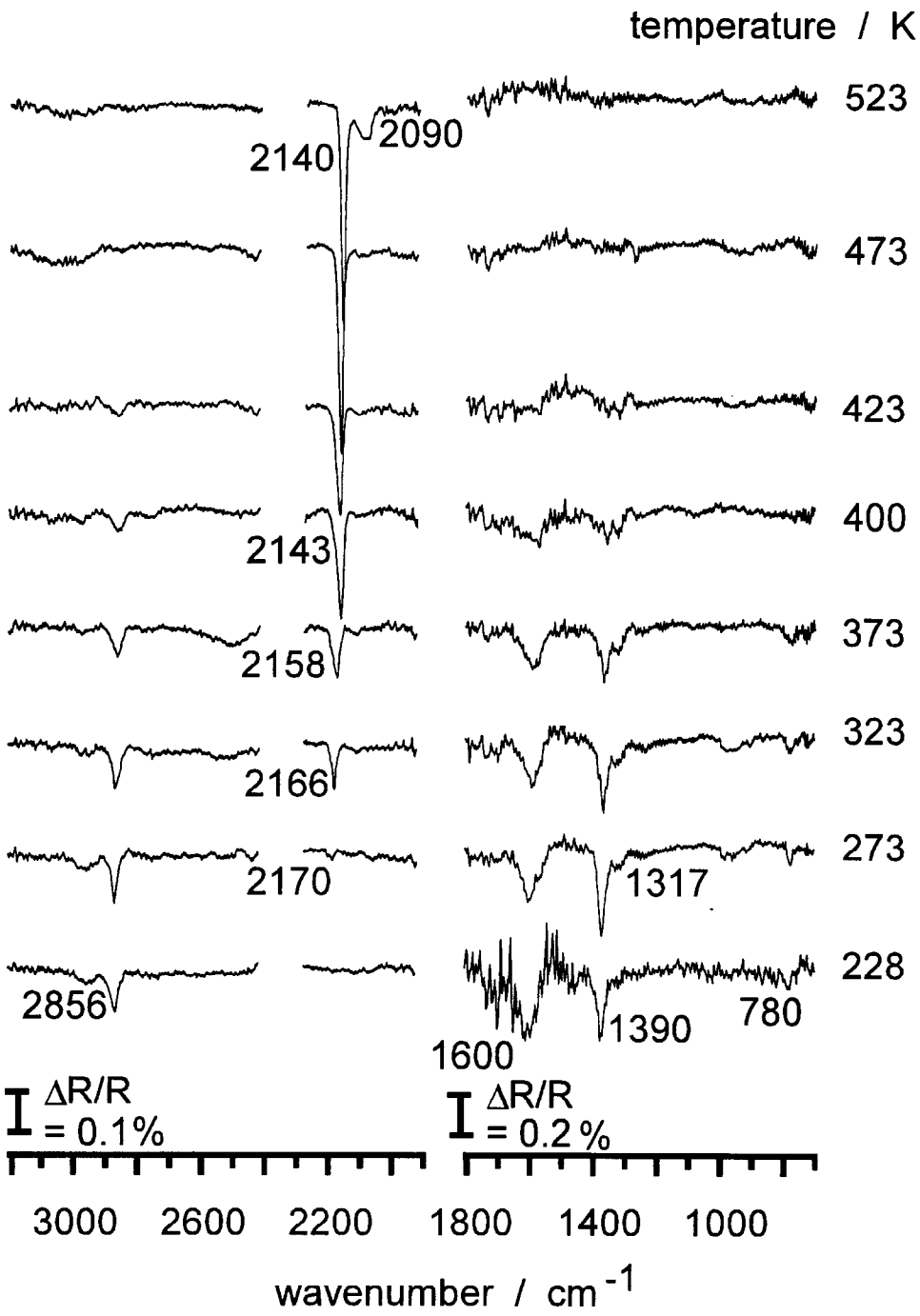

Fig. 4.4. IRA spectra of formate (HCOO) and CO co-adsorbed on NiO(111). The formate covered NiO(111) was first heated to the stated temperatures for a few minutes in vacuum. Then, the CO adsorption to the saturation coverage and the spectral measurement were carried out at 100 K.

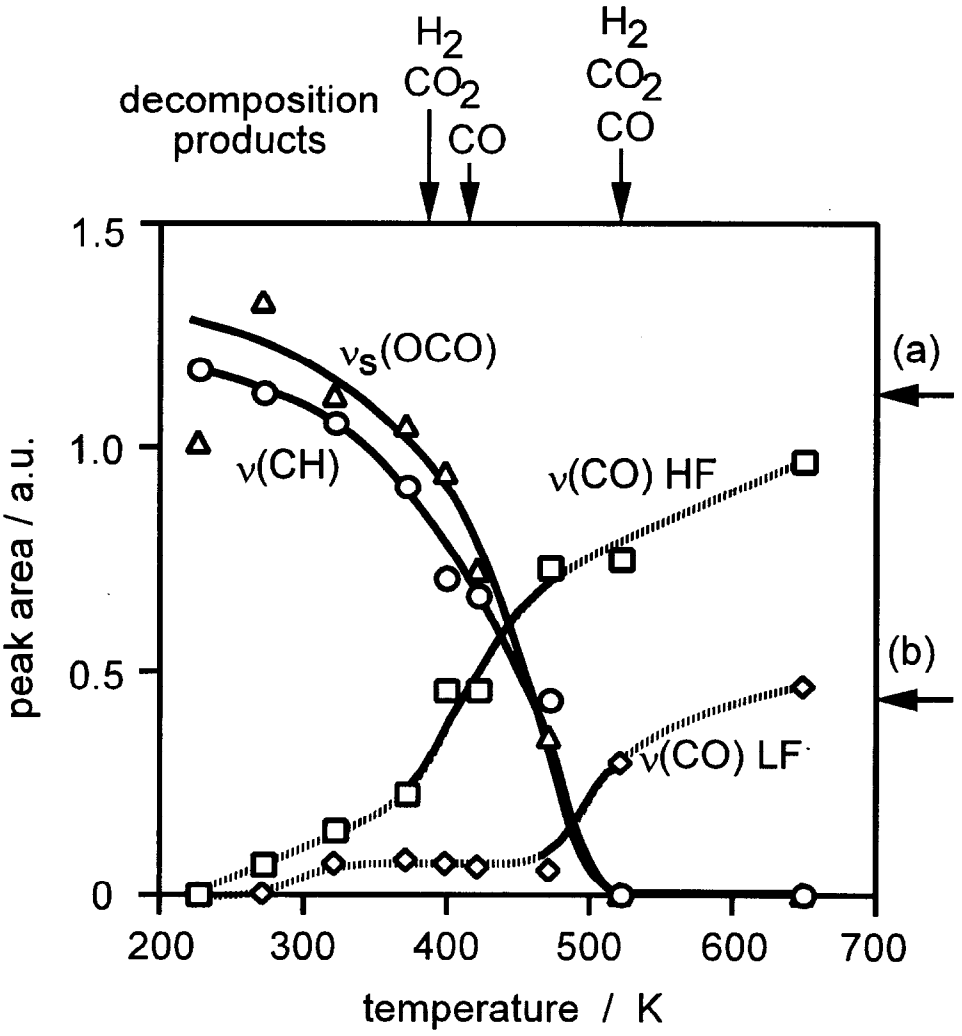

Fig. 4.5. Temperature dependence of the area intensities of the vibrational peaks of formate and CO. The areas were derived from the spectra shown in Fig. 4. The arrows (a) and (b) indicate the area intensities of the band by the CO adsorbed on HF and LF sites, respectively, of the initial surface without the adsorption of formic acid. The desorption peaks of the TPD signals are indicated on the top.

CO molecules did not adsorb. The IRAS bands of the CO appeared for surfaces annealed at and above 273 K. The intensity of the band at 2170 cm^{-1} coming from CO on the HF sites increased by increasing the annealing temperature. The band at 2090 cm^{-1} corresponding to the adsorbed CO on the LF sites gained the intensity when the surface was heated to 523 K. It must be noted that the frequency of adsorbed CO on the HF sites obtained from the formate covered surface at around 300 K is 17 cm^{-1} higher than that on clean NiO(111) when the CO coverage was small. This difference in frequency is considered to be due to interaction between CO and formate. Formate on a surface is regarded as an anionic species and the shift to higher frequency of co-adsorbed CO may be caused by withdrawing of the surface electrons to lessen the back-donation to the $2\pi^*$ state of CO by formate species [19, 20]. The arrows (a) and (b) in Fig. 4.5 indicate the area intensities of the bands by CO adsorbed on the HF and LF sites, respectively, of the initial NiO(111) surface before the adsorption of formic acid. It should be noted that the peak of CO on the HF sites gained drastically intensity at around 400 K but that on the LF sites gained at around 500 K. When the formate-covered surface was heated to 650 K, the CO peaks recovered their initial intensities, indicating that the surface structure was recovered. The feature suggests that the decomposition of formate at 340-415 K took place mainly on the HF sites since CO started to adsorb on the HF sites at this temperature. The decomposition of formate at 520 K, on the other hand, occurred at LF sites. It is thus concluded that the decomposition of formate on the fully-oxidized Ni cation sites on the terraces gave 340-415 K peaks on the TPD signals and those on the less-oxidized Ni sites at 520 K.

4.3.2 Behavior of hydroxyl species (-OD)

It is important to note the role of the surface hydroxyl species during decomposition of formate since a product of water should be originated from surface hydroxyl species. The behavior of hydroxyl species during decomposition of

formate has not been understood because of the low sensitivity of hydroxyl species for IRAS. Moreover, difficulty of detection of water in TPD also interfered with the understanding the reaction path of water production. The use of deuterated formic acid DCOOD enables us to detect the surface hydroxyl species on IRAS by taking advantage of much better signal-to-noise ratio in the O-D stretching region (~2700 cm^{-1}) than that in the O-H stretching region (~3700 cm^{-1}).

Hydroxyl species on NiO(111) were examined first without adsorption of formic acid. IRA spectra of surface hydroxyl species obtained from the dissociative adsorption of heavy water D_2O at the stated temperatures on NiO(111) are shown in Fig. 4.6. At the low adsorption temperature of 163 K, two peaks were observed at 2709 and 2624 cm^{-1} which are assigned to the O-D stretching modes of the dangling and hydrogen-bonded OD groups, respectively of the adsorbed D_2O molecule. In the temperature region between 228 and 550 K, a single peak was observed at 2719-2709 cm^{-1} and is assigned to the O-D stretching mode of the hydroxyl species [21, 22]. The peak position shifted from 2719 to 2709 cm^{-1} on increasing the substrate temperature from 228 K to 550 K, and might be due to the anharmonic coupling with low frequency modes such as the frustrated translation of the hydroxyl groups as suggested for the CO on metal surfaces [23]. The frequency of this peak suggests that the hydroxyl species do not interact with each other through hydrogen-bonding. The peak of the hydroxyl species disappeared at 650 K. The spectrum (a) was obtained after the surface was dosed by D_2O at 500 K and was cooled down to 163 K. A single peak was observed at 2721 cm^{-1}. The frequency shift dependent on the substrate temperature indicates that this peak is assigned to the band of isolated hydroxyl species.

The behavior of surface hydroxyl species produced by the decomposition of formic acid was different from that produced by the adsorption of water. Fig. 4.7 shows IRA spectra of the NiO(111) surface dosed by deuterated formic acid DCOOD in

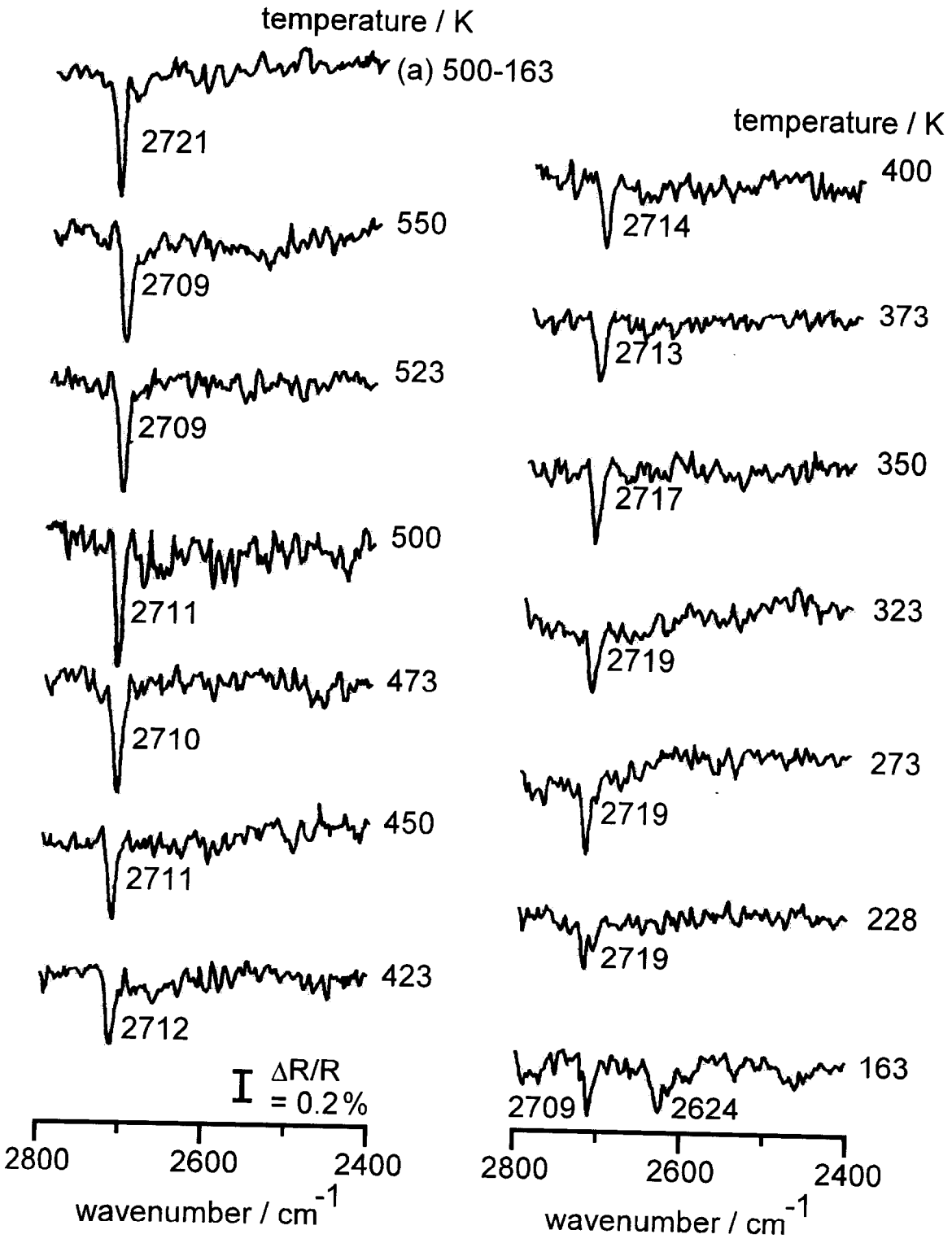

Fig. 4.6. IRA spectra of NiO(111) exposed to 10 L of D_2O at the stated temperatures. The spectrum (a) is obtained after the surface was dosed by D_2O at 500 K and cooled down to 163 K.

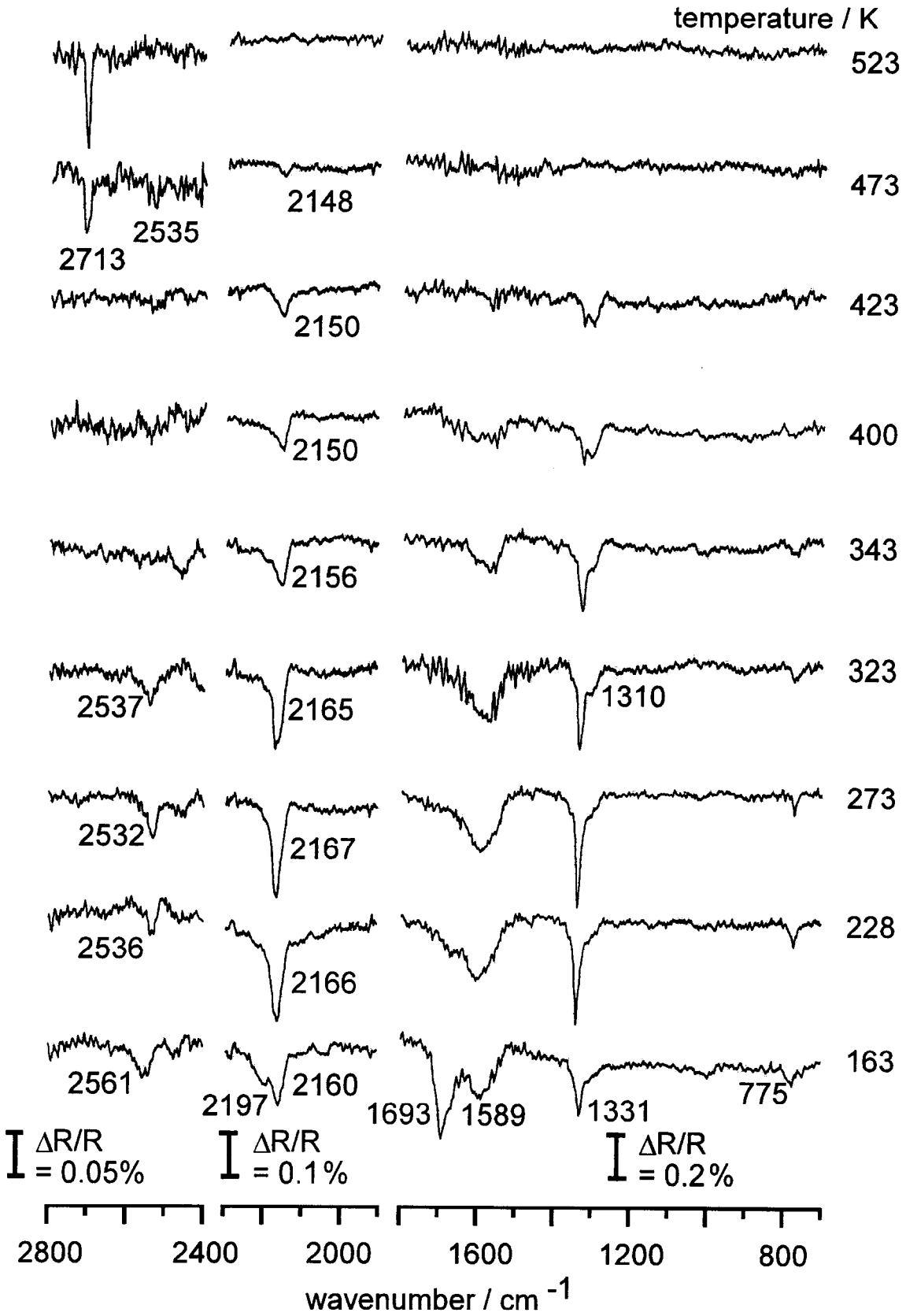

Fig. 4.7. Temperature dependent IRA spectra of formate (DCOO) adsorbed on NiO(111). The surface was exposed to DCOOD (10 L) at 163 K and then heated to the stated temperatures.

the same way as that of Fig. 4.2. The peaks at 2160, 1589, 1331, and 775 cm^{-1} were assigned to the C-D stretching, antisymmetric O-C-O stretching, symmetric O-C-O stretching and in-plane deformation modes of bidentate formate (DCOO-), respectively. A peak was observed at 2536 cm^{-1} at 228-323 K and is assigned to the O-D stretching mode of surface hydroxyl species produced by the dissociation of formic acid to formate. The frequency of 2536 cm^{-1} is by 180 cm^{-1} lower than that of the isolated hydroxyl species from D_2O. This indicates that the present hydroxyl species was perturbed by the co-adsorption of formate through either the hydrogen-bonding or electronic change of the adsorption site by the adsorption of anionic formate on the neighboring sites. The hydroxyl peak disappeared above 323 K and the hydroxyl species possibly desorbed at this temperature as D_2O. In conclusion, we considered that a part of water is produced and desorbs below 343 K by the decomposition of formic acid.

When the surface temperature was raised to 473 K, a new peak appeared at 2713 cm^{-1} and was also assigned to the O-D stretching mode of hydroxyl species. The frequency of the band is same as that of the hydroxyl species formed from D_2O indicating that these hydroxyl species are isolated. This type of hydroxyl species considerably is produced by the decomposition of the formate remaining at higher temperature to give the symmetric O-C-O stretching band at 1317 cm^{-1}. Although the TPD signal of water could not be detected, the IRA spectra clearly proves that there are two origins for the desorption of water by the decomposition of formic acid; one from the formate-perturbed hydroxyl species at around 343 K and the other from isolated hydroxyl species at around 650 K.

TPD spectra of DCOOH-dosed surface was measured to reveal which hydrogen in formic acid is the source for the hydrogen and water production, as shown in Fig. 4.8. The locations of TPD peaks of CO_2 and CO are almost the same as those observed for the HCOOH-dosed surface. It is seen that D_2 was produced from DCOOH but

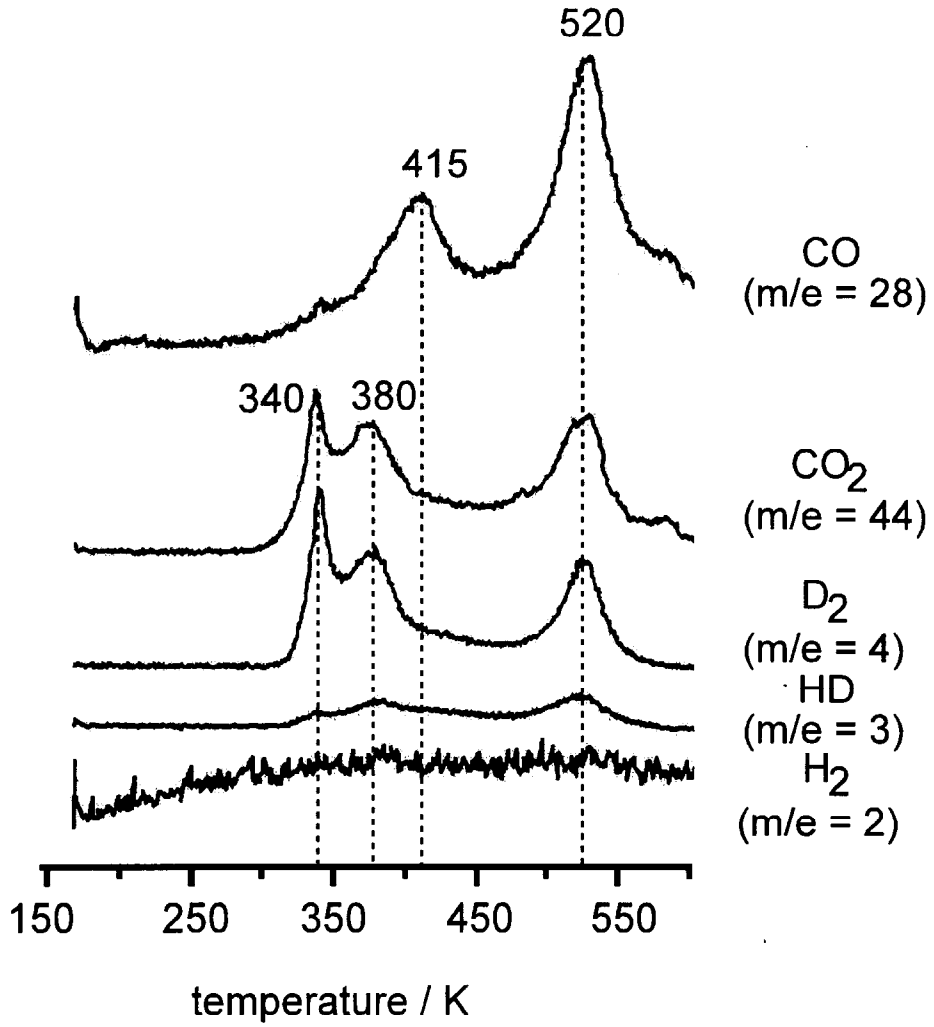

Fig. 4.8. TPD spectra of the DCOOH-dosed on NiO(111) surface. The surface was exposed to 10 L of DCOOH at 163 K.

the signals of H_2 or HD were hardly observable. It clearly indicates that the hydroxyl species produced at the oxygen sites on dissociative adsorption of formic acid desorbed primarily as water but not as hydrogen. It is thus reconfirmed that the disappearance of the IRAS peaks of the hydroxyl species is due to the desorption as water.

Desorption at 343 K of water produced from hydroxyl groups should leave behind an oxygen vacancy. However, the AES ratio of the O/Ni signals remained unchanged after several repetitions of TPD and thus created vacancies were apparently recovered by the oxygen atoms supplied by the further decomposition of formate. As a matter of fact, the change by the desorption of the hydroxyl species was not observed in the CO-probe measurements suggesting that the CO does not adsorb on the oxygen-vacancy sites generated from the desorption of water due possibly to the morphology of the sites or blocking by nearest formate species. We propose the scheme for the decomposition reaction as displayed in Fig. 4.9.

4.3.3 Adsorption of Formic acid on hydroxyl-covered NiO(111)

Next investigated was the adsorption of formic acid on the NiO(111) surface which was precovered by the D_2O-originated OD groups. The surface was prepared by exposing to the 10 L of D_2O vapor at 500 K. This hydroxylation condition is known to produce the largest amount of the isolated hydroxyl species on NiO(111) and disrupt the (2×2) microfacets [5]. Fig. 4.10 shows IRA spectra of formic acid adsorbed on hydroxylated NiO(111) as a function of temperature, where the shown spectra are the ratio spectra divided by those of hydroxylated NiO(111). When the surface was dosed at 163 K, large reduction of the peak intensity, that is the negative peak on the ratio spectra, was observed at 2711 cm^{-1}, and a peak appeared at 2534 cm^{-1} which was assigned to the hydroxyl species perturbed by formate. The intensity of the 2534 cm^{-1} peak was almost twice that observed on clean NiO(111). The feature suggests that the isolated hydroxyl species initially produced on the preparation

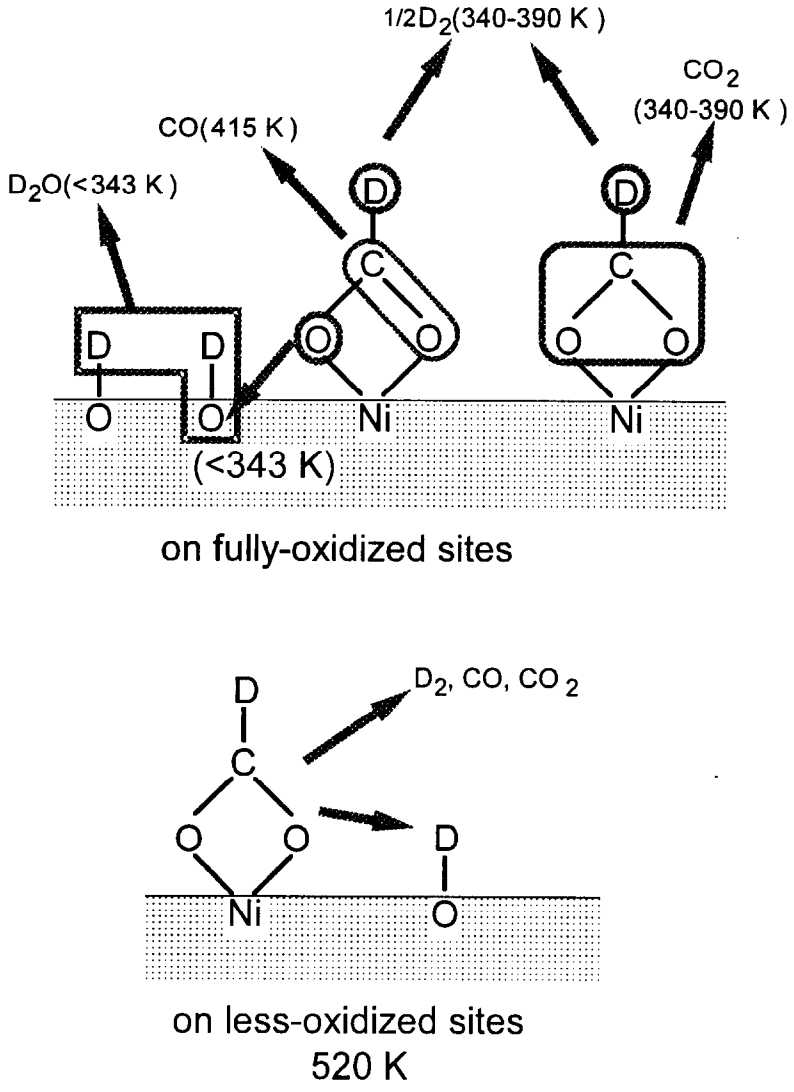

Fig. 4.9. Schematic model for the decomposition of formic acid on NiO(111).

transformed its structure to the hydroxyl species perturbed by formate. This peak disappeared at around 323 K as was the case on clean NiO(111) confirming that the formate-affected hydroxyl species desorbs at around 323 K irrespective of their origin. At the temperature higher than 473 K, the negative peak at 2711 cm^{-1} disappeared indicating that the isolated hydroxyl species was recovered by decomposition of formic acid.

The temperature dependent change of the formate peaks on hydroxylated NiO(111) was not different from that on the clean NiO(111). The intensity ratio of the antisymmetric and symmetric O-C-O stretching bands varies by the tilt angle of formate from the surface normal and the invariance suggest that the tilt angle on hydroxylated NiO(111) was the same as that on clean NiO(111). The formate stood vertical to the surface in the condition of the steady-state-reaction under continuous flow of formic acid [13].

4.4 Conclusion

The findings are summarized as follows.

(1) There are two decomposition temperatures, 340-415 and 520 K, for the formate on NiO(111). The frequency of the CO adsorbed on partially decomposed surface indicated that the decompositions at 340-415 and 520 K took place on the fully-oxidized Ni cation sites and the less-oxidized Ni cation sites, respectively.

(2) The IRAS peaks of surface hydroxyl species (OD) examined during formate decomposition on clean and hydroxylated NiO(111), revealed that , the 2530 cm^{-1} peak of hydroxyl species interacting with formate disappeared at around 323 K indicating that the hydroxyl species desorbs as water. On heating the substrate to 473 K, the isolated hydroxyl species was formed from the decomposition of formate giving the peak at 2711 cm^{-1}. It desorbed at 650 K with further heating.

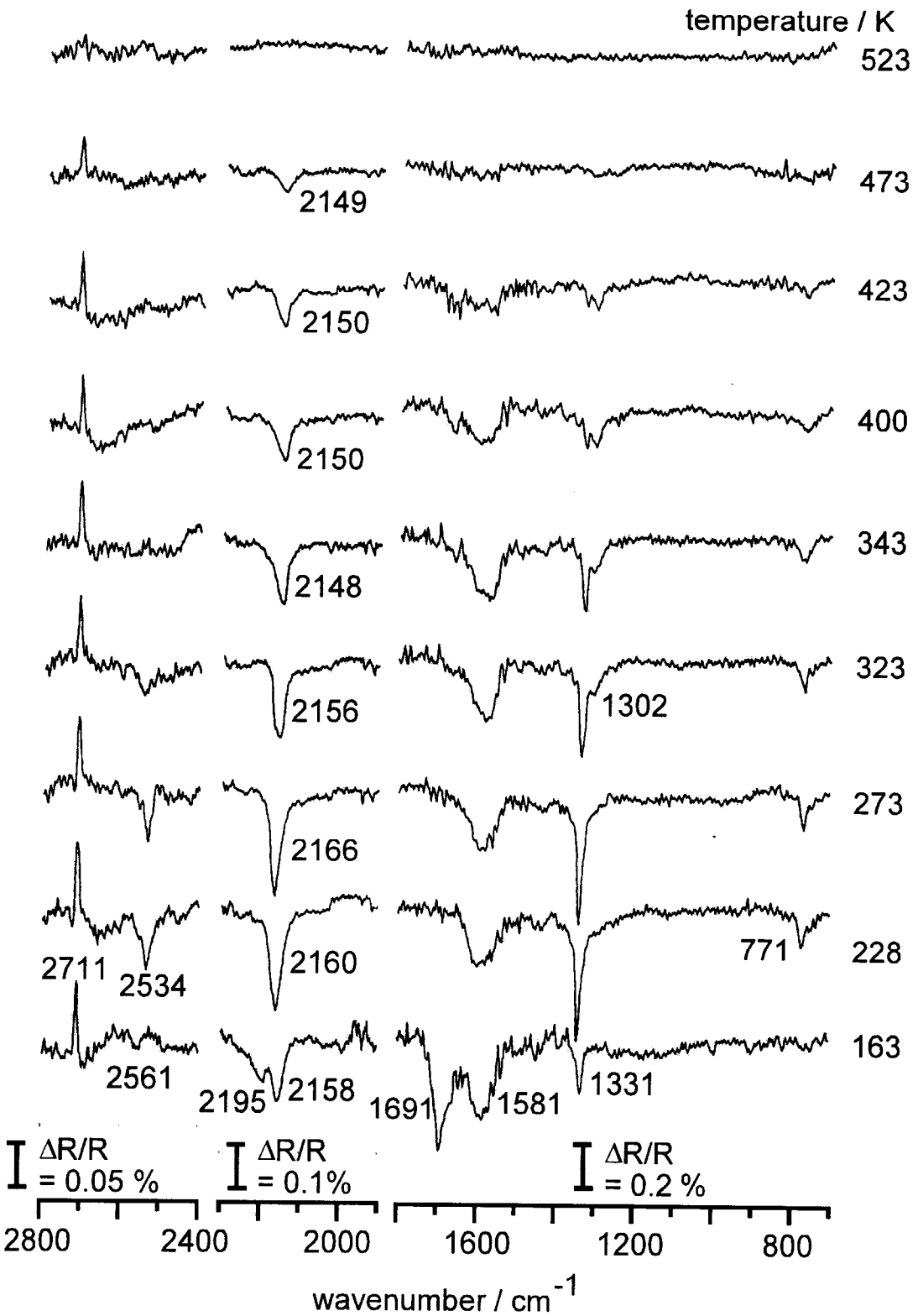

Fig. 4.10. Temperature dependence of IRA spectra of formate adsorbed on hydroxyl (-OD) precovered NiO(111). The surface was exposed to 10 L of D_2O at 500 K to produce isolated hydroxyl species. The hydroxyl covered NiO(111) was then exposed to the 10 L of DCOOD at 163 K and then heated to the stated temperatures. All spectra were normalized against the spectrum of the initial hydroxyl covered NiO(111) at 500 K

References

[1] V. E. Henrich and P. A. Cox, The Surface Science of Metal Oxides, 1st ed. (Cambridge U.P., New York, 1994).

[2] H. Kuhlenbeck, G. Odšrfer, R. Jaeger, G. Illing, M. Menges, Th. Mull, H.-J. Freund, M. Pohlchen, V. Staemmler, S. Witzel, C. Scharfshwerdt, K. Wennemann, T. Liedtke and M. Neumann, Phys,Rev. B. 43 (1991) 1969.

[3] K. Wulser and M. A. Langell, Catal. Lett. 15 (1992) 39.

[4] C. M. Troung, M. C. Wu, D. W. Goodman, J. Phys. Chem. 97 (1992) 9447.

[5] F. Rohr, K. Wirth, J. Libuda, D. Cappus, M. B. Öumer and H.-J. Freund, Surf. Sci. 315 (1994) L977.

[6] C. A. Ventrice, Th. Bertrams, H. Hannemann, A. Brodde and H. Neddermeyer, Phys. Rev. B49 (1994) 5773.

[7] C. Xu and D. W. J. Goodman, Chem. Soc. Faraday Trans. 91 (1995) 3709.

[8] C. Xu and D. W. Goodman, Catal. Today. 28 (1996) 297.

[9] M. Schönnenbeck, D. Cappus, J. Klinkmann, H.-J. Freund L. G. M. Petterson and P. S. Bagus, Surf.Sci. 347 (1996) 337.

[10] A. Bandara, J. Kubota, A. Wada, K. Domen and C. Hirose, Surf. Sci. 364 (1996) L580.

[11] A. Bandara, J. Kubota, A. Wada, K. Domen and C. Hirose, J. Phy. Chem. 100 (1996) 14962.

[12] J. Kubota, A. Bandara, A. Wada, K. Domen and C. Hirose, Surf. Sci. 368 (1996) 361.

[13] A. Bandara, J. Kubota, A. Wada, K. Domen and C Hirose, J. Phy. Chem. B. 101 (1997) 361.

[14] M. A. Henderson, J. Phys. Chem. 99 (1995) 12919.

[15] M.-C Wu and D. W. Goodman, Catal. Lett. 15 (1992) 1.

[16] W. T. Petrie and J. M. Vohs, Surf. Sci. 245 (1991) 315.

[17] P. A. Dilara and J. M. Vohs. J. Phys. Chem. 97 (1993) 12919.

[18] J. Yoshinobu, T. H. Ballinger, Z. Xu, H. J. JŠnsch, M. I. Zaki, J. Xu, Jr. and J. T. Yates, Surf. Sci. 225 (1991) 295.

[19] M. A. Zaki and H. Knšzinger, J.Catal. 119 (1989) 311.

[20] S. M. Vesecky, X. Xu and D. W. Goodman, J. Vac. Sci Technol. A12 (1994) 2114.

[21] H. E. Sanders, P. Gardner, D. A. King and M. A. Morris, Surf. Sci. 304 (1994) 159.

[22] J. N. Kondo, T. Yuzawa, J. Kubota, K. Domen and C Hirose, Surf. Sci. 343 (1995) 71.

[23] R. J. H. Clark and R. E. Hester, Spectroscopy of Surfaces (John Wiley & Sons Ltd., New York, 1988).

5 Adsorption structures of carbon dioxide on NiO(111) and hydroxylated NiO(111) studied by IRAS

Abstract

The adsorption of CO_2 on NiO(111)/Ni(111) and OD/NiO(111)/Ni(111) was studied by infrared reflection absorption spectroscopy (IRAS). When the surfaces were exposed to CO_2 at 123 K, peaks of adsorbates appeared at 1263 and 910 cm^{-1} on NiO(111), while a peak appeared at 1267 cm^{-1} on OD/NiO(111). The peaks at 1263 (or 1267) and 910 cm^{-1} could be assigned to the symmetric O-C-O stretching and out of plane deformation modes of monodentate carbonate, respectively. The much smaller deformation peaks in the spectra of carbonate on OD/NiO(111) indicates that the molecular axis is perpendicular to the surface. Furthermore, the change of the molecular geometry of CO_2 was attributed to the OD-induced change of surface structure of NiO(111), which was indicated by the weak perturbation of OD bands with the adsorbed CO_2.

5.1 Introduction

One of the powerful approaches for understanding the catalysis of oxides is the use of single-crystal oxide surfaces as models of the catalysts [1]. However, some single-crystal oxides are not suitable for observation by electron spectroscopies and infrared reflection absorption spectroscopy (IRAS) because of the problems of the low electroconductivity and low infrared reflectance, and some have the difficulty of the preparation. The preparation and the use of epitaxially grown films of oxides on metal substrates do not suffer from these problems and have been used for the study on oxide surfaces in the past several years [2-15].

NiO single crystal films on single crystal metal substrates are typical examples of epitaxial films which have been applied to the study of adsorption of molecules by several methods [4, 5, 7-15]. The NiO(111) surface is regarded as being more active than NiO(100) for chemical reactions because Ni cations at the surface have lower coordination number [8]. A bare NiO(111) surface has a (2×2) structure with oxygen termination in vacuum, and trigonal pyramids of the microfacets are disposed in order [5, 6, 9]. When the hydroxyl species were formed on (2×2)-NiO(111) by the dissociative adsorption of water, the low-energy electron diffraction (LEED) pattern changed into the (1×1) pattern and the (2×2) trigonal microfacets were disrupted [5].

The molecularly adsorbed CO_2 has been observed during the oxidation of CO and the decomposition or reduction of CO_2 on the surfaces of powder, evaporated films, supported catalysts [16], single-crystals, or single-crystal films [17]. CO_2 has often been used for probing the basic sites of oxide surfaces, where several types of carbonate species (CO_3^{2-}) are formed [18]. On the other hand, the adsorption of CO_2 on defect sites of an oxygen-modified Ni(111) surface results in dissociative adsorption [19]. Therefore, CO_2 is regarded as suitable for characterization of both the basic and the defect sites of oxide surfaces. We have studied the formation and property of OD species on the NiO(111) surface [20]. In this study, both the NiO(111) and the OD/NiO(111) surfaces are characterized and compared by IRA spectra of adsorbed CO_2, and the effect and the role of OD species are discussed.

5.2 Experimental

The experiments were carried out in an ultra-high vacuum chamber evacuated to 10^{-8} Pa as described in a previous paper [11]. 5-10 monolayers of the NiO film were grown on the Ni(111) surface by the cycles of exposure to 1000 L (1 L = 10^{-6} Torr s, 1 Torr = 133 Pa) of oxygen gas at 570 K and annealing at 650 K. The hexagonal LEED pattern which indicated a (2×2)-NiO(111) surface structure was observed on the

surface prepared this way. The OD/NiO(111) surface was prepared by exposing the NiO(111) to 10 L of D_2O and 500 K [15]. IRA spectra were acquired using a JEOL JIR-100 Fourier transform infrared spectrometer (FTIR) equipped with an InSb/MCT composite detector. The resolution was 4 cm^{-1} and the signals were averaged over 512 scans. The values of exposure were calculated from the pressures without correction and calibration to the real surface pressure.

5.3 Results and discussion

The temperature programmed desorption (TPD) spectra of CO_2 (m/e=44) from both the NiO(111) and the OD/NiO(111) surfaces showed a broad peak of CO_2 at 160 K with tailing to 250 K, and no peak of CO (m/e=28) was observed except for the fragment of CO_2. The amount of surface oxygen and the long range structure of the surfaces did not change after several repetitions of TPD of CO_2 as determined by AES and LEED measurements. This indicates that the adsorbed CO_2 on NiO(111) and OD/NiO(111) desorbs as CO_2 around 160 K. On an oxygen-modified Ni(111) surface, CO_2 desorbs around 395 K from anion vacant sites, and the CO produced by the dissociation of CO_2 as well as CO_2 itself desorbed at around 645 K from O^- sites during the disintegration of the oxide surface [19]. However, the absence of CO formation in the present study indicates that this surface does not have such anion vacancies or O^- sites.

Fig. 5.1 (a) and (b) show the IRA spectra of CO_2 adsorbed on NiO(111) with increasing exposure at 123 K and with increasing temperature of the 5 L exposed surface, respectively. Two peaks appeared at 1263 and 906 cm^{-1} and the intensities of both peaks increased with increasing exposure at 123 K and saturated at 0.5 L. When the CO_2-saturated surface was heated to the stated temperature, the peaks at 1261 and 908 cm^{-1} decreased in intensity with increasing temperature and disappeared completely at 248 K. The two peaks at 1263 (1261) and 906 (908) cm^{-1} behaved in

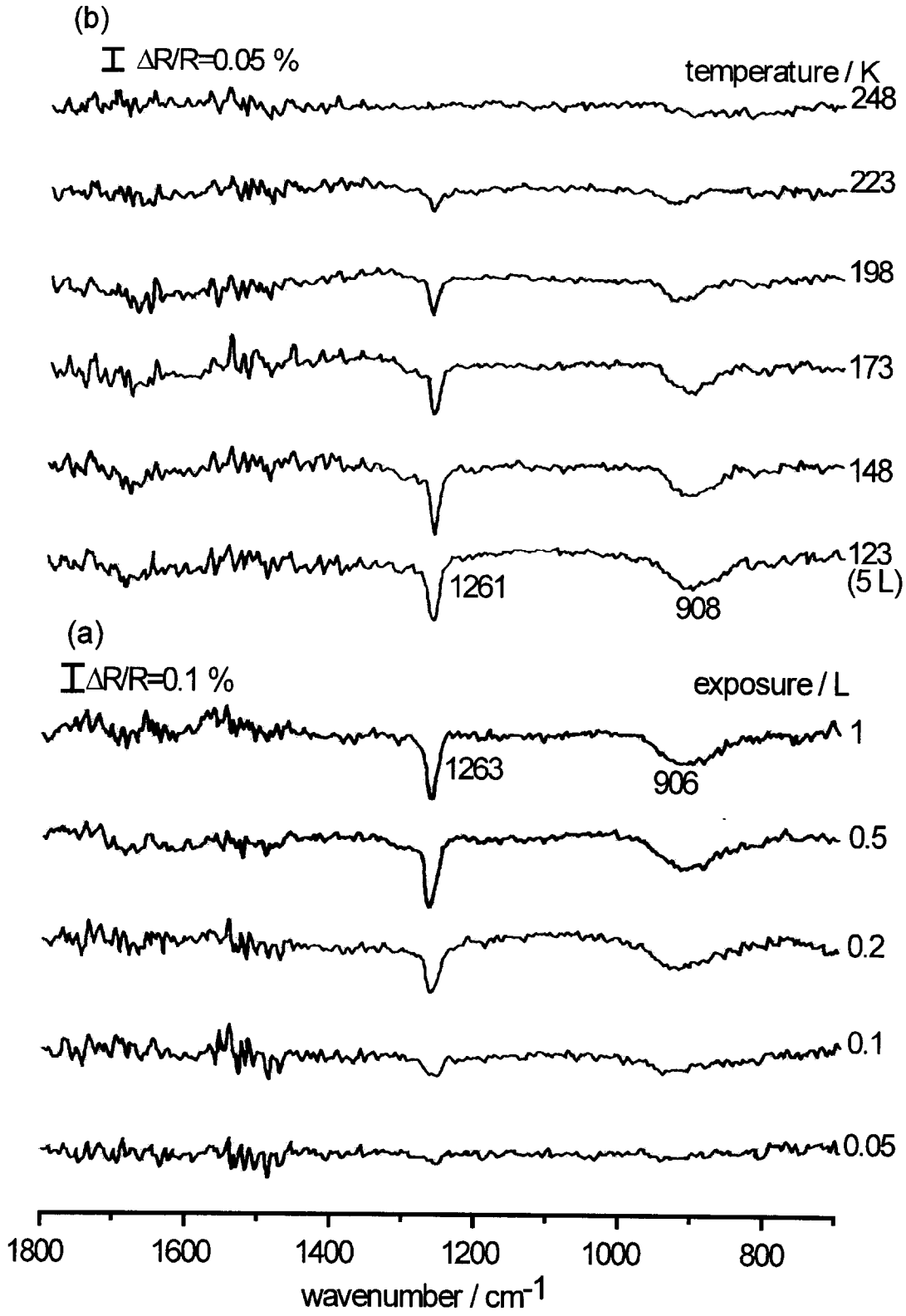

Fig. 5.1. IRA spectra of adsorbed CO_2 on NiO(111) (a) for various exposures at 123 K (lower half), and (b) at various temperatures of the 5 L exposed surface (upper half). The surfaces for the upper half were prepared at 123 K and heated to the stated temperatures after the exposure.

the same manner with changing coverage and temperature, so that both peaks were attributed to the same species.

The models of the adsorbed CO_2 on metals and oxides are illustrated in Fig. 5.2, and the frequencies of the CO_2-based species reported previously are listed in Table 5.1. The chemisorbed species originated from the adsorption of CO_2 are classified into two categories: carbonate (CO_3^{2-}), which is produced by the reaction with an oxygen atom on the surface, and chemisorbed CO_2. Three types of configuration are known for the carbonates as depicted in Fig. 5.2. By comparing the frequencies of the observed peaks with references, the presently observed species was regarded as either the bidentate or the monodentate carbonate (Table 5.1). In the case of the bidentate carbonate, the peaks at 1263 and 906 cm^{-1} can be assigned to the asymmetric O-C-O stretching and out of plane deformation modes, and the symmetric O-C-O stretching band is absent on the spectra. In this case, the molecular axis of bidentate carbonate should be parallel to the surface. We consider that this assignment is unlikely and prefer the assignment of the peaks at 1263 and 906 cm^{-1} to the symmetric O-C-O stretching and the out of plane deformation modes of monodentate carbonate, respectively. The typical frequencies of vibrational modes of monodentate carbonates are as 1080-1040 cm^{-1} for the C-O stretching mode and 880-850 cm^{-1} for the out-of-plane deformation mode [16]. The comparison with the values in the reference also suggested that the wavenumber of 910 cm^{-1} could be assigned to the out-of-plane deformation mode. In the monodentate structure, the asymmetric O-C-O stretching mode is inactive to IRAS and the transition dipole moment of this mode is parallel to the surface. Because of the appearance of the out of plane deformation band, the molecular axis of the carbonate is thus tilted to the surface while keeping the transition dipole moment of the asymmetric O-C-O stretching mode parallel to the surface. It is considered that the tilting of the carbonate reflects the inclined plane of the NiO(111) surface with (2×2) microfacets. It remains the possibility that

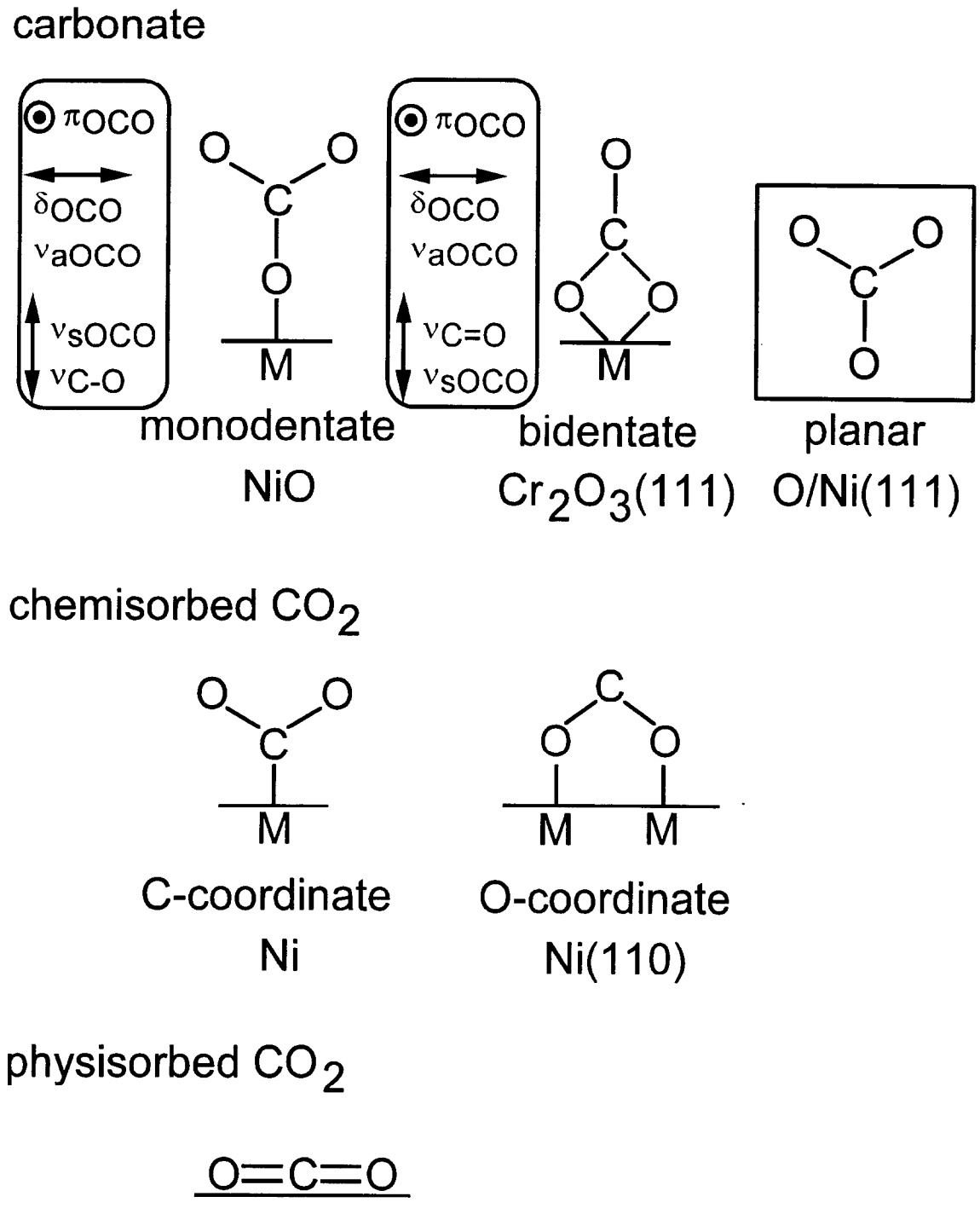

Fig. 5.2. Schematic drawings of the species on metal and oxide surfaces produced by the adsorption of CO_2. The orientations of the transition dipole moments of monodentate and bidentate carbonate are also indicated.

Table 5.1. The wavenumbers of the peak assigned to the mode of CO_3^{2-} and CO_2

system	NiO(111)	$[Co(NH_3)_5CO_3]Br$	$[Co(NH_3)_4CO_3]Cl$	O/Ag(110)	
method	IRAS	IR	IR	HREELS	IR
δOCO	-	756	673	660/1280	667/1286
π	906	850	834		
νC-O	-	1070			
νsO-C-O	1260	1373	1031	1390	1388
νaO-C-O	-	1453	1265	2350	2349
νC=O			1593		
assignment	CO_3^{2-}	CO_3^{2-}	CO_3^{2-}	CO_2	CO_2
configration	monodentate	monodentate	bidentate	physisorbed	gas
reference	this work	[16]	[16]	[21]	[21]

system	NiO	$Cr_2O_3(111)$	O/NiO(100)	Ni	Ni(110)
method	IR	HREELS	HREELS	IR	HREELS
δOCO	-	-			750
π	-	920	850		
νC-O	-		1050		
νsO-C-O	1390	1035	1330	1410	1130
νaO-C-O	1640	1285	-	1640	1620
νC=O		1630			
assignment	CO_3^{2-}	CO_3^{2-}	CO_3^{2-}	CO_2	$CO_2^{\delta-}$
configration	monodentate	bidentate	planar	C-coordinate	O-coordinate
reference	[16]	[22]	[23]	[16]	[24]

δ_{O-C-O}: inplane deformation; π: out of plane deformation: ν_{C-O}: C-O stretching; ν_{sO-C-O}: symmetric O-C-O stretching; ν_{aO-C-O}: asymmetric O-C-O stretching; $\nu_{C=O}$: C=O stretching.

the peak at 910 cm^{-1} is due to the C-O stretching band. We, however, believe from the result of the next experiment that the absorption coefficient of the C-O stretching could be too small for the peak to be observed. The peak at 910 cm^{-1} was broader than the peak at 1260 cm^{-1}. It is probably due to the inhomogeneous broadening since the out of plane deformation vibration is more affected by the inhomogeneity of the surface than the symmetric O-C-O stretching vibration which is located far from the surface.

Fig. 5. 3 (a) and (b) show the IRA spectra of the CO_2 on OD/NiO(111) measured at various exposures at 123 K and temperature-dependent IRA spectra of OD/NiO(111) after the exposure to 5 L of CO_2 at 123 K, respectively. The peak at 2721 cm^{-1} was assigned to the O-D stretching mode of the isolated hydroxyl species [15]. The frequency and sharpness of the peak clearly show that the hydroxyl species was isolated and not hydrogen-bonded. It is also suggested from the frequency of the O-D stretching mode of hydroxyl species that the hydroxyl groups adsorb on the three-fold hollow sites [20].

When CO_2 was introduced onto the OD/NiO(111) surface, a peak at 1267 cm^{-1} appeared. The intensity of the peak increased with increasing exposure and saturated at 0.2 L, while the OD band did not shift but slightly broadened with increasing the exposure of CO_2. This indicates that the adsorbed CO_2 does not strongly interact with the hydroxyl species through the hydrogen-bonding. As for the temperature-dependence of the IRA spectra, the peak at 1267 cm^{-1} weakened at higher temperature and disappeared at 248 K. This peak was assigned to the symmetric O-C-O stretching mode of the monodentate carbonate because of the similarities of the frequency and desorption temperature to those observed on NiO(111). It should be noted that the peak assigned to the out of plane deformation mode is much weaker in the spectra of the OD/NiO(111) surface. The molecular axis of the carbonate on OD/NiO(111) is thus considered to be oriented normal to the surface. The change of

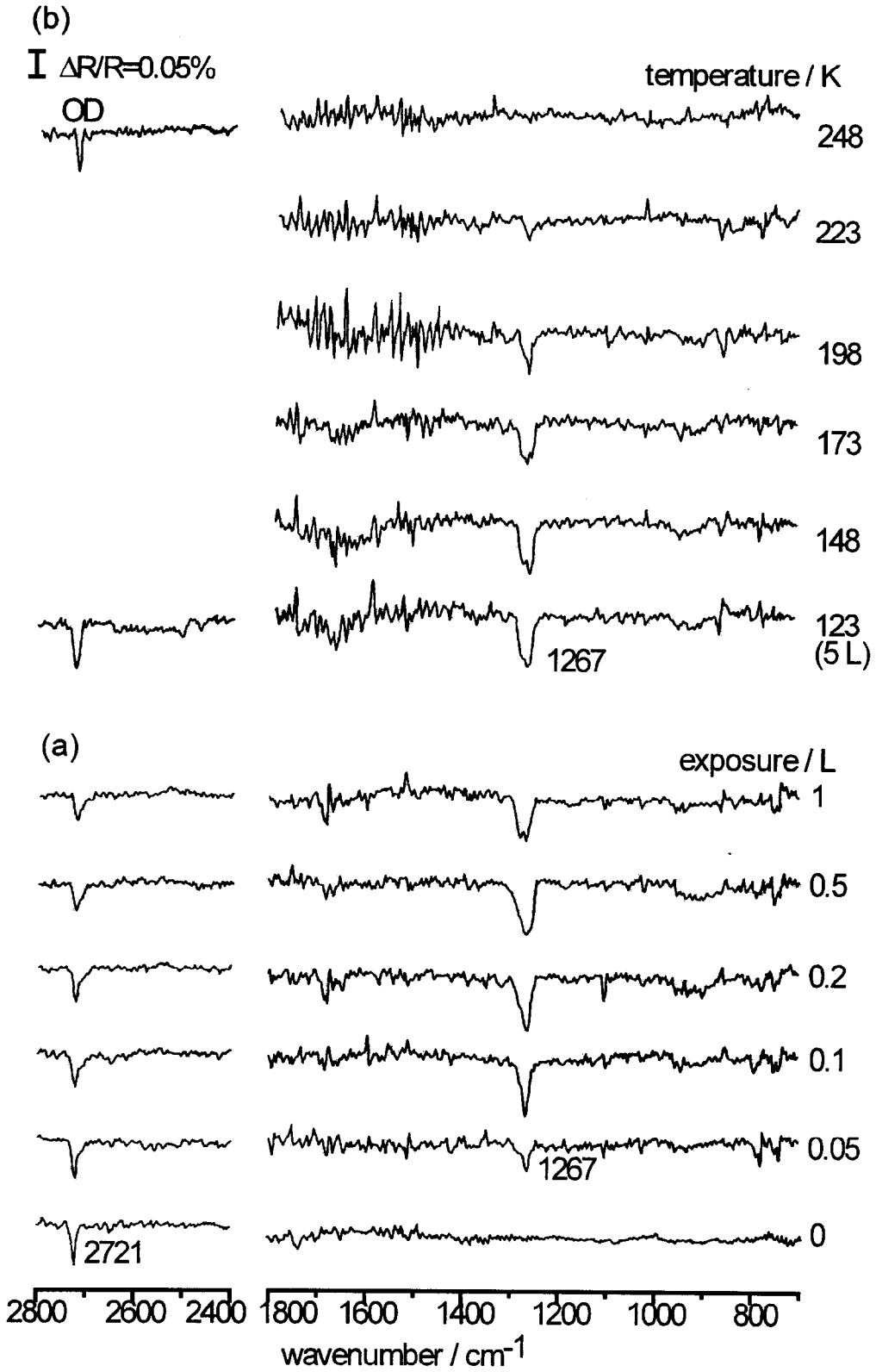

Fig. 5.3. IRA spectra of adsorbed CO_2 on OD/NiO(111) (a) with various exposures at 123 K (lower half) and (b) at various temperatures of the 5 L exposed surface (upper half). The surfaces for the upper half were prepared at 123 K and heated to the stated temperatures after the exposure.

the orientation of the carbonate from the NiO(111) to the OD/NiO(111) surfaces is not due to the direct interaction with hydroxyl groups because the desorption temperature of CO_2 is the same, and because no noticeable change occurred in the frequency of the stretching band of the hydroxyl species. The dissociative adsorption of water is known to change the long-range structure as based on the change of the LEED pattern from (2×2) into (1×1)[5]. The change of the orientation would reflect the disruption of the (2×2) microfacets by hydroxyl species. A broad and small peak for OD/NiO(111) was observed at 910 cm^{-1}. We suspect that an OD/NiO(111) surface has some defect sites and some tilted carbonate was observed on the defect sites.

Two adsorption sites of CO_2 on (2×2)-NiO(111) are conceivable. One is the O-terminated sites [11] and the other is the Ni cation sites with O-adatoms. Some oxygen adatoms could be present on the surface and they react with CO_2 adsorbs to form carbonate. In both cases, we think either orientation of the carbonate standing vertical or tilting cannot be excluded reasonably.

Comparing the spectra for two surfaces, we can reconfirm our assignment of the carbonate bands. The transition dipole moments of the symmetric O-C-O stretching and the C-O stretching modes of monodentate carbonate have the same direction, while that of the out of plane deformation is perpendicular to this direction. It means that the monodentate carbonate should show the peaks of the symmetric O-C-O stretching and the C-O stretching modes at the same time, and the intensity of the out of plane deformation band reflects the orientation of the carbonate. The peak at 910 cm^{-1} for OD/NiO(111) is much weaker and broader than that for NiO(111). We prefer the explanation that the peak at 910 cm^{-1} is assigned to the out of plane deformation band; the change of the intensity of this peak is due to the change of the orientation of carbonate and the absence of the stretching mode is due to the small absorption coefficient. It is conceivable as one possibility that the peak at 910 cm^{-1} is assigned

to the C-O stretching band and the change of this peak intensity is due to the some physical interaction of carbonate with hydroxyl groups only for the C-O stretching band. The interaction between carbonate and hydroxyl groups, however, must be small since the hydroxyl peak was little perturbed by the production of carbonate.

5.4 Conclusion

We have studied the adsorption of CO_2 on bare and hydroxylated NiO(111) surfaces using IRAS. The symmetric O-C-O stretching (1263 cm^{-1}) and the out of plane deformation (906 cm^{-1}) bands of monodentate carbonate were observed on NiO(111) but the later band is much weaker on hydroxylated NiO(111). Therefore, the monodentate carbonate was tilted away from the surface normal on NiO(111) but was oriented along the surface normal on OD/NiO(111). The absence of strong interaction between hydroxyl species and carbonate and the similarity of the desorption temperature around 248 K between both surfaces show that hydroxyl species does not directly affect the structure of carbonate. It is considered that the formation of the hydroxyl species changes the structure of microfacets on NiO(111) leading to the difference of the orientations of monodentate carbonate between NiO(111) and OD/NiO(111)

References

[1] V. E. Henrich and P. A. Cox, (The Surface Science of Metal Oxides, 1st ed. ,Cambridge U.P., New York, 1994)

[2] H. Kuhlenberg, G. Odorfer, R. Jaeger, G. Illing, M. Munges, Th. Mull, H.-J. Freund, M. Pohlchen, V. Staemmler, S. Witzel, C. Scharafshwerdt, K. Wennemann T. Liedtke and M.Neumann, Phys. Rev. B43 (1991) 1969.

[3] K. Wulser and M. A. Langell, Catal. Lett. 15 (1992) 39.

[4] C. M. Troung, M. C. Wu and D. W. Goodman, J. Phys. Chem. 97 (1992) 9447.

[5] F. Rohr, K. Wirth, J. Libuda, D. Cappus, M. Böumer and H.-J. Freund, Surf. Sci. 315 (1994) L977.

[6] C. A. Ventrice, Th. Bertrams, H. Hannemann, A. Brodde and H. Neddermeyer, Phys. Rev. B49 (1994) 5773.

[7] C. Xu and D. W. Goodman, J. Chem. Soc. Faraday Trans. 91 (1995) 3709.

[8] C. Xu and D. W. Goodman, Catal. Today. 28 (1996) 297.

[9] M. Schonneback, D. Cappus, J. Klinkmann, H.-J. Freund, L. G. M. Petterson and P. S. Bagus, Surf. Sci. 347 (1996) 337.

[10] A. Bandara, J. Kubota, A. Wada, K. Domen and C. Hirose, Surf. Sci. 364 (1996) L580.

[11] A. Bandara, J. Kubota, A. Wada, K. Domen, C. Hirose, J. Phys. Chem. 100 (1996) 14962.

[12] J. Kubota, A. Bandara, A. Wada, K. Domen and C. Hirose, Surf. Sci. 368 (1996) 361.

[13] A. Bandara, J. Kubota, A. Wada, K. Domen and C. Hirose, J. Phys. Chem. B101 (1997) 361.

[14] D. W. Goodman, J. Vac. Sci. Technol. A 14 (1996) 1526

[15] T. Matsumoto, A. Bandara, J. Kubota, C. Hirose and K. Domen, J. Phys. Chem. B102 (1998) 2979.

[16] L. H. Little, (Infrared Spectra of Adsorbed Species, Willmer Brothers Ltd., Britain, 1966).

[17] H.-J. Freunt and M. W. Roberts, Surf. Sci. Rep. 25 (1996) 225.

[18] Lavelley, J. C. Catal. Today. 27 (1996) 377, and the reference therein.

[19] D. E. A. Gordon and R. M. Lambert, Surf. Sci. 287/288 (1993) 114.

[20] J. N. Kondo, T. Yuzawa, J. Kubota, K. Domen and C. Hirose, Surf. Sci. 343 (1995) 71.

[21] E. M. Stuve, R. J. Madix and B. A. Sexton, Chem. Phys. Letters, 89 (1982) 48.

[22] H. Kuhlenbeck, C. Xu, M. Dillmann, M. Haßel, B. Adam, D. Ehrlich, S. Wohlrab, H.-J. Freund, U. A. Ditzinger, M. Neddermayer, M. Neuber, M. Neumann and Ber. Bunsenges. Phys. Chem. 96 (1992) 15.

[23] R. J. Behn and C. R. Brundle, Surf. Sci. 255 (1991) 327.

[24] B. Bartos, H.-J. Freund, H. Kuhlenbeck, M. Neumann, H. Linder and K. Müller, Surf. Sci. 179 (1987) 59.

6 STM studies of oxygen adsorption on Cu(111)

Abstract

The adsorption of O_2 on Cu(111) at room temperature has been investigated by scanning tunneling microscopy (STM) and low energy electron diffraction (LEED). Adsorption of oxygen leads to formation of a surface oxide by incorporation of Cu atoms from step edges and terraces. This process is most rapid along the close packed direction of the surface and leads to mesoscopic changes in surface morphology. Three characteristic features were observed during the initial stage of adsorption; dark fringes along the Cu(111) step edges, dark domains within the Cu(111) terrace, and rather mobile light patches on top of the Cu terraces. Within these regions atomic scale features could be imaged and the structure related to that of Cu_2O. The dark fringes and dark domains grew slowly in oxygen, whereas the bright patches only became visible when gas-phase O_2 was evacuated.

STM observation at elevated temperatures indicates mobilization and rearrangement of surface features formed during room temperature adsorption. O/Cu(111) surfaces annealed at 473-623 K indicated a well ordered ($\sqrt{73}$ R5.8°× $\sqrt{21}$ R-10.9°) lattice structure ('44'-structure) on the terraces which was also confirmed by LEED. Annealing up to 723 K exhibited slight disordering of this lattice structure presumably due to inter-diffusion of O and Cu atoms with the bulk. The mesoscopic process of oxygen adsorption onto the clean Cu(111) surface was investigated at elevated temperature by scanning tunnelling microscopy (STM). The reaction of the surface maintained at temperatures between 373 and 773 K was investigated for oxygen pressures in the 10^{-5}-10^{-3} Pa range. The oxidized surface formed at 373 K was largely disordered with only small areas of the '44'-structure

($\sqrt{73}$R5.8°×$\sqrt{21}$R-10.9°). Well-ordered adlattices of the '44'-structure were formed upon O_2 exposure at 473 K. Such surfaces could be converted to the '29'-structure ($\sqrt{13}$R46.1°×7R-21.8°) by annealing at 673 K in vacuum. On the basis of the STM images we propose a new model for the "29" structure. Annealing at higher temperatures (~773 K) retrieved the '44'-structure in small domains on a disordered background. Disordered oxide surfaces which were produced at room temperature and annealed at 723 K can be ordered into the '44'-structure by O_2 exposure and heating at 623 K.

6.1 Introduction

Scanning tunneling microscopy (STM) has been applied to study oxygen adsorption on Cu(110) and Cu(100) surfaces previously. Well-ordered oxide films, (2×1)O-Cu(110), *c*(6×2)O-Cu(110) [1-5], *c*(2×2)O-Cu(100), (2$\sqrt{2}$ ×2)*R*45°-Cu(100) [6] are formed on these Cu single-crystal surfaces. These structures and the processes of oxide formation have been examined in some detail. Many catalytic model reactions have also been investigated on these surfaces; these include the partial oxidation of methanol [7-21] and alkenes [22, 23], the decomposition of formic acid [24-31], and the oxidation of formaldehyde [32].

The (111) surface of Cu is considered to be the most stable in terms of surface coordination, and the reactions on oxidized Cu(111) surface have been reported less than those on other crystallographic planes partly because this surface is relatively unreactive. Many researchers have observed that Cu oxide films can be formed epitaxially on Cu(111) surfaces by exposure to O_2 with subsequent annealing. The formation of Cu_2O thin films having the structure of Cu_2O on Cu(111) are frequently reported to be well-ordered [33-35], but many other types of ordered structures formed by oxidation elevated temperature have also been reported [36-45]. Some researchers reported that only disordered structures were formed on Cu(111) by oxidation, not only

at room temperature but also even at elevated temperatures [46-49]. This diversity of surface structures has been hindering researchers from examining reactions on the Cu(111) surface. Site specific and mechanistic information on the Cu(111) oxidation is necessary in order to better understand catalysis on the Cu surfaces.

It is advantageous to prepare well-ordered flat surfaces in order to gain an understanding of chemical reactions occurring on these surfaces on the nanoscale. A series of well-ordered oxidized Cu(111) surfaces can be produced, however, at elevated temperatures [42-44]. STM and low-energy electron diffraction (LEED) reveals that the ordered '29'-($\sqrt{13}$ R46.1°×7R-21.8°) and '44'- ($\sqrt{73}$ R5.8°× $\sqrt{21}$ R-10.9°) structures are produced on Cu(111) by exposure to O_2 at elevated temperature or by annealing [42-44]. The '29' and '44' notations will be used hereafter for clarity. These structures were described as comprising distorted hexagonal arrays of O atoms arranged in parallel lines in the first layer [42-44], with unit cell areas 29 and 44 times larger than that of the substrate Cu(111). Both oxide overlayers were considered to be analogous to crystallographic planes of Cu_2O(111) which has a structure with equilateral hexagons of oxygen atoms in the first layer [42-44].

Imaging of oxide surfaces, and in particular oxides grown on metals, is problematic due to O having a low density of states available for tunneling. Thus, on Cu for example [1-6], images of the oxide are likely to be dominated by the metal states with the O atoms appearing dark. The strong influence of electronic effects in the contrast mechanism when imaging oxide surfaces therefore requires consideration of the apparent height of the tip. In general STM images of oxides cannot always be interpreted as topographic maps of the surface.

In this study, we carefully observed the oxidation of Cu(111) at room and elevated temperature by STM. The site where oxidation initiates and the structure of the oxide islands were revealed at atomic resolution. We found that the '44'-structure was produced at lower temperature than that reported previously [42-44]. The effect of

annealing of these pre-oxidized surfaces was also studied. Oxygen pressure and elevated temperature annealing were also found to influence the structure of the surface.

6.2 Experimental

The new Cu(111) crystal surface was cleaned by many cycles of Ar ion bombardment and annealing, and routinely prepared before experiments by 4 cycles of ion bombardment at room temperature for 15 minutes and at 823 K for 4 minutes, followed by vacuum annealing at 773 K for 10 minutes. This process gave a well-ordered clean surface providing LEED patterns with sharp integral order spots and low background intensity. Good order was also seen by the STM, with little evidence of contamination (seen as bright as asperities, combined with poor imaging), and verified by Auger electron spectroscopy (VG RFA). All STM images were acquired in the constant-current mode, and sample bias voltages and tunneling currents were noted for each STM images.

6.3 Results and discussion

6.3.1 Cu(111) surface oxidized at room temperature

6.3.1.1 Oxidation of Cu(111) at room temperature

Fig. 6.1 shows STM images which give an overview of the Cu(111) oxidation process. The bold arrows in panels (a, b, c, d, e and f) indicate the same point on the surface. Panel (a) shows a large area scan (1000Å) of a terrace including some vacancy islands (one is shown by the arrow) observed on the clean Cu(111) surface. The step edges of the clean surface are rather smooth in Fig. 6.1 (a), but become angular upon exposure to 7×10^{-5} Pa O_2, Fig. 6.1 (b). These angular step edges adjoin a new surface structure, which appears with an apparent height intermediate between terraces separated by a single step. The spatial extent of these new structure areas is limited to the old Cu(111) step edges which were present before introduction of O_2.

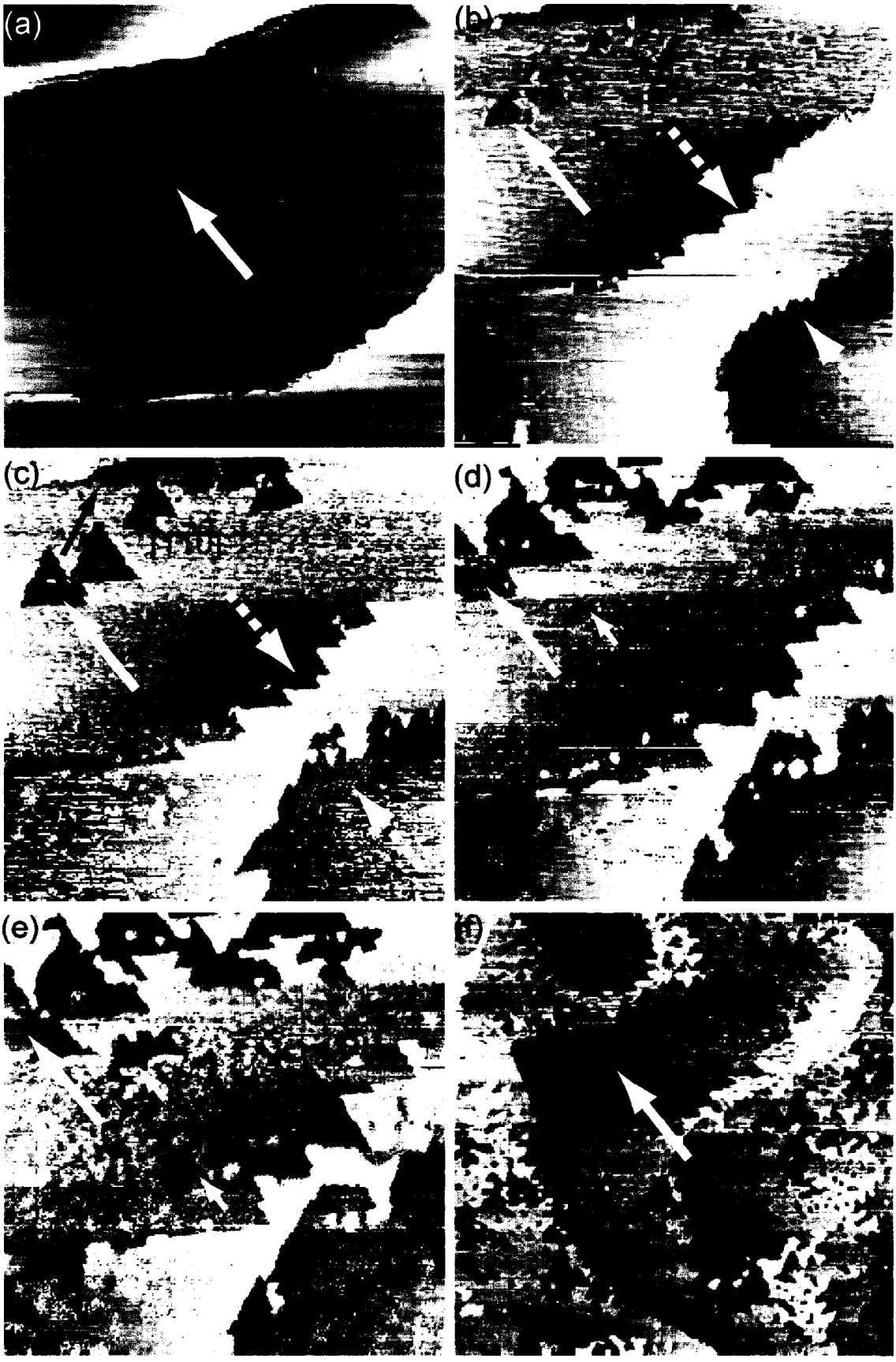
(a)
(b)
(c)
(d)
(e)
(f)

Fig. 6.1. STM images of clean Cu(111) and Cu(111) reacting in a pressure of O_2 at 7×10^{-5} Pa at room temperature. (a) Clean Cu(111) (1000×1000 Å^2, V=500 mV, I=0.03 nA). (b) Recorded after 10 min in oxygen, the dashed arrows indicate the original position of the step edge (1200×1200 Å^2, V=700 mV, I=0.07 nA). (c) After 20 min exposure the step edges have retreated (dashed arrows as before) (1200×1200 Å^2, V=700 mV, I=0.03 nA). (d) 33 min (1000×1000 Å^2, V=700 mV, I=0.03 nA). (e) 39 min (1000×1000 Å^2, V=700 mV, I=0.03 nA). The small arrows indicate new "terrace oxide" formed in the latter stages of adsorption. (f) 66 min (3000×3000 Å^2, V=700 mV, I=0.03 nA). The large solid arrow indicates the same position in each image.

This indicates the preferential formation of an oxide from step edge Cu atoms – the oxide grows into the upper terrace from the step edge. We therefore denote this material as "step oxide" to highlight its formation from Cu atoms from the upper terrace at a step edge.

Within the flat Cu(111) terraces, the initial image (a) shows vacancy islands, which expand to form triangles with exposure to O_2, images (b-d). As we shall discuss later there is structure within these islands and we denote this triangular pit structure as "terrace oxide" to highlight its mode of formation. The large solid arrows in Fig. 6.1 (b), (c), (d), (e), and (f) indicate the position of the growing "terrace oxide" which originated from the vacancy island. The step edges and perimeters of the triangles on the oxidized Cu surfaces prefer the close packed directions of the atomic rows of Cu(111), namely, $[1\bar{1}0]$ and equivalent directions. In Fig. 6.1 (d) the surface is notably more streaked, with the appearance of structure on top of the terraces. The density of this structure increases with exposure and will be remarked upon shortly.

Fig. 6.1 (d) and (e) show new small dark triangular features of "terrace oxide" (short arrows) produced in the middle of the Cu terrace without obvious association with any previous feature. The formation of both terrace oxide as triangular pits in the terrace from existing vacancy islands and from the defect free surface after higher exposure to O_2 lead us to conclude that oxygen is capable of abstracting Cu from the terraces. This process is accompanied by the formation of a third oxide species that

appears as bright straggly features on top of the terraces. These begin to dominate the surface in the latter stages of adsorption and disrupt the growth of the "terrace oxide" triangles, leading to irregular rather than triangular edges, Fig. 6.1 (d), (e), and (f). We denote this oxide, which forms upon the terrace, as "added oxide" as it has grown on top of the terrace rather than in the terrace or at the step edge.

A great deal of surface restructuring is apparent by the time we reach the final panel, Fig. 6.1 (f), with the loss of the clear triangular features of Fig. 6.1(b) and (c). Even the 3-fold symmetry is not so obvious. Additionally, although the step edges were, and continue to be, etched by O_2 adsorption, the extent of the "step oxide" onto the lower terrace remains pinned at the position of the original step edge. We shall return to the growth mechanisms in comparison to other Cu surfaces shortly.

6.3.1.2 The surface structures observed in the initial stages of oxidation of Cu(111)

Fig. 6.2 (a) is an STM image of the Cu(111) surface in a pressure of O_2 at 1-2.4×10^{-5} Pa after exposure for 10 min. Step edges were angular and some dark triangles were formed as observed in Fig. 6.1 (c) and (d). The surrounded area indicates a part of Fig. 6.2 (b). Fig. 6.2 (b) shows a similar area and was obtained immediately after evacuation of the gas phase O_2 (total exposure ~100 L). This Fig. 6 shows significant differences to Fig. 6.2 (a) despite the similar exposures. The islands of "added oxide" appear clearly on the terraces.

The added and terrace oxide islands are shown at atomic resolution in Fig. 6.2 (c), which is a high-resolution image of the marked region in Fig. 6.2 (b). The "terrace and added oxide" islands are both composed of small unit features with similar orientation and separation. We therefore consider these units to be copper oxide molecular units, most probably imaging a single prominent Cu atom. The nearest-neighbor distance of these units is 5.5-7 Å, and some parts have a nearly hexagonal

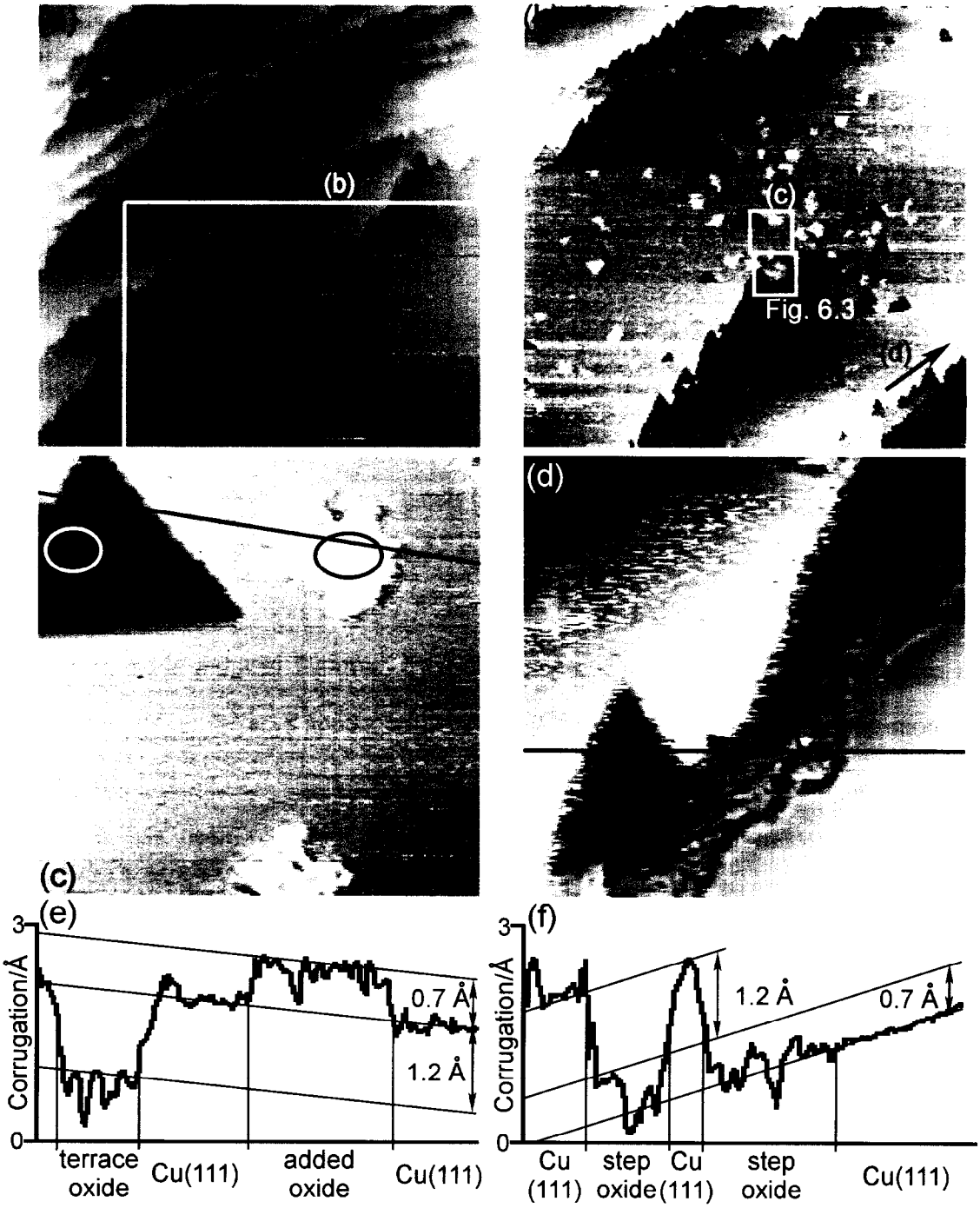
(b)
(c)
Fig. 6.3
(a)
(d)
(c)
(e)
3
0
Corrugation/Å
0.7 Å
1.2 Å
terrace oxide
Cu(111)
added oxide
Cu(111)
(f)
3
0
Corrugation/Å
1.2 Å
0.7 Å
Cu (111)
step oxide
Cu (111)
step oxide
Cu(111)

Fig. 6.2. STM images of Cu(111) during and after exposure to O_2 at 1-2.4×10^{-5} Pa for 15 min at room temperature. (a) Oxidized Cu(111) surface in O_2 (2000×2000 Å^2, V=500 mV, I=0.05 nA). Surrounded area is a part of the area seen in the Fig. 6.2 (b). (b) Oxidized Cu(111) surface scanned in large area after evacuation of O_2 (2000×2000 Å^2, V=500 mV, I=0.05 nA). Square and arrows indicate the area observed in Fig. 6.2 (c), Fig. 6.2 (d), and Fig. 6.3. (c) Terrace and added oxide islands showing some degree of internal order (200×200 Å^2, V=500 mV, I=0.05 nA). (d) Step oxide growing into a step edge (200×200 Å^2, V=500 mV, I=0.1 nA). Again the oxide shows some ordering of internal structure. (e and f) Corrugation of terrace and added oxide along the solid line marked in Fig. 6.2 (c) and (d), respectively. The values for the X axis indicate the length from the left side along the black lines.

lattice structure. Fig. 6.2 (d) shows a dark domain of the "step oxide" along a step edge a few angstroms to the right of the area of Fig. 6.2 (b) at atomic resolution. The etched step edge displays sharp triangular facets but the front fringe edge forms a smooth curve. Within the "step oxide" atomic scale features can be resolved. Again, the distance between the small features is 5.5-7 Å and some of these dots are arranged hexagonally. All three oxide induced features, fringes at step edges, triangular pits in terraces and added islands on terraces appear to have the same structure despite differing modes of formation.

It has been reported that the (111) plane of Cu_2O possesses a hexagonal symmetry, and the lattice constant is 6 Å [1, 2]. This suggests that the observed surface oxide layers may have a structure close to the Cu_2O (111) topmost layer.

Fig. 6.2 (e) shows a cross section of the oxidized surface along the black line in Fig. 6.2 (c). In Fig. 6.2 (e), the level of the "terrace oxide" is apparently 1.2 Å lower than that of the Cu(111) terrace, while the level of the tip scanning the "added oxide" is 0.7 Å higher than Cu(111). Then the apparent height difference between these two oxide islands is about 1.9 Å, similar to the monoatomic step height of the Cu(111) surface (2.1 Å), as one would expect for identical oxides growing on terraces separated by a single atomic step.

A screw dislocation was observed at atomic resolution in Fig. 6.3 and is recorded as an enlargement of Fig. 6.2 (b) at an early stage of reaction. This image shows clearly the striking similarity between oxide structures formed at step edges and in and on terraces. We therefore conclude that all three oxide phases formed are the same despite differing modes of formation and differing location.

We can estimate the composition of the copper oxide by analyzing the areas of oxide grown in the STM images. If we assume the small features observed in Fig. 6.2 (c) and (d) are unit cells of the oxide, then we can let the area density of Cu in the cell to be $2x / (\sqrt{3}\,(6\ \text{Å})^2)$ where x is the no. of Cu atoms per cell and 6Å the nearest neighbor distance obtained above for the cell size. Fortunately, we can also estimate the number of Cu atoms removed from the Cu(111) terraces upon exposure to O_2. The amount of mobilized Cu is equivalent to sum of areas of the dark triangles, and of the retreat of the original Cu step edges. These areas released $2/ (\sqrt{3}\,(2.55\ \text{Å})^2)$ Cu atoms per unit area. Within Fig. 6.2 (b), the islands added to the terrace represent the part of newly generated oxide, and the darker domains represent the area of Cu(111) replaced by oxide. The mass balance for Cu is then formulated as:

$$(\text{Area of surface etched})/(2.55\ \text{Å})^2$$

$$= x \times (\text{Area of surface etched} + \text{area of added oxide})\ /(6\ \text{Å})^2$$

The area of the domains was measured from Fig. 6.2 (b), and the obtained value for x is 3.6. Therefore we associate each oxide unit with 3.6 added Cu atoms. This is close to the value of 3 Cu atoms added per unit cell for the growth of Cu_2O on the surface. It is therefore likely that the small individual features correspond to Cu_2O [42-44], and the excess amount of Cu liberated during oxidation may be present as Cu atoms mobilized on Cu(111) terraces but not trapped into an ordered structure. We have some evidence for mobile species as discussed below.

Fig. 6.3. STM image showing atomic structure of the oxide growing at a screw dislocation at high resolution (200×200 Å^2, V=500 mV, I=0.05 nA). Arrays of depressions are observed in the oxidized areas in a loosely hexagonal pattern.

Fig. 6.4. Change of STM image contrast with redosing O_2 to the oxidized surface. The partially oxidized surface shown in Fig. 6.2 (b) was exposed to the O_2 at 1.6×10^{-4} Pa at room temperature for 4 min. (a) Terrace and added oxide islands before redosing O_2 (500×500 Å^2, V=500 mV, I=0.05 nA). (b) Indistinct light patches almost in the same place as in (a) just after redosing O_2 (300×300 Å^2, V=500 mV, I=0.05 nA). A kink has formed in the terrace island edge as the surrounding Cu terrace is etched. (c) Distinct light patches in the same place as (a) and (b) after evacuation of O_2 (300×300 Å^2, V=500 mV, I=0.05 nA). The kink in Fig. 6 (b) has moved along the step in the direction of the arrow, i.e. $<01\bar{1}>$.

6.3.1.3 Structural alteration of O/Cu(111) by the presence of O_2 in the gas phase

The effect of the gas phase oxygen on the "added oxide" islands on the surface was studied by imaging during the early stage of oxidation. Fig. 6.4 (a) is a STM image obtained for O/Cu(111) after evacuating O_2 where "terrace and added oxide" structures were observed at atomic resolution. Fig. 6.4 (b) shows an image for the same surface with O_2 present at a pressure of 1.6×10^{-4} Pa. The light patches became indistinct but were just observable in almost the same positions as before. The surface became heavily streaked, which is commonly observed when imaging mobile species. Fig. 6.4 (c) was acquired in vacuum after introducing O_2 for a total time of 4 minutes. The light patches were clearer again, appearing in almost the same place as shown in (a) and (b), but have grown considerably. We believe that the oxygen adsorbs onto the surface and reacts with Cu atoms to form a mobile precursor phase. These oxide precursors attach to existing islands of "added oxide" (and in some cases nucleate new island growth). When oxygen is removed from the gas phase the equilibrium concentration of precursor drops rapidly allowing easier imaging.

The "terrace oxide" islands, which form triangular pits in the terraces, supply some of the copper to the mobile precursor. In Fig. 6.4 (a-c) the lower edge of the triangle is etched by oxygen adsorption with a large kink (10-20 angstroms width) moving along the step edge. This etching process is initiated at the corners of the triangular islands, Fig. 6.4 (b) (circled), and traverses the entire step length in the typical directions as indicated by the arrow in Fig. 6.4 (c). The width of a kink is much larger than a single Cu-Cu distance in the surface. We consider that as the lattice constants for the Cu(111) surface and the copper oxide are different and thus stable oxide islands may only form when the coincidence between the two lattices is complementary. Thus wide kinks tend to form which represent a favorable conjunction between surface lattices and the step edge.

6.3.1.4 Effect of heating on surface structure

STM images of the Cu(111) surface after O_2 adsorption at room temperature were also taken at elevated temperatures to investigate annealing of the surface. Fig. 6.5 (a) and (b) were acquired at 473 K, and (c) and (d) at 623 K in vacuum after delivery of O_2 at 7×10^{-5} Pa for 66 minutes at room temperature. In Fig. 6.5 (a) islands of "added oxide" on top of the terraces were not observed, the density of the "terrace oxide" forming pits in the terrace was reduced and the step edges more rounded in comparison to images taken at RT. In the near atomic-resolution image, Fig. 6.5 (b), many small bright features were observed on top of the oxide surface which was not previously imaged at room temperature. These small individual features are possibly Cu adatoms on top of the oxide surface which are imaged in a similar manner to the Cu adatoms on top of (2×1) and c(6×2) oxygen structures on Cu(110) [1-6]. Raising the temperature still further to 623 K, (Fig. 6.5 (c) and (d)) produces straighter step edges than those in (a) and the disappearance of the bright features. The surface morphology became flattened with increasing the annealing temperature and in small area scans the step edges appeared "frizzy". The "frizziness" of step edges and the lack of atomic scale surface structure implies mobilization of the surface species.

Room-temperature STM images were taken of the O/Cu(111) surface after annealing in an attempt to regain atomic resolution on the high temperature annealed surfaces. The STM images and the LEED patterns of Fig. 6.6 were recorded at room temperature for O/Cu(111) prepared by room temperature adsorption of O_2 at 108 L (Langmuir=10^{-6} Torr· s) followed by annealing at 473 K in vacuum for 5 minutes. In Fig. 6.6 (a), equally spaced stripes are seen on the terraces, indicating that the surface was well ordered over hundreds of angstroms. Domain boundaries between the large ordered islands were also observed within one single terrace. Small area scans show, Fig. 6.6 (b), a well-ordered array of atomic-scale features. These are similar to the '44'-structures reported by Besenbacher et al on O/Cu(111) [42-44]. A structural

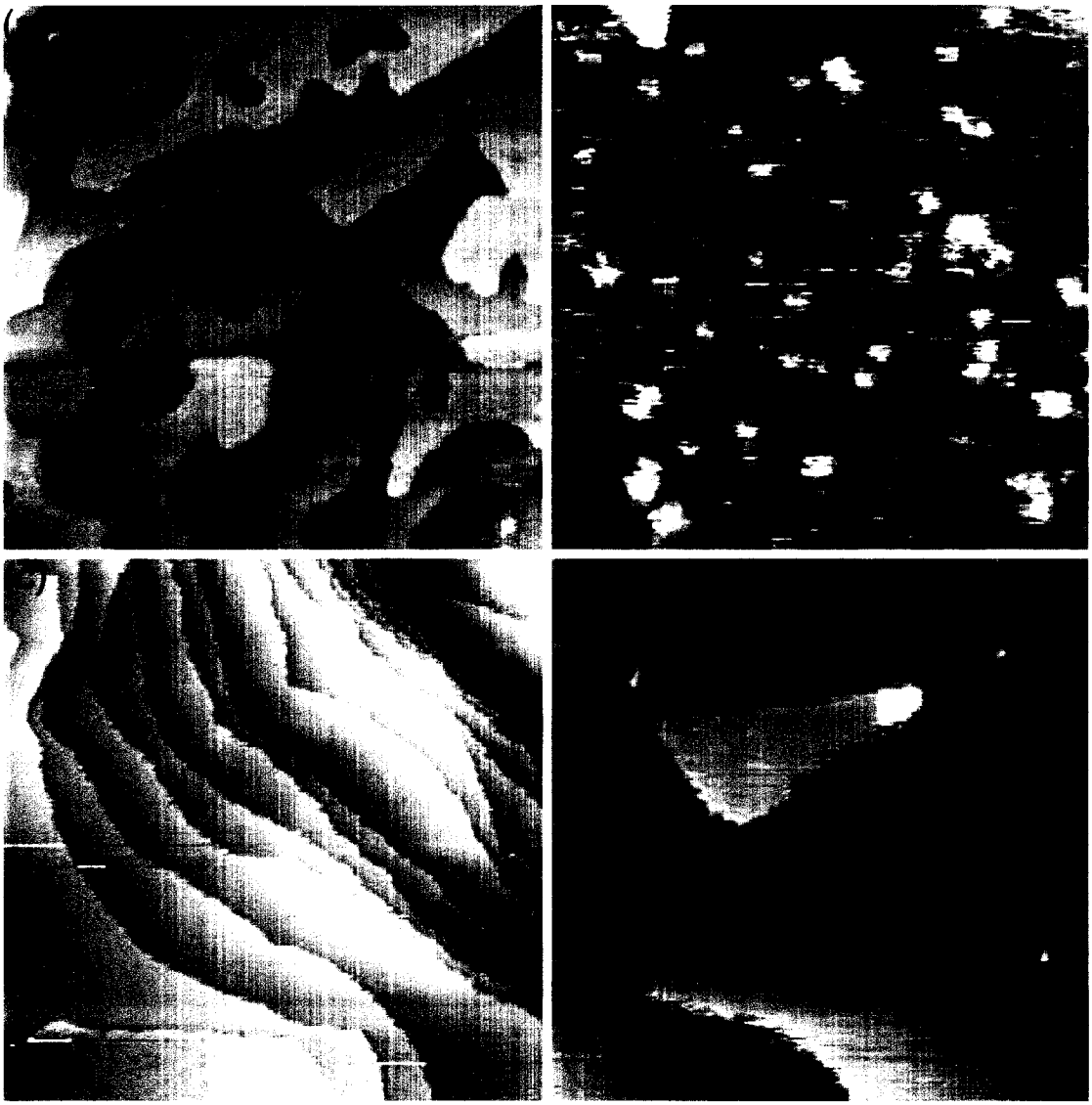

Fig. 6.5. STM images of the oxidized surface shown at room temperature in Fig. 6.1 (f) now imaged at the stated temperatures. (a) At 473 K (2000×2000 Å^2, V=700 mV, I=0.03 nA). (b) At 473 K (250×250 Å^2, V=700 mV, I=0.03 nA). (c) At 623 K (3000×3000 Å^2, V=1000 mV, I=0.3 nA). (d) At 623 K (800×800 Å^2, V=1000 mV, I=0.3 nA).

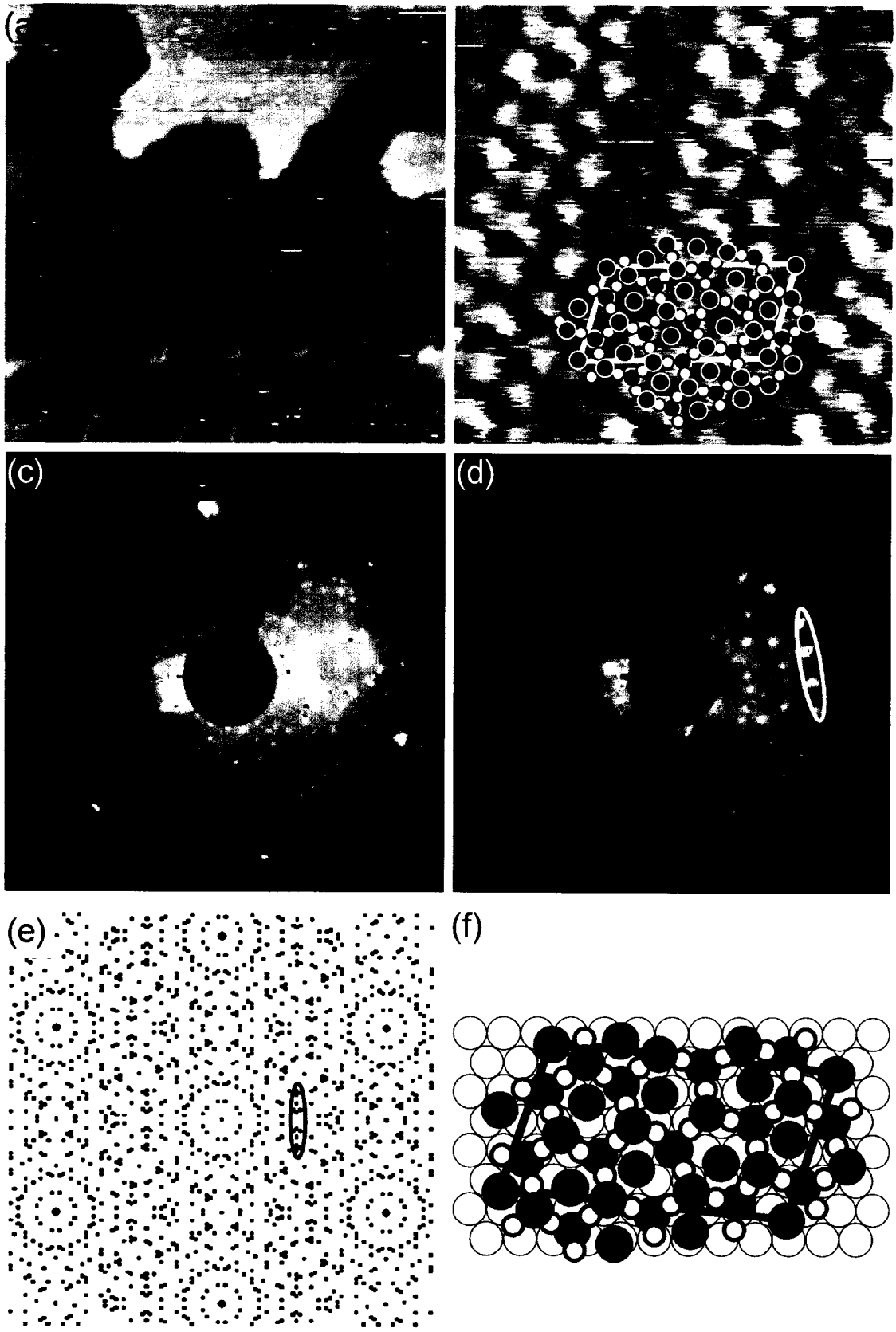
(c)
(d)
(e)
(f)

Fig. 6.6. STM images and LEED patterns for the surface oxidized at room temperature and annealed at 473 K for 5 min. The O_2 was dosed at 0.2-1×10^{-5} Pa for 40 min. STM images were observed at room temperature. The LEED pattern was also observed at room temperature. (a) Well-ordered surface in a large area (500×500 Å^2, V=1000 mV, I=0.3 nA). (b) Well-ordered surface at atomic resolution (50×50 Å^2, V=700 mV, I=0.2 nA). White parallelogram lines indicate the unit cell for the '44'-structure. The structural model is depicted with the open and filled circles indicate the Cu and O atoms in the model, respectively. (c) LEED pattern at primary energy of 55eV. This LEED pattern corresponds with the '44'-structure. Highlighted spots correspond to those in the calculated LEED pattern (e). (d) LEED pattern at primary energy of 19 eV. Surrounded spots correspond to those in the calculated pattern (e). (e) Calculated LEED pattern for the '44'-structure for 6 equivalent domains. (f) Schematic model of the overlayer oxide on the Cu(111) surface with Cu and O atoms of the oxide shaded as in (b), the substrate Cu atoms are light gray.

model of O atoms relative to the Cu atoms of the substrate Cu(111) surface is inserted in Fig. 6.6 (b). The open and filled circles indicate the Cu and O atoms, respectively. Besenbacher et al. [44] modeled this '44'-structure by laying one single slightly deformed (111) oxygen net plane, embedded in the 3-dimensional Cu_2O crystal, onto the Cu(111) surface. The unit cell of the Cu_2O(111) plane was adjusted so as to make it commensurate with the Cu(111) by forming the '44' superlattice unit cell. The coordination number and configuration of O atoms around one Cu atom were almost unchanged from the original Cu_2O crystal structure. Fig. 6.6 (c) and (d) are LEED patterns of this surface taken at a primary energy of 55 and 19 eV, respectively. Sharp hexagonally arranged spots were observed in a relatively complex pattern. The six outer hexagonal bright spots in Fig. 6.6 (c) are the integral order spots of the Cu(111) substrate. These LEED patterns can be assigned to the 6 equivalent domains with the structure represented by ($\sqrt{73}$ R5.8°×$\sqrt{21}$ R-10.9°) in the Wood notation, varying by rotation and reflection due to the substrate symmetry. The reciprocal lattice plot for ($\sqrt{73}$ R5.8°×$\sqrt{21}$ R-10.9°) is shown in Fig. 6.6 (e) to simulate the LEED pattern. All of the spots in this plot were recognized in the LEED patterns obtained. The ($\sqrt{73}$ R5.8°×$\sqrt{21}$ R-10.9°) super lattice is equivalent to the '44' lattice proposed by

Besenbacher et al [42-44]. We have shown that the disordered surface formed by room temperature O_2 adsorption is converted to a well-ordered adlattice by annealing in vacuum.

The effect of annealing this structure to an even higher temperature and for an extended period of time was also studied. The Cu(111) surface was exposed to O_2 at room-temperature, annealed at 723 K for 20 minutes and was cooled to room temperature. Fig. 6.7 (a) shows a large-area STM image. Rhomboidal and trapezoidal structures were found on the large scale, apparently composed of criss-crossed steps on the surface. The surface appears to be ordered over an extended area. The surface at atomic resolution is shown in Fig. 6.7 (b). The surface was structured but the features were not arranged regularly. Fig. 6.7 (c) is the LEED pattern for the surface at a primary beam energy of 53 eV. The arrangement of diffraction spots is the same as the ($\sqrt{73}$ R5.8°×$\sqrt{21}$ R-10.9°) structure with apparently stronger background in comparison to those in Fig. 6.6 (c) and (d). The STM image, Fig. 6.7 (d) was acquired after annealing at 723 K for 30 minutes. Many light dots were observed on the terraces, which we again associate with Cu adatoms on the oxide surface. The origin of this Cu is probably the oxide film itself that is beginning to decompose as oxygen is lost by dissolution into the bulk during the long annealing time.

Though LEED gave distinct diffractions spots, no well ordered structure was recognizable in the STM. This apparent contradiction can be resolved in the following manner. The STM images, such as shown in Fig. 6.7 (b) and (d), do in fact contain well-ordered 2-dimensional lattices although the surface looks disordered at a glance. Fig. 6.8 shows a 2-dimensional Fourier-transformation of the STM image in Fig. 6.7 (b) and (d). This Fourier-transformed image involves a well-ordered array of spots, representing the reciprocal lattice detected within Fig. 6.7 (b) and (d). The set of unit vectors of this reciprocal lattice is recognized as congruent to that of ($\sqrt{73}$ R5.8°×$\sqrt{21}$ R-10.9°).

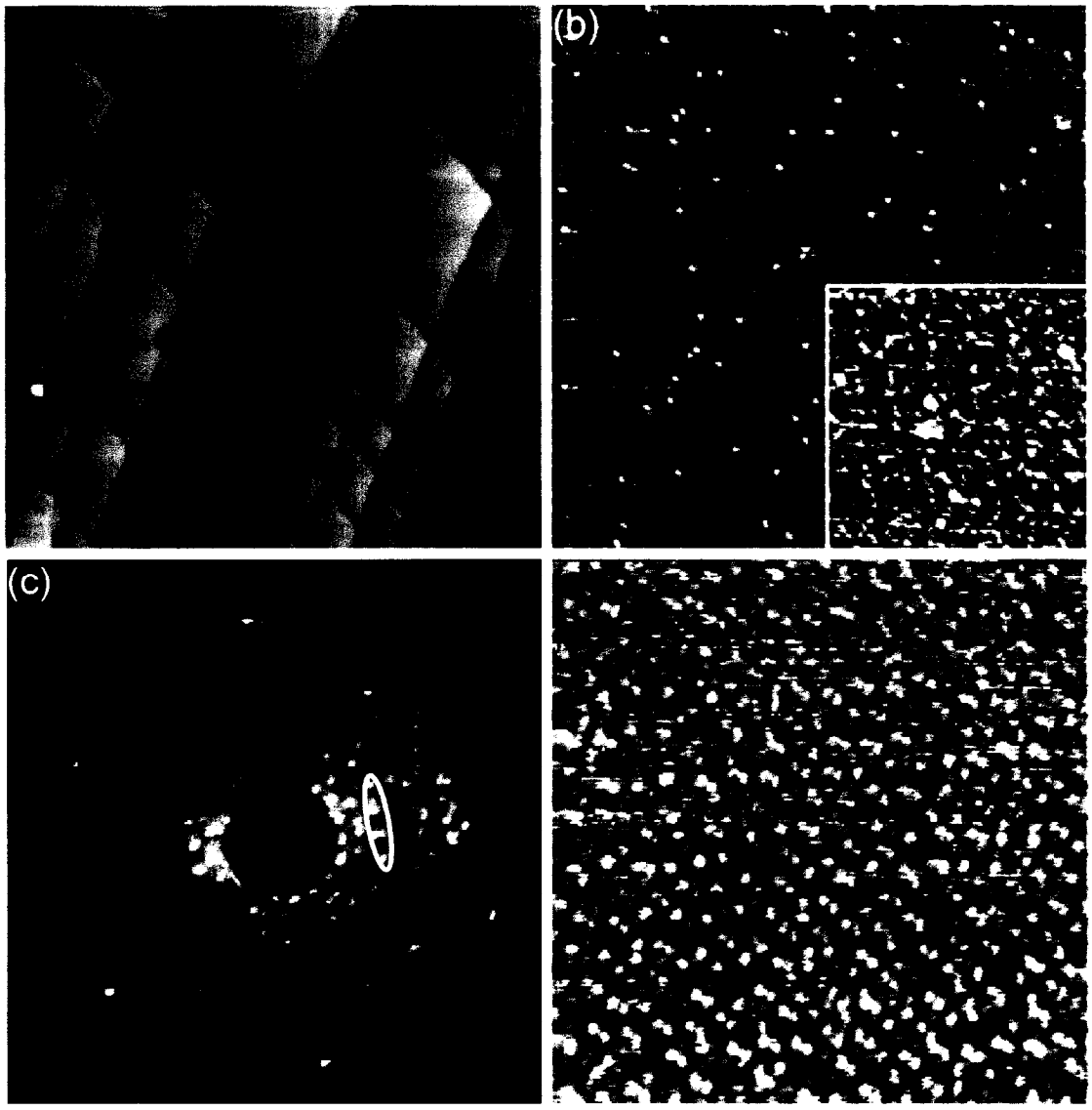

Fig. 6.7. STM images and LEED pattern at room temperature for the surface oxidized at room temperature and annealed at 723 K for 20 min. The O_2 was dosed at $1\text{-}4\times10^{-5}$ Pa at for 30 min. (a) Triangular rhomboid, and trapezoid structures forming terraces in a large area image (3000×3000 Å^2, V=500 mV, I=0.5 nA). (b) Structure at atomic resolution for the surface shown in (a) (500×500 Å^2, V=300 mV, I=0.05 nA (lower right insert: 150×150 Å^2)). (c) LEED pattern at primary energy with 53 eV. The surrounded spots correspond to those in Fig. 6.6 (e). (d) STM image for the surface annealed at 723 K for more 30 min (200×200 Å^2, V=100 mV, I=0.05 nA).

6.3.1.5 O/Cu(111) compared with O/Cu(110) and O/Cu(100)

The oxidation process of Cu surfaces is dependent on the crystallographic plane of the surface. On Cu(110), Cu atoms diffuse from step edges and uniform (2×1)-O oxide islands are formed on terraces as stripes [1-5]. On Cu(100), the oxide islands are formed on terraces by squeezing out Cu atoms from the terraces and the step edges are less important during oxidation.

In this study, three pathways were found for the oxidation of Cu(111). The first is the formation of oxide domains growing into step edges through ejection of Cu. The second is the association of the released Cu atoms with diffusing O atoms to form "added oxide" islands on the terrace. The third is the ejection of Cu atoms from. terraces after most of the surface is covered with oxide islands as shown in Fig. 6.1 (e). The last process is similar to the oxidation processes for Cu(110) and Cu(100) surfaces regarding mass transport. However, the existence of the first mechanism for Cu(111) that the oxidation starts from, and etches into, the step edges is essentially different from those for Cu(110) and Cu(100), surfaces. On Cu(110) (2×1) chains of –O-Cu-O-Cu- grow on the surface in long narrow islands with the majority of Cu for these added structures removed from the step edges. Only when there is insufficient supply of Cu from step edges do vacancy islands appear in the terraces as Cu is removed. The O-(2×1) islands form an ordered grating across the surface which remains aligned across step edges running along $<1\bar{1}0>$ direction. There appears to be no preferential growth at the step edges, however, the alignment of (2×1) islands over the step edge implies considerable gain in surface stability by such alignment. In a similar manner the "terrace oxide" that forms as triangular pits with the edges which are also directed in the $<1\bar{1}0>$ directions shows preferential growth by removal of wide swathes of Cu from the edges rather than a monatomic row. As we discussed earlier this may be related to the matching of Cu and Cu_2O crystal lattices. On both surfaces it is presumably the orientation of Cu-O bonds at this step edge that dictate the local structure and reactivity.

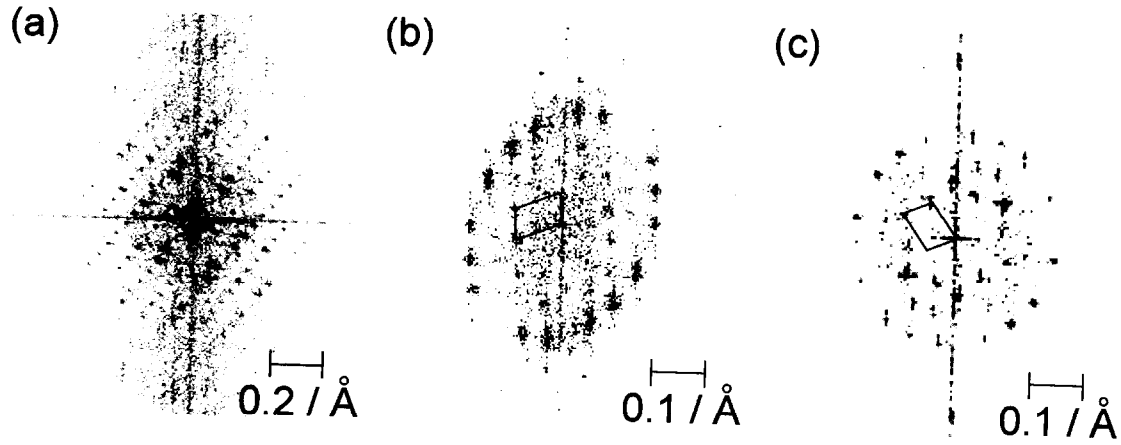

Fig. 6.8. Fourier transforms of the STM images showing the '44'-structure (the same surface as shown in Fig. 6.7 (a), Fig. 6.7 (b), and Fig. 6.7 (d) are shown in the figure (a), (b), and (c), respectively. The size of the transformed images are 1.31×1.31, 0.68×0.68, and 0.68×0.68 / Å^2 for (a), (b), and (c), respectively. The parallelograms represent the unit cells and their sizes were almost the same 0.049×0.094 / Å^2. The angles given by the unit vectors were also the same ~103°. This indicates that all these spots correspond to the reciprocal lattice representation of the surface structure in the STM image and to the LEED pattern for the observed area of the '44'-structure.

6.3.2 Cu(111) surface oxidized at elevated temperature

6.3.2.1 Oxidation of Cu(111) at 373 K

The Cu(111) surface was observed by STM in a flow of oxygen at $3\text{-}4\times10^{-4}$ Pa with the substrate temperature maintained at 373 K . Fig. 6.9 (a) shows an STM image of a clean Cu(111) surface at 373 K. All step edges are smooth, which is in contrast to the jagged edges observed at room temperature as seen in Fig. 6.1. A higher resolution image is shown in Fig. 6.9 (b). The step edges look almost straight and somewhat streaky. It is likely that some Cu atom diffusion occurs from the step edges. Fig. 6.9 (c) was obtained 9 minutes after introducing O_2. The step edges became angular and domains of a new structure (indicated by the arrow) were formed along the step edges on the metallic Cu(111) terraces. These types of domain seem to be equivalent to the random Cu_2O monolayer observed after room temperature adsorption. Atomic resolution could not be obtained and the boundaries of the oxide are often streaky, indicating that the Cu and O atoms of the oxide may be mobile. Fig. 6.9 (d) is a larger scale STM image for the surface oxidized for 10 minutes in a flow of O_2. The sharply pointed step edges can be clearly observed. By analyzing the cross sections of this image, this surface is revealed to be composed of terraces of bare Cu(111) with jagged edged down steps to the lower terrace on which the oxide monolayer grows. On a terrace of bare Cu(111) dark triangles are also seen due to oxide growth in a pit (marked with arrows). These fringes and triangles are presumed to have the same Cu/O composition as those formed at room temperature. Fig. 6.9 (e) shows the surface oxidized for 60 minutes. A partially ordered structure was observed with atomic resolution, randomly covering the surface. The diffusion of atoms was suppressed by this full oxidation of the surface as also seen in the study at room temperature as seen in Fig. 6.1 (d). A patch of well-ordered structure was found as shown in Fig. 6.9 (f) (highlighted), and seems to have the '44'-structure. The oxidation at 373 K resulted in the aggregation of diffusing Cu and O atoms into an oxide area along step edges.

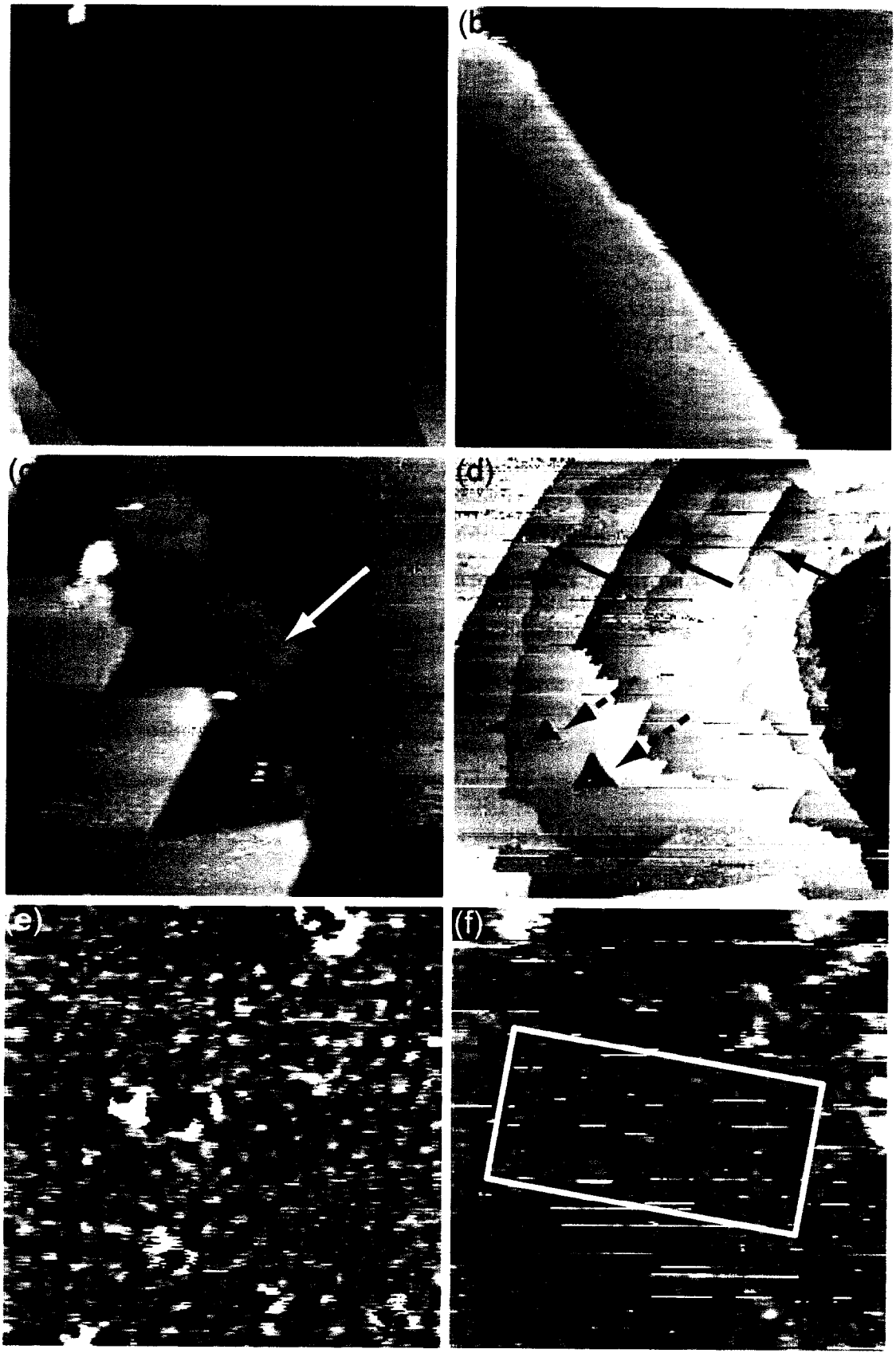
(b)
(d)
(e)
(f)

Fig. 6.9. STM images of the Cu(111) surface at 373 K before and after exposure to oxygen at 3-4×10^{-4} Pa. (a) Clean surface in a large scale (5000×5000 Å^2, V=1000 mV, I=0.1 nA). (b) Clean surface step edge at high resolution (300×300 Å^2, V=1000 mV, I=0.1 nA). (c) Oxidized surface in a large scale after 9 minutes (1500×1500 Å^2, V=600 mV, I=0.5 nA). The step edge has become etched in triangular motifs with the formation of oxide (arrowed) in the etched region extending in an irregular shape onto the terrace. (d) Large area image of the oxidized surface after 10 minutes exposure (4000×4000 Å^2, V=1000 mV, I=0.1 nA). The solid arrows indicate oxide domains formed from the originally straight step edges that are now facetted. The dashed arrows indicate triangular pits formed in the Cu terrace. (e) Oxidized surface at atomic resolution without ordered structure (150×150 Å^2, V=100 mV, I=0.1 nA). (f) Oxidized surface at atomic resolution with ordered structure marked (200×200 Å^2, V=500 mV, I=0.1 nA).

6.3.2.2 Formation of the '44'-structure by oxidation at 423-573 K

The '44'-structure extending over hundreds of angstrom wide areas could be formed by oxidation at 423-573 K. Fig. 6.10 is a series of images during oxidation of the Cu(111) surface at 573 K. The pressure of O_2 was 1-7×10^{-5} Pa. Fig. 6.2 (a) shows a large area scan of the clean Cu(111) surface before oxidation at 573 K. The step edges are generally smooth with streaks. Fig. 6.10 (b)-(e) show large area scans of the Cu(111) surface oxidized for 5, 10, 11, 14 minutes after O_2 introduction, respectively. Oxide domains (arrows) were produced along the step edges in Fig. 6.10 (b). No atomic resolution was obtained presumably because of rapid diffusion of surface species. The oxide area near the step edges extended with time and exposure as shown in Fig. 6.10 (c). The Cu step edge became straighter (marked in the image) while the boundaries of the oxide domains became poorly resolved. Fig. 6.10 (d) shows that the metallic terrace has retreated as the oxide advances until the metallic terrace eventually disappears (the white lines indicate the step lines observed in Fig. 6.10 (c)). These observations indicate that the oxide is an added structure and uses Cu atoms from the step edge. Step retreat during oxygen layer formation has also been seen for the added row (2×1) reconstruction on Cu(110) [5]. The oxygen diffusion over the metallic part

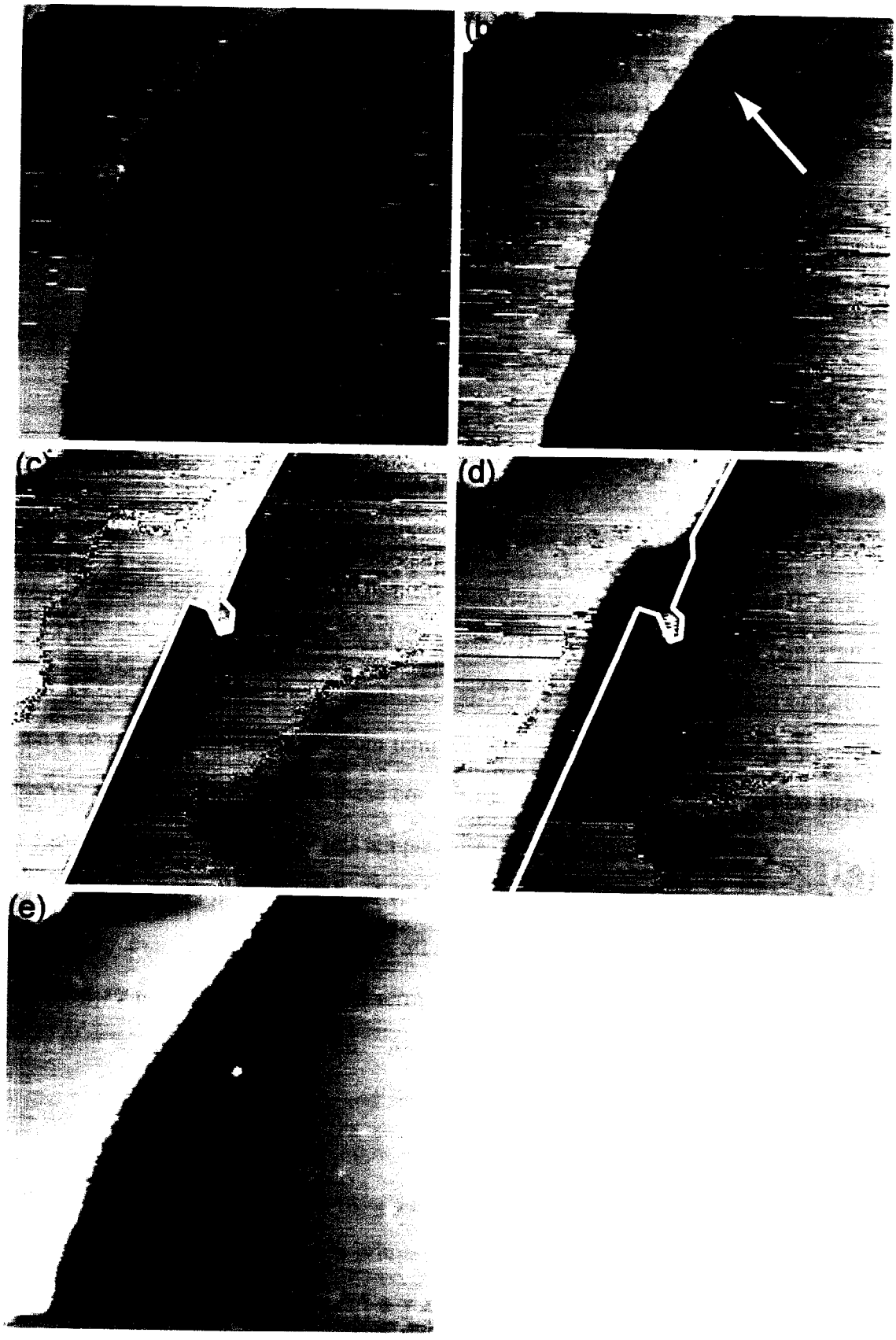
(b)
(c)
(d)
(e)

Fig. 6.10. Reaction sequence of the oxidation of Cu(111) at 573 K. The Cu(111) surface was exposed to oxygen at 1-7×10^{-5} Pa. The images were obtained after stated time. (a) Clean surface step edge 0 minutes (1000×1000 Å^2, V=700 mV, I=0.1 nA). (b) After 5 minutes the oxide areas have grown along the step edges as indicated by the arrows (1000×1000 Å^2, V=700 mV, I=0.1 nA). (c) 10 minutes exposure leads significant movement of the step edge and oxide formation on the lower terraces. A solid white line marks the step edge (1000×1000 Å^2, V=700 mV, I=0.1 nA). (d) Image taken after 11 minutes (1000×1000 Å^2, V=700 mV, I=0.1 nA). The solid white line represents the step edge observed in figure (c). The step has clearly retreated rapidly from its original position while the oxide areas grow. (e) The step has retreated to the growing oxide on its upper terrace and stopped retreating after 14 minutes, (1000×1000 Å^2, V=500 mV, I=0.1 nA).

towards the step edges is strongly enhanced at this temperature and adds as oxide at the Cu-oxide interface thus adding the growing oxide front. By tracking the expanding dark fringes of oxide, we could confirm that a monolayer oxide (Fig. 6.10 (e)) covered the whole surface. This process was obviously faster than that at room temperature taking 14 minutes to cover the whole surface at 573K rather than in excess of 66mins to reach a comparable coverage at room temperature. Dark triangular patches were not observed during oxidation under these conditions. The step edge could not be altered any further by exposure to O_2 at this temperature.

The Cu(111) surface oxidized (2-6×10^{-5} Pa O_2 for 23 minutes) at 573 K was imaged after evacuation of oxygen and after cooling to 300K. Fig. 6.11 (a) shows a large area scan in which one of the terraces is several hundreds angstroms wide and shows feint bands in a single domain. Atomic-resolution images were obtained, such as the one displayed in Fig. 6.11 (b), and showed the '44'-structure. These features were not observed at 573 K during oxidation, and therefore O_2 in the gas phase is considered to effect the diffusion of the atoms composing the oxide. Fig. 6.11 (c) is a LEED pattern observed for this surface at primary energy at 104 eV. The spots were sharp with a low background indicative of a well-ordered surface. This LEED pattern is identical to the reciprocal plot of the '44'-structure in Fig. 6.6 (e). STM and LEED

results revealed that the '44'-structure could be produced at even lower temperature than the oxidation at 673 K and annealing at 773 K in UHV as reported before [42-44].

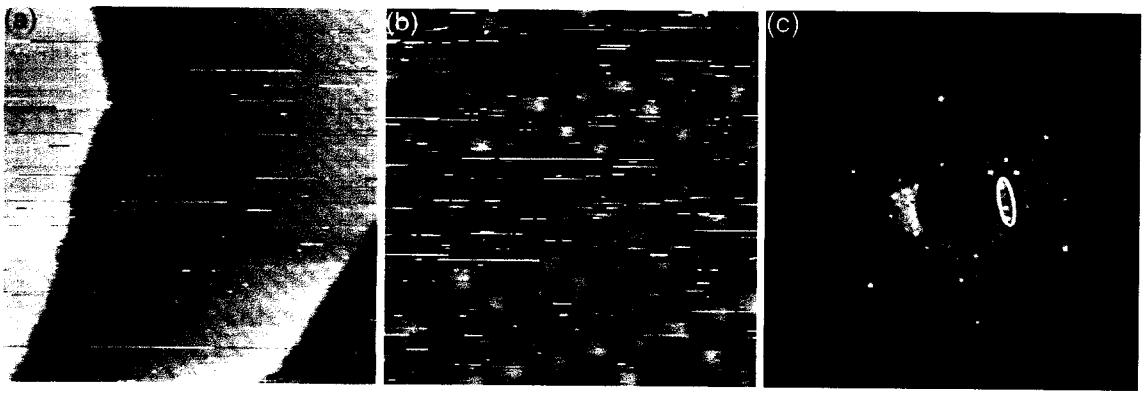

Fig. 6.11. STM images and LEED pattern for the Cu(111) surface oxidized at 573 K showing complementary evidence for the formation of a well-ordered '44' structure. (a) Large scale STM image of the well-ordered structure at 573 K (500×500 Å^2, V=1000 mV, I=1 nA). (b) STM image at atomic resolution at 573 K (50×50 Å^2, V=500 mV, I=1 nA). (c) LEED pattern at primary energy of 104 eV at room temperature. The surrounded spots correspond to those in Fig. 6.6 (e).

6.3.2.3 Transformation of the '44'-structure to the '29'-structure by annealing at 673 K

Emergence of the '29'-structure has been reported [43] to occur on annealing the '44'-structure at 673 K in vacuum. We have prepared the initial '44'-structure by exposure of the Cu(111) surface to O_2 at $3\text{-}4\times10^{-5}$ Pa for 60 minutes at 423 K. This surface structure was confirmed by LEED taken at room temperature. Raising the temperature to 448 K resulted in smearing of the LEED fractional order spots. Below 423 K the LEED pattern remained well defined. In contrast STM images of the '44'-structure were observed to be reasonably stable even up to 493 K. Fig. 6.12 (a) shows a STM image of the well-ordered '44'-structure observed at 493 K in vacuum. Continued heating to 573 K and imaging in-situ produced a surface as shown by the STM image in Fig. 6.12 (b). This image is similar to the '29'-structure as previously reported [42-44] indicating conversion of the '44'-structure to the '29'-structure. Annealing to still higher temperatures (673 K) resulted in the terraces imaged in the STM appearing with no corrugation, however 'frizzy' step edges were still visible.

Fig. 6.12 (c) shows the LEED pattern acquired after cooling the surface annealed at 673 K as shown in Fig. 6.12 (b) down to room temperature. The reciprocal lattice plot for the '29'-structure [42-44] is shown in Fig. 6.12 (d). It was confirmed that every LEED spot could be assigned to the 29'-structure with 6 domains (three rotational with two mirror images). Thus, annealing at 673 K in vacuum brought about conversion of the '44'-structure to the '29'-structure.

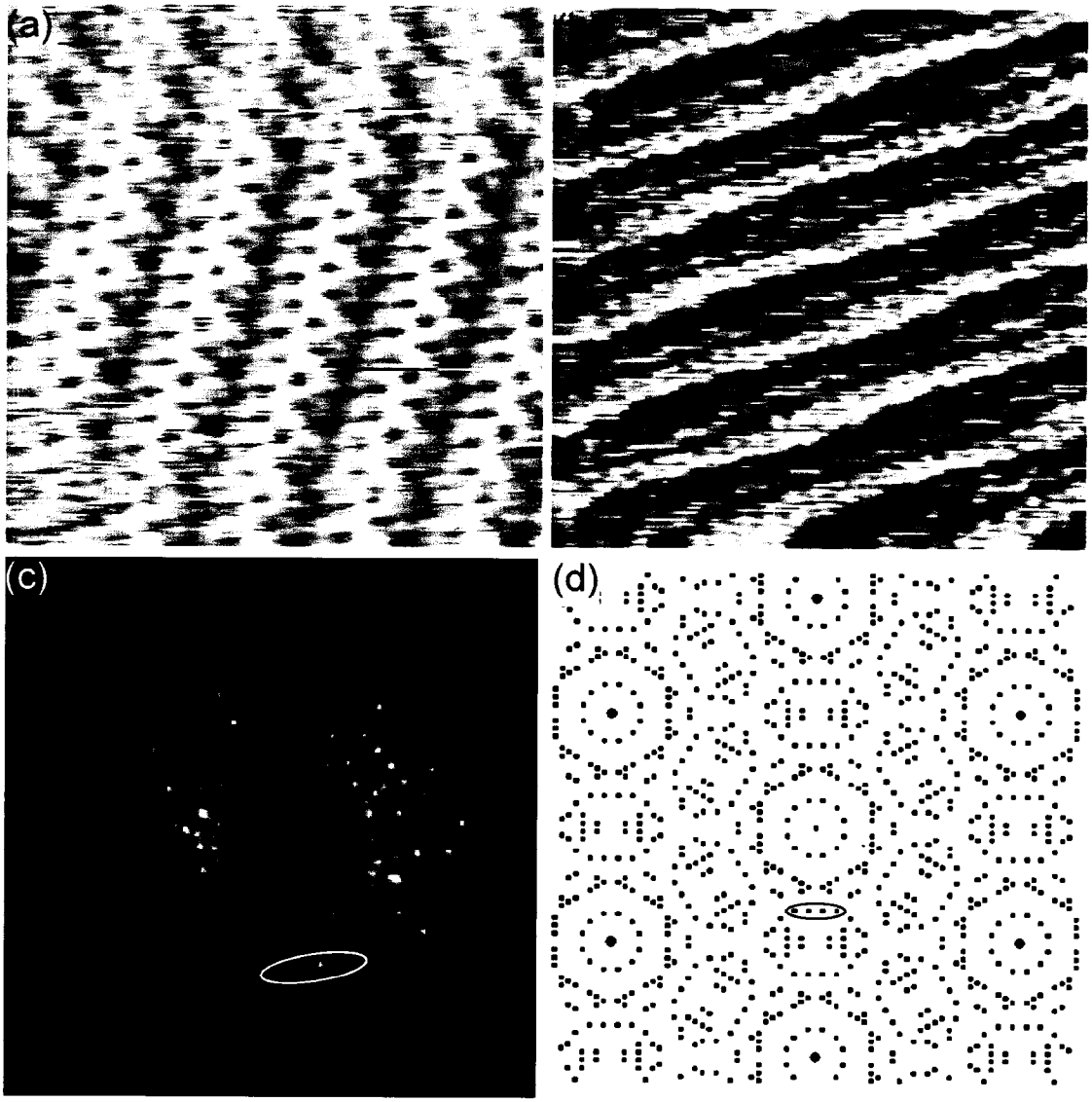

Fig. 6.12. Change of the surface structure from the '44'-structure at 423 K to the '29'-structure at 673 K. The surface with the '44'-structure was produced by the exposure of Cu(111) surface to oxygen at $3\text{-}4\times10^{-5}$ Pa for 60 minutes at 423 K. (a) The '44'-structure observed at 493 K in UHV (100×100 Å^2, V=500 mV, I=1 nA). (b) The '29'-structure observed at 573 K in UHV (100×100 Å^2, V=1000 mV, I=0.1 nA). (c) LEED pattern for the '29'-structure at primary energy of 55 eV (room temperature after 673 K anneal). The surrounded spots correspond to those in the calculated LEED pattern (d). (d) The reciprocal lattice plot for ($\sqrt{13}$ R46.1°×7R-21.8°) superlattice ('29'-structure).

6.3.2.4 The fine structure of the '29' adlayer

A well-ordered '29' surface was prepared on Cu(111) in a flow of O_2 at 5×10^{-5} Pa for 30 minutes at 673 K followed by annealing at 723 K for 5 minutes in UHV. Atomic resolution was not attained at 723 K, but was possible at room temperature, Fig. 6.13 (a). A well-ordered lattice is seen over an extended area to within ~20Å of the step edge which appear both linear (lower step) and a smoothly curved (upper step). Ordered atomic features were seen along the top of the step edge with some disordered structures at the boundary with the '29'-structure. This disordered part might be produced by accommodation of the strain in the overlayer or due to the difficulty in completing the large unit cell structure at the step edge. Fig. 6.13 (b) shows a magnified view of one of the terraces. The size and orientation of unit cell is the same as that of the '29'-structure. The Fourier transformation of Fig. 6.13 (b) is also identical to the reciprocal lattice of the '29'-structure. The inset structural model shows the relationship between the proposed positions of O and Cu atoms, represented with the filled and open circles respectively, and the STM image. LEED patterns for this surface observed at primary energies of 63, and 29 eV are shown in Fig. 6.13 (c) and (d), respectively. Again sharp diffraction spots were observed. This LEED pattern is identical to that of the '29'-structure. Fig. 6.13 (e) shows a proposed model of the '29'-structure, the unit cell is marked by the parallelogram. The dark spots in Fig. 6.13 (b) are assigned to the O atoms adsorbed on three-fold sites as observed for the '44'-structure (Fig. 6.6). The dark spots form a distorted hexagonal superstructure with a periodicity of ~ 6 Å which some similarity to the array of the O atoms of the Cu_2O (111) and the '44'-structure surfaces [42-44]. The distortion of the ideal hexagonal net of Cu-O are significant at the '29'-structure surface and result in the observation of bright stripes in the form of series of ×-shapes running just to the right of centre of the unit cell marked in Fig. 6.13 (b). These features indicate that the '29'- structure may be different from a complete layer of the simple hexagonal structures as

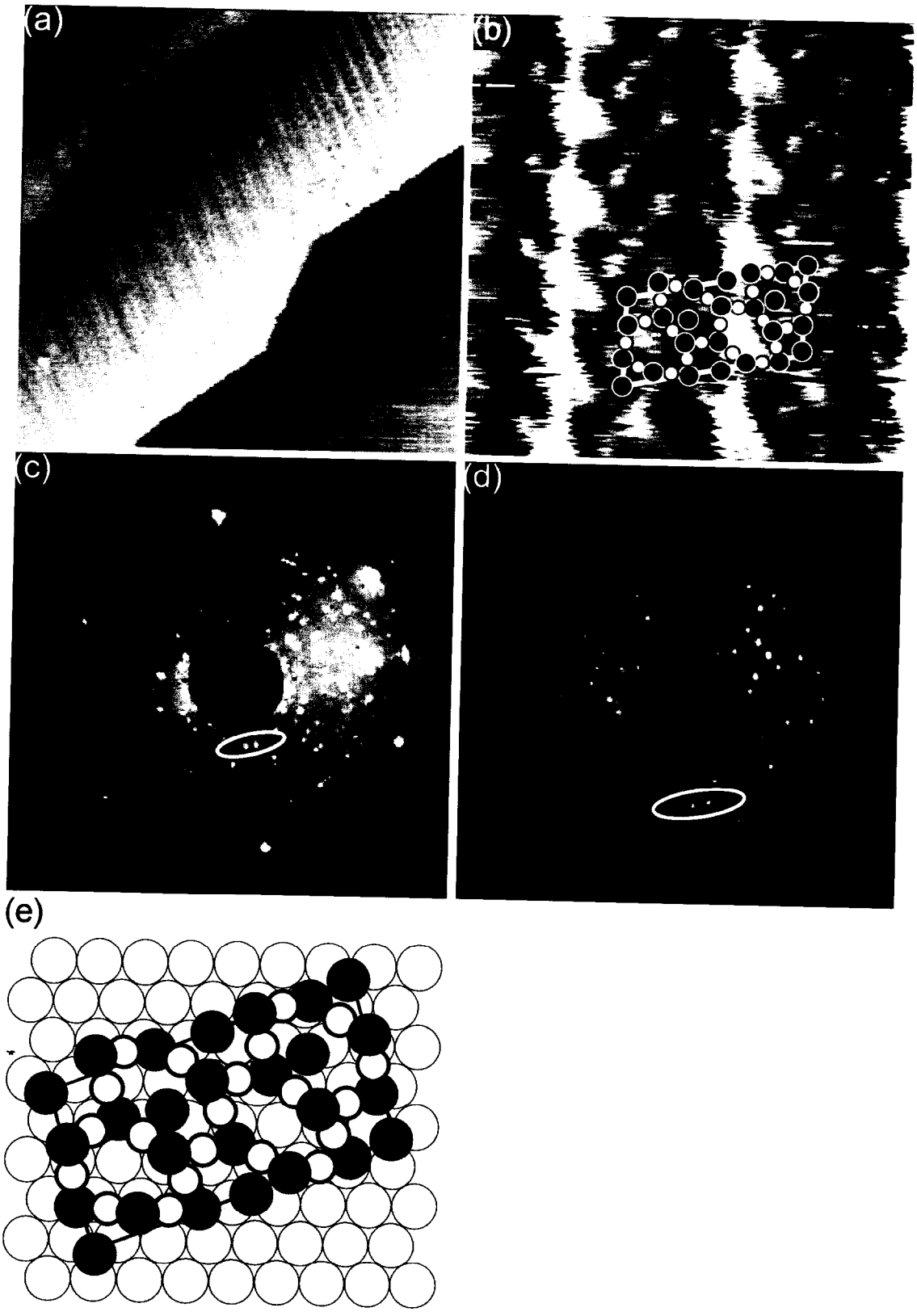
(a)
(b)
(c)
(d)
(e)

Fig. 6.13. STM images and LEED patterns for the '29'-structure at room temperature. This surface was produced by exposure of Cu(111) surface to oxygen at 5×10^{-5} Pa for 30 minutes at 673 K and sequent annealing at 723 K for 5 minutes. (a) STM image of the well-ordered surface in a large scale where both straight and curved step edges were observed (400×400 Å^2, V=700 mV, I=0.1 nA). (b) STM image at atomic resolution. The white parallelogram indicates the unit cell for the '29'-structure (43×43 Å^2, V=700 mV, I=0.03 nA). The filled and open circles indicate the speculated positions of O and Cu atoms, respectively. (c and d) LEED patterns at primary energy of 63 and 29 eV respectively. The surrounded spots correspond to those in Fig. 6.4 (d). (e) Proposed model of the '29'-structure. The parallelogram shows the unit cell of the '29'-structure. The filled and the open circles represent the O and Cu atoms, respectively. The filled black and grey circles indicate O atoms which adsorb on the three-fold sites of the light grey Cu(111) surface and O atoms forming the Cu-O nets in the STM images of Fig. 6.13 (b), respectively.

seen in the '44'-structure or $Cu_2O(111)$ surface. We propose that some hexagonal nets without central O atoms (filled black circles) are produced between the hexagonal Cu-O nets containing the dark centre O atoms. These missing oxygen atoms in the hexagonal array produce the visibly lighter ×-shapes in the STM images.

In this structure the surface density of the O atoms relative to the Cu atoms of the substrate for this model is 16/29=0.552, and very similar to 24/44=0.545, that for the '44'-structure. Thus conversion of the 44 to 29 structure requires little overall change in surface O atom density while the high mobility of Cu at elevated temperatures is sufficient to maintain stoichiometry. In comparison, the '44'-structure contains one center O atom in the bridge-site while all others are 3-fold coordinated whereas in the '29'-structure all center O atoms are assigned to the stable three-fold sites. The suggested model is proposed solely from the STM image and consideration of the relative ease of interconversion of the structures without gain or loss of oxygen. Corroborative structural techniques such as AFM (atomic force microscope), EXAFS (extended X-ray absorption fine structure), LEED-IV and XPD (x-ray photoelectron diffraction) would need to be employed to determine further detail of the '29'-structure.

6.3.2.5 Transformation of the '29'-structure to the '44'-structure by annealing at 773 K

The '29'-structure was formed by annealing the '44'-structure at 673 K, but the '44'-structure could be restored by annealing at 773 K in vacuum. This conversion was also reported previously [42-44]. The '29'-structure obtained for Fig. 6.13 was further annealed at 773 K for 5 minutes according to the recipe in these reports, and imaged to produce Fig. 6.14 (a). This surface was composed of many small rotational patches with an average diameter below 250 Å. The domain size in Fig. 6.14 (a) is obviously smaller than those for the original '29'-structure in Fig. 6.5. STM could not resolve each atom in the domains. Fig. 6.14 (b) shows a LEED pattern measured at primary energy of 54 eV. The complex spots observed in this pattern correspond to the '44'-structure, i.e. ($\sqrt{73}$R5.8°×$\sqrt{21}$R-10.9°). It has been reported in the previous work [42-44] that annealing the '29'-structure produced the '44' -structure is reproduced.

The '44'-structure was changed to the '29'-structure, and returned to the '44'-structure again as the annealing temperature increased. However, these two '44-structures are different from each other in detail. The '44'-structure produced by annealing a '29' surface at 773 K had smaller domains than those formed by adsorption of O_2 on the clean surface below 573 K. The small domains were separated by disordered regions which may be formed by out diffusion of Cu from the substrate or dissolution of oxygen in the bulk.

The '44'-structure produced at 423-623 K was transformed to the '29'-structure at 573-673 K. This surface appeared uncorrugated at 773 K presumably because of rapid diffusion of surface species. The Cu(111) surface oxidized at 300 K was annealed at 623 K where the '29'-structure is expected to be observed but could not be observed at atomic resolution. These uncorrugated surfaces were found to have the '44'-strucrture at 300 K indicating that rapid diffusion stopped below the temperature for production of the '29'-structure to form the '44'-structure.

6.3.2.6 Reoxidation of the disordered surface

Disordered oxide layers can be ordered by exposure to O_2 at high temperature. We prepared a disordered O/Cu(111) surface by room-temperature adsorption of O_2 on clean Cu(111) at 1-4×10^{-4} Pa for 30 minutes and annealing at 723 K in vacuum. Then this disordered surface was reoxidized in a flow of O_2 at 1×10^{-4} Pa at 673 K for 15 minutes. A large area of the resulting surface is shown in the STM image of Fig. 6.15 (a). The surface is now well-ordered over a large area. Each terrace was often covered by one domain which is several hundreds of angstroms wide. The size of one domain was much larger than that shown in Fig. 6.14 (a). The morphology was observed at atomic resolution and exhibited the '44'-structure. Fig. 6.15 (b) is a LEED pattern at primary energy with 29 eV and identical to the reciprocal lattice plot for the '44' structure in Fig. 6.6 (e). By mobilizing the surface species by high temperature and O_2 impingement, the disordered surface was changed to the well-ordered '44'-structure.

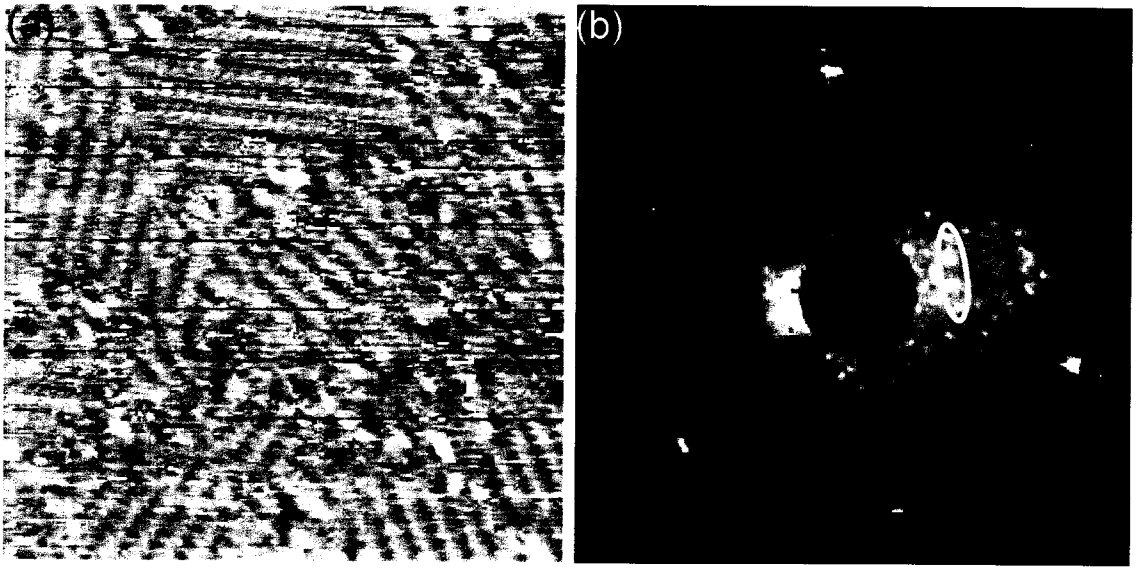

Fig. 6.14. The results of annealing the surface shown in Fig. 6.13 at 773 K for 5 minutes. (a) STM images at room temperature showing many small domains and disordered background (500×500 Å^2, V=1000 mV, I=0.4 nA). (b) LEED pattern at primary energy of 54 eV. This pattern is assigned to the '44'-structure and the surrounded spots correspond to those in Fig. 6.6 (e).

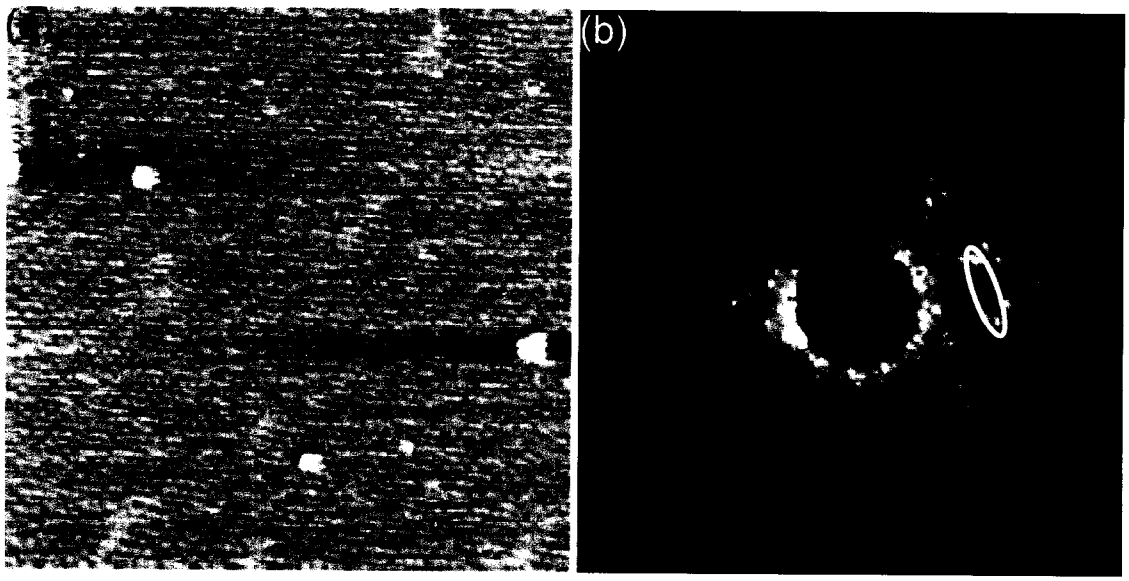

Fig. 6.15. STM image and LEED pattern for a reoxidized disordered oxide surface which was produced by oxidation in a flow of oxygen at 1-4×10^{-5} Pa for 30 min at room temperature and annealed at 723 K for 20 min (shown in Fig. 6.8 (b)). The surface presented here was produced by re-exposure to oxygen at 2-7.3×10^{-5} Pa at 673 K for 15 min. (a) STM image with the '44'-structure in a large scale (500×500 Å^2, V=800 mV, I=0.04 nA). (b) LEED pattern at primary energy of 47 eV. This pattern is assigned to the '44'-structure and the surrounded spots correspond to those in Fig. 6.6 (e).

6.4 Conclusion

The O_2 adsorption on Cu(111) surface at room temperature was investigated using STM. The step edges were observed to be etched to form an oxide attached to the step edges. Small vacancy islands on the terraces rapidly oxidized to form triangular islands that grow with exposure to oxygen by ejection of Cu in a one dimensional reaction propagating along the newly created step edges. Cu atoms were also released from the step edges as oxidation proceeded. Diffusing O and Cu atoms aggregated to produce added oxide islands on top of the terraces. This added oxide overlayer encouraged the displacement of Cu atoms from the terrace, forming new triangular oxide islands growing in the terrace. The Cu(111) surface displayed poorly ordered structures when oxidized at room temperature but was ordered by annealing at 473 K. Annealing also resulted in significant changes in surface morphology, with the removal of all angular features at step edges. By further annealing at 723 K, the surface again exhibits poorly ordered features, due to loss of oxygen either into the Cu bulk or to the background gas.

O_2 adsorption on the Cu(111) surface at elevated temperatures was also observed. An oxygen structure was formed, starting from the step edges, by treatment in oxygen at surface temperatures above 373 K. The '44'-structure was produced at 423 K, which is a lower temperature than that reported previously [42-44]. The '44'-structure produced by oxidation at 423-573 K changed to the '29'-structure by annealing at 673 K in UHV. We have presented evidence for and proposed a new model for the "29"-structure. The '29'-structure could be returned to the '44'-structure by annealing at 773 K in vacuum. Disordered oxide layers on Cu(111) formed at room temperatures and annealed at 723 K can order upon exposure to O_2 at high temperatures.

References

[1] R. Feidenhans'l, F. Grey, M. Nielsen, F. Besenbacher, F. Jensen, E. Lægsgaard, K. W. Jacobsen, J. K. Nørskov and R. L. Kohnson, Phys. Rev. Lett. 65 (1990) 2027.

[2] D. J. Coulman, J. Wintterlin, R. J. Behm and G. Ertl, Phys. Rev. Lett. 64 (1990) 1761.

[3] Y. Kuk, F. M. Chua, P. J. Silverman and J. A. Meyer, Phys. Rev. B 41 (1990) 12393.

[4] F. Jensen, F. Besenbacher, E. Lægsgaard and I. Stensgaard, Phys. Rev. B 41 (1990) 10233.

[5] D. J. Coulman, J. Wintterlin, J. V. Barth, G. Ertl and R. J. Behm, Surf. Sci. 240 (1990) 151.

[6] F. Jensen, F. Besenbacher, E. Lægsgaard and I. Stensgaard, Phys. Rev. B 42 (1990) 9206.

[7] M. Bowker, S. Poulston, R. A. Bennett and P. Stone, J. Phys. Condens. Matter. 10 (1998) 7713.

[8] M. Bowker, R. A. Bennett, S. Poulston and P. Stone, Catal. Lett. 56 (1998) 77.

[9] A. H. Jones, S. Poulston, R. A. Bennett, M. Bowker, Surf. Sci. 380 (1997) 31.

[10] F. M. Leibsle, S. M. Francis, R. Davis, N. Xiang, S. Haq and M. Bowker, Phys. Rev. Lett. 72 (1994) 2569.

[11] F. M. Leibsle, S. M. Francis, S. Haq and M. Bowker, Surf. Sci. 318 (1994) 46.

[12] S. M. Francis, F. M. Leibsle, S. Haq, N. Xiang and M. Bowker, Surf. Sci. 315 (1994) 284.

[13] F. M. Leibsle, P. W. Murray, S. M. Francis, G. Thornton and M. Bowker, Nature. 318 (1993) 706.

[14] C. Barnes, P. Pudney, Q. Guo and M. Bowker, J. Chem. Soc. Faraday Trans. 86 (1990) 2693.

[15] S. L. Silva, R. M. Lemor and F. M. Leibsle. Surf. Sci. 421 (1999) 135.

[16]S. L. Silva, R. M. Lemor and F. M. Leibsle, Surf. Sci. 421 (1999) 146.

[17] F. M. Leibsle, J. Phys. Condens. Matter. 9 (1998) 8787.

[18] P. R. Davies and G. G. Mariotti. Catal. Lett, 46 (1997) 133.

[19] P. R. Davies and G. G. Mariotti, J. Phys. Chem. 100 (1996) 19975.

[20] A. F. Carley, P. R. Davies, G. G. Mariotti, S. Read, Surf. Sci. 364 (1996) L525.

[21] I. E. Wachs and R. J. Madix, J. Catal. 53 (1978) 208.

[22] J. Kubota, J. N. Kondo, K. Domen, C. Hirose, J. Phys. Chem. 98 (1994) 7653.

[23] D. A. Outka, C. M. Friend, S. Jorgensen and R. J. Madix, J. Am. Chem. Soc. 105 (1983) 3468.

[24] P. Stone, S. Poulston, R. A. Bennett, N. J. Price and M. Bowker, Surf. Sci. 418 (1998) 71.

[25] R. A. Bennett, S. Poulston and M. Bowker, J. Phys. Chem. 108 (1998) 6916.

[26] S. Poulston, A. Jones, R. A. Bennett and M. Bowker, Surf. Sci. 377 (1997) 66.

[27] M. Bowker, S. Poulston, R. A. Bennett, P. Stone, A. H. Jones, S. Haq and P. Hollins, J. Mol. Catal. A131 (1998) 185.

[28] M. Bowker, S. Haq, R. Holroyd, P. M. Parlett, S. Poulston and N. Richardson, J. Chem. Soc. Faraday. Trans. 92 (1996) 4638.

[29] M. Bowker, E. Rowbotham, F. M. Leibsle and S. Haq. Surf. Sci, 349 (1996) 97.

[30] F. M. Leibsle and S. Haq, B. G. Frederick, M. Bowker, N. V. Richardson, Surf. Sci. 343 (1995) L1175.

[31] S. Haq and F. M. Leibsle, Surf. Sci. 375 (1997) 81.

[32] B. A. Sexton, A. E. Hughes and N. R. Avery. Surf. Sci. 155 (1985) 366.

[33] K. R. Lawress and A. T. Gwathemy, Acta. Metal. 4 (1956) 153.

[34] J. H. Ho and R. W. Vook, J. Crystal. Growth. 44 (1978) 561.

[35] McDonnell and D. P. Woodruff, Surf. Sci. 46 (1974) 505.

[36] G. Ertl, Surf.Sci. 6 (1967) 208.

[37] G. W. Simmons, D. F. Mitchell and K. R. Lawless, Surf. Sci. 8 (1967) 130.

[38] T. Delcher and F. C. Tompkins, Surf. Sci. 8 (1967) 165.

[39] A. Oustry, L. Lafourceade and A. Escaut, Surf. Sci. 40 (1973) 545.

[40] A. Spitzer and H. Lüth, Surf. Sci. 118 (1982) 136.

[41] R. W. Judd, P. Hollins and J. Pritchard, Surf. Sci. 171 (1988) 643.

[42] F. Jensen, F. Besenbacher, E. Lægsgaard and I. Stensgaard, Surf. Sci. 259 (1991) L781.

[43] F. Jensen, F. Besenbacher and I. Stensgaard, Surf. Sci. 269/270 (1992) 400.

[44] F. Besenbacher and J. K. Nørskov, Prog. in Surf. Sci. 44 (1993) 5.

[45] T. Matsumoto, J. Kubota, J. N. Kondo, C. Hirose and K. Domen, Langmuir. *in prepararion*

[46] L. H. Dubois, Surf. Sci. 119 (1982) 399.

[47] F. H. P. M. Habraken, E. Ph. Kieffer and G. A. Bootsma, Surf. Sci. 83 (1979) 45.

[48] H. Niehus, Surf. Sci. 130 (1983) 41.

[49] S. M. Thurgate and P. J. Jennings, Surf. Sci. 131 (1983) 309.

7 Adsorption and decomposition of formic acid on an ordered oxidized Cu(111) surface

Abstruct

The decomposition of formic acid on the well-ordered oxidized Cu(111) with the '29'-structure was examined by temperature programmed desorption (TPD), and infrared reflection absorption spectroscopy (IRAS). Formic acid dissociated to formate around 173 K, and the D atoms released during the dissociation of DCOOD were observed to desorb as D_2O at 173 K with reducing the surface by TPD and IRAS experiments. Formate decomposed to desorb as D_2O and CO_2 at 378 K reacting with surface oxygen, and also as D_2 and CO_2 at 387 K. These reaction temperatures were lower than those on the other metallic and oxidized copper surfaces reported previously.

7.1 Introduction

Formate on copper and copper oxide has been regarded as an important intermediate of various catalytic reactions such as water gas shift reaction, methanol synthesis, and methanol oxidation. Oxygen atoms on surfaces are also known to act as a key species. The decomposition reaction of formate species formed by dissociative adsorption of formic acid has been studied on Cu(100) [1], Cu(110), Cu(110)-O(2×1), Cu_2O, and CuO surfaces [2, 3]. As the (111) surface is considered to be the most stable of copper surfaces, it is important to study the behavior of formate on the oxidized Cu(111) surface. It was reported that the (111) plane of Cu_2O film produced on Cu(111) is parallel to the Cu(111) plane [4-7]. However, the surface structure is sensitive and changes depending on the oxidation condition. Various ordered surface structures have been observed on the oxidized Cu(111) surfaces by the oxidation at elevated temperatures [8-16], and only disordered structure was

found by the oxidation at room temperature [17-19]. Due to the diversity of the oxidized surface structures, researchers refrained from studying chemical reactions on the ordered oxidized Cu(111) surfaces except for the CO adsorption [20]. The structure of adsorbate has also rarely been examined on these surfaces using vibration spectroscopies.

The '29'-structure is one of the ordered structures of the oxidized Cu(111) surfaces, and resembles the structure of the $Cu_2O(111)$ surface in the position of oxygen atoms [14-16]. The unit cell of the $Cu_2O(111)$ surface consists of the oxygen atoms located regular-hexagonally at the top layer. The unit cell of the '29'-structure is 29 times larger than that of the Cu(111) surface, and includes a hexagonal structure distorted from the unit cell of the $Cu_2O(111)$ surface. In this study, the decomposition temperature of formic acid on the oxidized Cu(111) surface with the '29'-structure was revealed to be lower than those on oxidized Cu(110) and Cu(100) surfaces. The reaction mechanism is discussed in this report.

7.2 Experimental

The copper single crystal was supported by Ta wires through the holes of a sample piece. The Cu(111) surface was prepared by the Ar sputtering at 573 K and annealing at 973 K. IRA spectra were acquired using JEOL JIR-100 Fourier transform infrared spectrometer (FTIR) equipped with an InSb/MCT composite detector. The resolution was 4 cm^{-1}, and the signals were averaged over 512 scans.

7.3 Results and discussion

The oxidized Cu(111) surface was produced by the exposure of Cu(111) to oxygen at 773 K and 12000 L (6×10^{-5} Torr×200 s; 1 Torr=133 Pa; L=10^{-6} Torr×s). The structure and the amount of oxygen on the surface were examined using low energy electron diffraction (LEED) and Auger electron spectroscopy (AES), respectively.

The observed LEED pattern of the oxidized Cu(111) surface is shown in Figs. 7.1 (a) and (b) with primary electron beam energies of 24 and 100 eV, respectively. Fig. 7.1 (c) shows a reference LEED pattern for Cu(111) with a primary energy of 100 eV. The LEED spots in Fig. 7.1 (b) which are located almost at the same position as those for Cu(111) in Fig. 7.1 (c) are possibly due to the Cu(111) surface structure of substrate. The LEED spots observed in this study were basically consistent with those for the six equivalent domains of the '29'-structure [14-16] varying by rotation and reflection due to the substrate symmetry. These LEED spots diffused and disappeared around 450 K by heating, and were recovered by cooling. The Auger spectra of this surface was also obtained, and the Auger intensity ratio of $O(KL_{23}L_{23})$ to $Cu(L_3M_{45}M_{45})$ was found to be about 0.6. The relative Auger sensitivity $O(KL_{23}L_{23})$ to $Cu(L_3M_{45}M_{45})$ is known to be about 2.5 indicating that the ratio of the numbers of oxygen atoms to copper atoms detected by AES is less than 0.5 [21]. The composition of oxygen atoms to copper atoms for the '29'-structure surface is known to be about 0.5 [15]. The present oxide film is thought to have a few monolayer thickness which is less than the attenuation length of Auger electron [21].

Fig. 7.2 shows a temperature programmed desorption (TPD) spectra acquired after the exposure of the oxide surface to DCOOD at the stated amounts at 110 K. Mass signals were observed for D_2 (m/e=4), D_2O (m/e=20), CO (m/e=28), CO_2 (m/e=44), and DCOOD (m/e=48). The CO signals were not detected except for the fragment of DCOOD and CO_2 produced in quadrupole mass spectrometer (QMS). The desorption peaks of D_2O, CO_2, and DCOOD appeared at 157 K are due to DCOOD from the multilayer. D_2O desorption peak was observed at 173 K, and is considered to result from the desorption of D_2O and not the fragment of DCOOD. The sharp peaks at 378 K were observed for D_2O and CO_2, and the peaks at 387 K for D_2 and CO_2. The peaks at 378 and 387 K are supposed to be due to the reaction of formate and the oxygen atoms on the surface and to the decomposition reaction of remaining formate,

Fig. 7. 1 LEED spots observed for the oxidized Cu(111) surface with primary energies of 24 eV (a), and 100 eV (b), and that observed for Cu(111) surface with primary energy of 100 eV (c).

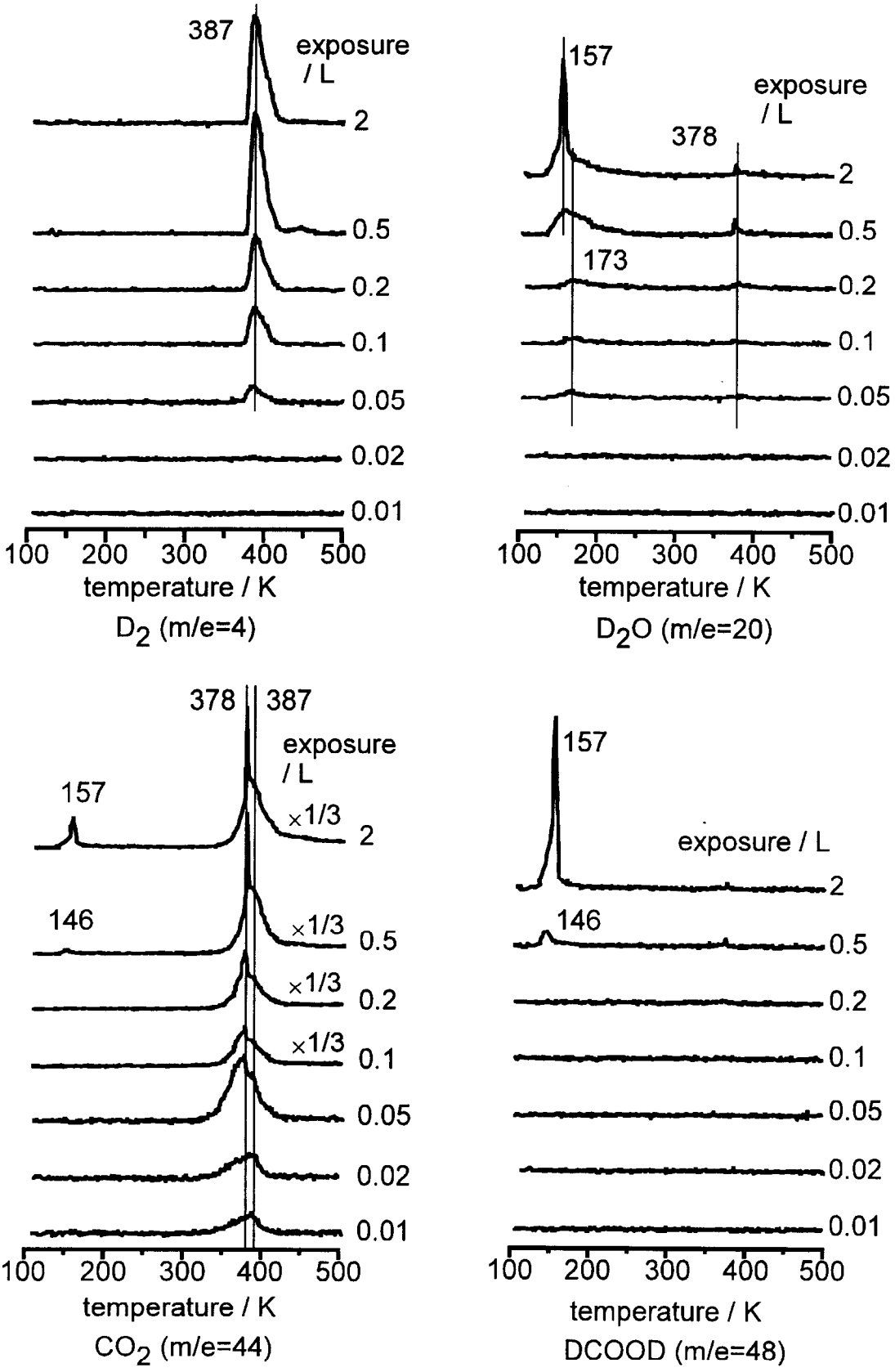

Fig. 7.2. TPD spectra of DCOOD on a well-ordered oxidized Cu(111) surface after the exposure at the stated exposure and 110 K. The heating rate was 1 K/s.

respectively. The desorption peak at 378 K is much sharper than that at 387 K. The sharpness of the peak may indicate that the reaction at 378 K is self-promoted (auto-catalytic) [22].

Temperature dependence of IRA spectra of the oxidized Cu(111) surface with the '29'-structure exposed to 2 L DCOOD at 110 K is shown in Fig. 7.3. The two bottom spectra were observed at 110 K and 165 K, and the other spectra at 240 K after flashing the surface to the indicated temperatures. The peaks assignable to the bands of DCOOD multilayer were observed at 110 K. The peaks at 2222, 2110, 2052, 1708, 1257, 997, 901, and 723 cm^{-1} are assigned to ν(C-D), δ(C-D)+π(O-D), ν(O-D), ν(C=O), ν(C-O), δ(C-D), π(C-D), and π(O-D) [23, 24]. (ν; stretching mode, δ; deformation mode, π; out-of-plane bending mode.) The DCOOD peaks almost disappeared at 165 K, which corresponds to the desorption of DCOOD multilayer at 157 K as observed in the TPD experiment. The peaks appeared at above 165 K are assigned to the vibrational modes of formate. The peaks at 2175-2171, 1672-1570, 1336-1317, and 768-762 cm^{-1} are assigned to ν(C-D), ν_{as}(OCO), ν_s(OCO), and δ(C-D) [25]. (ν_{as}; antisymmetric stretching mode, ν_s; symmetric stretching mode). It is considered that formic acid dissociates to form formate around 173 K where the D_2O desorption was observed on the TPD spectrum. The formate observed at above 340 K is thought to be a bidentate or a bridge type from the difference of the frequencies between the antisymmetric and symmetric OCO stretching modes [26]. The transition dipole moment of the antisymmetric OCO stretching band is perpendicular to the molecular axis (the C-H bond). Some molecular axes of formate molecules are considered to tilt from the surface normal at 370 K because only the vibrations containing its component vertical to the surface is active for IRAS [27]. The asymmetric OCO stretching peak disappeared but the other formate peaks remained at 380 K. The molecular axis of formate observed at 380 K are considered to be vertical to the surface since the transition dipole moments of the C-D stretching, the symmetric OCO

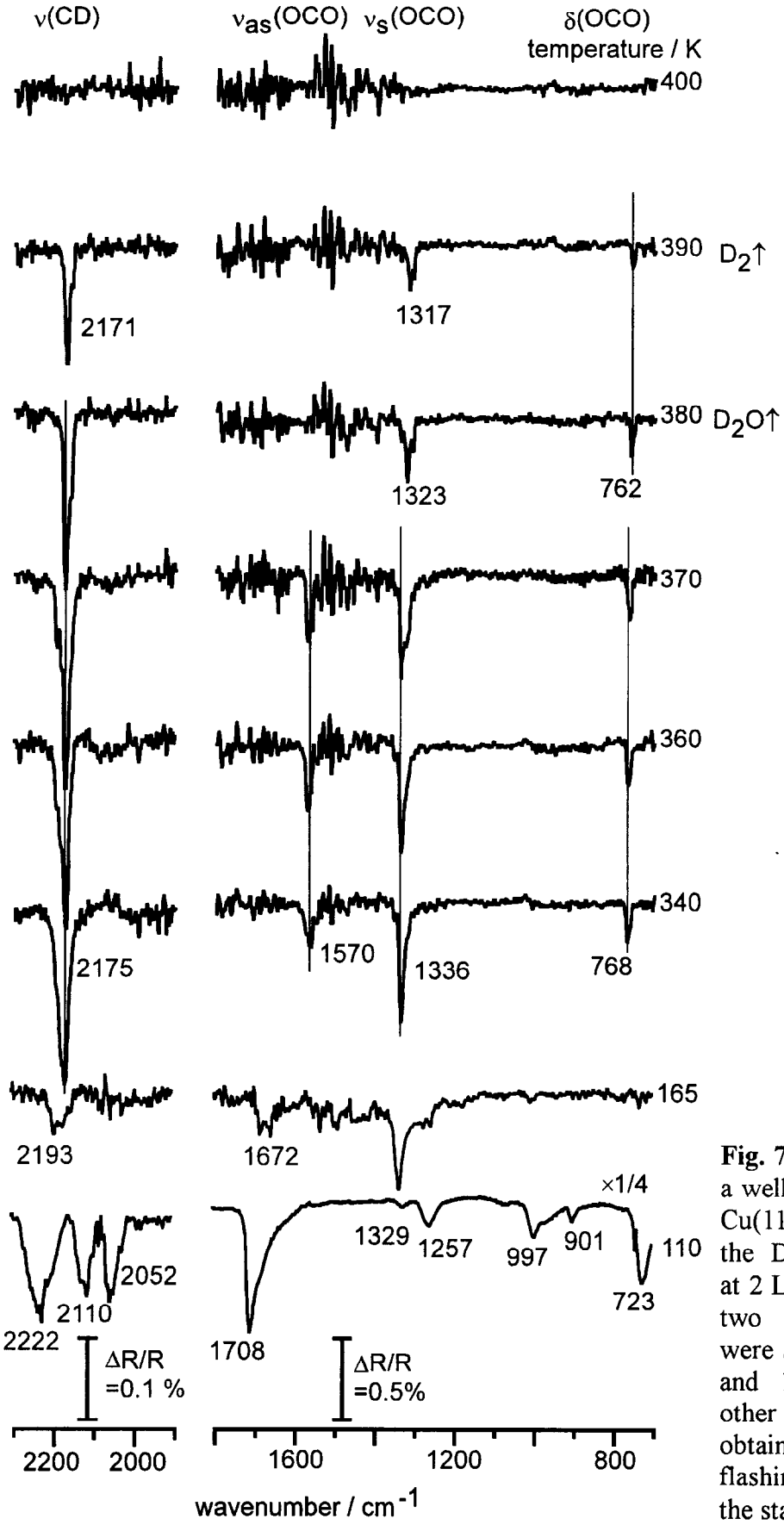

Fig. 7.3. IRA spectra of a well-ordered oxidized Cu(111) surface after the DCOOD exposure at 2 L at 110 K. The two bottom spectra were acquired at 110 K and 165 K, and the other spectra were obtained at 240 K after flashing the surface to the stated temperatures.

stretching, and the OCO deformation modes of formate are parallel to the molecular axis. Thus, two kinds of formate species were conceivable on the surface, and it is suggested that the tilted formate decomposed to produce D_2O and CO_2 at 378 K and the standing formate was dehydrogenated to produce D_2 and CO_2 at 387 K. The oxidation and the dehydrogenation of formate were reported on the other oxidized and metallic copper surfaces as listed in Table 7.1. The reaction temperatures of formate on the oxidized Cu(111) surface are lower than those for the Cu(100), Cu(110), and Cu(110)-O(2×1) surfaces.

Main reaction pathways observed in this study are summarized as follows.

$$DCOOD\ (multilayer) \rightarrow DCOOD(g) \qquad \text{at 157 K}$$

$$2DCOOD(a)+O(a) \rightarrow 2DCOO(a)+D_2O(g) \qquad \text{at 173 K}$$

$$2DCOO(a)+O(a) \rightarrow 2CO_2(g)+D_2O(g) \qquad \text{at 378 K}$$

$$2DCOO(a) \rightarrow 2CO_2(g)+D_2(g) \qquad \text{at 387 K}$$

No LEED spots were observed after flashing to 400 K. This indicates that the surface structure was disordered with the decomposition of formic acid.

Table 7.1. Reaction temperatures for the oxidation and dehydrogenation of formic acid on copper and oxidized copper surfaces.

Sample	Temperature / K	Reference
Oxidation reaction		
oxidized Cu(111)	378	in this study
powdered CuO	390	[2]
powdered Cu_2O	510	[2]
Dehydrogenation reaction		
oxidized Cu(111)	387	in this study
Cu(100)	490	[1]
Cu(110)	450	[2]
Cu(110)-O(2×1)	410, 450	[2]

7.4 Conclusion

The oxidized Cu(111) surface with the '29'-structure was prepared by the exposure to oxygen at 12000 L at 773 K. Formic acid adsorbed molecularly on the oxidized Cu(111) surface at 110 K, and dissociated to formate with reducing the surface at 173 K. The formate reacted with the oxygen atoms on the surface to form D_2O and CO_2 at 378 K, and was dehydrogenated to form D_2 and CO_2 at 387 K. These reaction temperatures were lower than those on the other metallic and oxidized copper surfaces. The structure of the oxidized Cu(111) surface was disordered by the decomposition of formic acid.

References

[1] L. H. Dubiois, T. H. Ellis, B. R. Zegarski and S. D. Kevan, Surf. Sci. 172 (1986) 385.

[2] M. Bowker, E. F. Rowbotham, M. Liebsle and S. Haq, Surf Sci. 349 (1996) 97.

[3] J. Lin, K. G. Neoh and W. K. Teo, J. Chem. Soc. Faraday. Trans. 90 (1994) 355.

[4] K. R. Lawress and A. T. Gwathemy, Acta. Metal. 4 (1956) 153.

[5] J. H. Ho and R. W. J. Vook, J. Crystal. Growth. 44 (1978) 561.

[6] L. McDonnell and D. P. Woodruff. Surf. Sci. 46 (1974) 505.

[7] L. H. Dubois, Surf.Sci. 119 (1982) 399.

[8] G. Ertl, Surf.Sci. 6 (1967) 208.

[9] G. W. Simmons, D. F. Mitchell and K. R. Lawless, Surf. Sci. 8 (1967) 130.

[10] T. Delcher and F. C. Tompkins, Surf.Sci. 8 (1967) 165.

[11] A. Oustry, L. Lafourceade and A. Escaut, Surf.Sci. 40 (1973) 545.

[12] A. Spitzer and H. Lüth, Surf.Sci. 118 (1982)136.

[13] R. W. Judd, P. Hollins and J. Pritchard. Surf. Sci. 171 (1988) 643.

[14] F. Jensen, F. Besenbacher, E. Lægsgaard and I. Stensgaard, Surf. Sci. 259 (1991) L781.

[15] F. Jensen, F. Besenbacher and I. Stensgaard. Surf. Sci. 269/270 (1992) 400.

[16] F. Besenbacher and J. K. Nørscov. Prog. Surf. Sci. 44 (1993) 5.

[17] F. H. P. M. Habraken, E. Ph. Kieffer and G. A. Bootsma, Surf.Sci. 83 (1979) 45.

[18] H. Niehus, Surf. Sci. 130 (1983) 41.

[19] S. M. Thurgate and P. J. Jennings, Surf. Sci. 131 (1983) 309.

[20] P. Hollins and J. Pritchard, Surf. Sci. 134 (1983) 91.

[21] D.; Briggs, M. P. Segh: Practical surface analysis (John Wiley & Sons Ltd., England, 1983.)

[22] R. J. Madix, J. L. Gland, G. E. Mitchell and B. A. Sexton, Surf Sci. 125 (1983) 481.

[23] R. C. Millikan and K. S. Pitzer, J. Am. Chem. Soc. 80 (1958) 3515.

[24] Y. Mikawa, J. W. Brasch and R. J. Jakobosen, J. Mol. Spectrosc. 24 (1967) 314.

[25] T. Matsumoto, A. Bandara, J. Kubota, C. Hirose and K. Domen, J. Phy. Chem. B102 (1998) 2979.

[26] T. Shido and Y. Iwasawa, J. Catal. 141 (1993) 71.

[27] F. M. Hoffmann, Surf. Sci. Rep. 3 (1983) 107.

8 Concluding remarks and outlook

The formation of oxide thin films on the Ni(111) and Cu(111) surfaces were observed using scanning tunneling microscopy (STM) and low energy electron diffraction (LEED). The chemical reactions on their oxide surfaces were investigated by temperature programmed desorption (TPD) and infrared reflection absorption spectroscopy (IRAS). Adsorption and decomposition of formic acid and carbon dioxide were observed on NiO(111)/Ni(111), and decomposition of formic acid was observed on oxidized Cu(111) surfaces.

In chapter 3, the oxidation process of the Ni(111) surface and the structure of the oxidized Ni(111) surface were observed at elevated temperature by LEED and STM. Two oxidation processes were observed at 573 K; the first process is the formation of the flat oxide layer on Ni(111) terraces and the second is the formation of small islands on the flat oxide. On the surface of the small islands, the (2×2)-NiO(111) structure was observed over the area having a few nanometers width after flashing to 623 K the surface oxidized at 573 K.

In chapter 4, the decomposition of formic acid was studied on NiO(111)/Ni(111) by TPD and IRAS. Formic acid molecules adsorbed dissociatively on the surface to form formate which decomposed to H_2, CO_2, H_2O, and CO at 340-415 and 520 K. The sites of decompositions at 340-415 and 520 K were revealed to be the fully-oxidized Ni cation sites and less-oxidized Ni cation sites, respectively.

In chapter 5, the adsorption of CO_2 on NiO(111)/Ni(111) and OD/NiO(111)/Ni(111) was studied by IRAS. Monodentate carbonate was observed, and the molecular geometry of CO_2 changed by the weak perturbation with hydroxyl species.

In chapter 6, the adsorption of oxygen on Cu(111) was investigated by STM and LEED. Three oxidation steps were found at room temperature, and the one step at elevated temperature. The oxide islands similar to the Cu_2O(111) structure was observed after oxidation at 300 K. The ordered '44'- and '29'-structures were observed at elevated temperatures, and the models of their structures are suggested.

In chapter 7, the decomposition of formic acid on the oxidized Cu(111) surface with the '29'-structure was studied by TPD and IRAS. Formic acid dissociated to formate at around 173 K with reducing the surface. Formate decomposed to D_2O and CO_2 at 378 K by the reaction with surface oxygen, and to D_2 and CO_2 at 387 K.

These reaction temperatures are lower than those on the other metallic and oxidized copper surfaces reported previously.

The surface structures and the formation process of oxide thin films on Ni(111) and Cu(111) reflect the substrate structure, temperature, and the coverage of O atoms. The Ni(111) and the Cu(111) surfaces are considered to be stable form the coordination number of the atoms at the surface. However, the oxide thin films produced on their metal surfaces could be polar surfaces due to epitaxy, and they are very active for decomposition of formic acid. Formic acid on their oxide surfaces dissociatively adsorbs at low temperature, and decomposes depending on the surface conditions.

Publication list

Chapter 3

[1] T. Matsumoto, J. Kubota, J. N. Kondo, M. Hara, C. Hirose and K. Domen: STM observation of NiO(111)/Ni(111) and NiO(100)/Ni(111), *in preparation.*

Chapter 4

[2] T. Matsumoto, W. A. Bandara, J. Kubota, C. Hirose and K. Domen: Adsorption and reaction of formic acid on a (2×2) NiO(111)/Ni(111) surface. 3. IRAS studies on the characterization of reaction sites using CO and the behavior of surface hydroxyl species, J. Phys. Chem. B, 102 (1998) 2979-2984.

[3] T. Matsumoto, W. A. Banadara, J. Kubota, C. Hirose and K. Domen: IRAS observation of decomposition of formic acid on NiO(111)/Ni(111), J. Surf. Sci. Soc. Japan, 18 (1997) 435-440.

Chapter 5

[4] T. Matsumoto, J. Kubota, J. N. Kondo, C. Hirose and K. Domen: Adsorption structures of carbon dioxide on NiO(111) and hydroxylated NiO(111) studied by infrared reflection spectroscopy, Langmuir, 15 (1999) 2158-2161.

Chapter 6

[5] T. Matsumoto, P. Stone, R. Bennett, T. Yamada, K. Domen and M. Bowker: STM observation of oxygen adsorption on Cu(111), Studies in Surf. Sci. and Catal. *in press.*

[6] T. Matsumoto, P. Stone, R. Bennett, T. Yamada, K. Domen and M. Bowker: STM studies of oxygen adsorption on Cu(111), Surf. Sci. 471 (2001) 225-245.

Chapter 7

[7] T. Matsumoto, J. Kubota, J. N. Kondo, C. Hirose, K. Domen, T. Yamada, P. Stone, R. Bennett, and M. Bowker: Adsorption and decomposition of formic acid on an ordered oxidized Cu(111) surface, *in preparation.*

Reference Paper

[8] M. Endo, T. Matsumoto, J. Kubota, K. Domen and C. Hirose: In-situ IRAS observation of catalytic deep oxidation of methanol on Pt(111) under ambient pressure conditions, J. Phys. Chem. B. *in press.*

[9] M. Kato, T. Matsumoto, J. Kubota, J. N. Kondo, C. Hirose and K. Domen: IRAS study of adsorbed formic acid on a chromium oxide film grown on Cr(110), J. Surf. Sci. Soc. Japan, 21 (2000) 438-439.

[10] M. Endo, T. Matsumoto, J. Kubota, K. Domen and C. Hirose: Formation of formate in the deep oxidation of methanol on Pt(111) under UHV condition studied by IRAS, J. Phys. Chem. B, 104 (2000) 4916-4922.

[11] M. Endo, T. Matsumoto, J. Kubota, K. Domen and C. Hirose: Oxidation of methanol by molecularly adsorbed oxygen on Pt(111) under vacuum and ambient pressure conditions studied by infrared reflection absorption spectroscopy: identification of formate intermediate, Surf. Sci. Lett., 441 (1999) L931-L937.

[12] T. Matsumoto, J. Kubota, J. N. Kondo, C. Hirose and K. Domen: Ammonia decomposition by UV-light irradiation on NiO(111)/Ni(111), *in preparation.*

Acknowledgement

I wish to express my most sincere appreciation to Professor Kazunari Domen of Tokyo Institute of Technology for giving me opportunity for challenging researches and tolerant guidance.

I am truly grateful to Professor Chiaki Hirose, Professor Akihide Wada, Professor Michikazu Hara, Dr. Junko N. Kondo, Dr. Jun Kubota, Dr. Ken Onda, and Dr. Toshio Kamisuki of Tokyo Institute of Technology for important supports and suggestions.

I am greatly indebted to Professor Michael Bowker, Dr. Roger Bennett, and Dr. Peter Stone of University of Reading in UK for instruction in STM experiment, patient discussion and the hospitality in UK.

I owe a debt of gratitude to Professor Taro Yamada of Waseda University taking much time for discussion on the analysis of STM results.

I thank Ms. Malisa Williams without end for training me in English.

I deeply appreciate that Dr. Toshiaki Ohtani, Dr. Akira Yamakata, and Dr. Shigeru Ichihara of IRAS group discussed producing and using experimental apparatuses. I especially appreciate Dr. Athula Banadara's kindness to provide much information not only on experiments but also on manners abroad.

I acknowledge all help and encouragement given by every member of Professor Domen's laboratory, Professor Hirose's laboratory, Professor Maruya's laboratory, Professor Wada's laboratory, and Professor Hara's laboratory from the bottom of my heart.